

Revista Română de Inginerie Civilă
Indexată în bazele de date internaționale (BDI)
ProQuest, INSPEC, EBSCO
INDEX COPERNICUS, ULRICH'S și JOURNALSEEK

Volumul 5 (2014), Numărul 1
ISSN 2068-3987

The possibility of replacing solid walls with water curtain applicable to a large underground garage	1-8
<i>Ivan Antonov, Rositsa Velichkova, Kamen Grozdanov, Ivancho Bogoev, Kiril Mavrov</i>	
Experimental Study Of Acoustic Barriers In Urban Environment	9-18
<i>Tiberiu Catalina, Vlad Iordache, George Craciunescu</i>	
The influence of different flow velocities on the heat transfer inside a ventilated façade	19-26
<i>Monica Chereches, Nelu-Cristian Chereches, Sebastian Hudisteanu</i>	
Conception of a simplified seated thermal manikin for CFD validation purposes	27-35
<i>Angel Dogeanu, Bode Florin, Alexandru Iatan, Cristiana Croitoru, Ilinca Nastase</i>	
Experimental and theoretical study regarding the thermal performances of the heat exchangers with steel panels and extended surfaces	36-45
<i>Anica Ilie, Răzvan Calotă</i>	
Consecințe energetice ale încălzirii intermitente a clădirilor	46-58
<i>Florin Iordache, Vlad Iordache</i>	
Analiza performanței energetice a unei instalații solare de preparare a apei calde de consum în diverse condiții de utilizare	59-67
<i>Răzvan Popescu, Lelia Popescu, Andrei Damian</i>	
The behaviour analysis of an anaerobic sludge digester exposed on thermic action	68-78
<i>Lucian Valentin Sorohan</i>	
An experimental study on convective drying of quince	79-86
<i>Tzempelikos Dimitrios, Bardakas Achilleas, Vouros Alexandros, Tsepenekas Dionysios, Filios Andronikos, Margaritis Dionissios</i>	

COLEGIUL EDITORIAL

Prof.dr.ing. Ioan BOIAN, *Universitatea Transilvania Braşov*
Prof.dr.ing. Alexandru CĂTĂRIG, *Universitatea Tehnică Cluj Napoca*
Conf.dr.ing. Victoria COTOROBAL, *Universitatea Tehnică Gh. Asachi Iaşi*
Prof. dr. mat. Rodica DĂNEŢ, *Universitatea Tehnică de Construcţii Bucureşti*
Prof.dr.ing. Carlos Infante FERREIRA, *Delft University of Technology, The Netherlands*
Prof.dr.ing. Dragoş HERA, *Universitatea Tehnică de Construcţii Bucureşti – redactor şef*
Prof.dr.ing. Ovidiu IANCULESCU, *director editorial*
Prof.dr.ing. Gheorghe Constantin IONESCU, *Universitatea Oradea*
Prof.dr.ing. Florin IORDACHE, *Universitatea Tehnică de Construcţii Bucureşti*
Prof.dr.ing. Carmen Elena MAFTEI, *Universitatea Ovidius Constanţa*
Prof.dr.ing. Ion MIREL, *Universitatea Politehnica Timişoara*
Prof.dr.ing. Dan GEORGESCU, *Universitatea Tehnică de Construcţii Bucureşti*
Prof.dr.ing. Mircea PETRINA, *Universitatea Tehnică Cluj Napoca*
Conf.dr.ing. Dorel PLĂTICĂ, *Universitatea Tehnică Gh. Asachi Iaşi*
Prof.dr.ing. Nicolae POSTĂVARU, *Universitatea Tehnică de Construcţii Bucureşti-redactor şef*
Prof.dr.ing. Daniela PREDA, *Universitatea Tehnică de Construcţii Bucureşti*
Prof.dr.ing. Ioan SÎRBU, *Universitatea Politehnica Timişoara*
Prof.dr.ing. Ioan TUNS, *Universitatea Transilvania Braşov*

ISSN 2068-3987

MATRIX ROM
OP CHIAJNA CP 2
077040 – ILFOV
Tel. 021 4113617 Fax. 021 4114280
e-mail: office@matrixrom.ro
www.matrixrom.ro

The possibility of replacing solid walls with water curtain applicable to a large underground garage*

Ivan Antonov¹, Rositsa Velichkova¹, Kamen Grozdanov¹, Ivancho Bogoev², Kiril Mavrov¹

¹Technical University of Sofia.

1000Sofia, 8 Kl.Ohridski Ave, Bulgaria

E-mail: mfantonov@abv.bg, rositsavelichkova@abv.bg, alekcandra_s_b@abv.bg, mavrov@gmail.com

² VFU „Chernoriztes Hrabar”

9007 Varna Chaika resort, Bulgaria

E-mail: ivanchobogoev@abv.bg

Abstract. *The work is considered the replacement of fire barriers with hard water curtain sprinkler system created by the devices. The main focus is the duration of activation of sprinkler devices and parameters they generate water curtain. It is isolate specific cell cars using water curtain to prevent the spread of fire to neighboring and adjacent cars.*

Key words: sprinkler device, fire, water curtain

1. Introduction

In large public parking with a few hundred or thousand cars the major problem is to ensure the fire safety, respectively the protection of arising the fire and its isolation and turning out. The main goal is to prevent the spread of fire to neighboring cars. This can be done by using of fire walls or as proposed in this work with dense water curtain, which is create of certain of a number of sprinklers located around the cell (Fig. 1).

2. Theoretical formulation of the problem

The idea of the application of eventually change fire walls with dense water curtain comes down to this: Over the burning vehicle arises vertical convective jet whose initial velocity is proportional to the power of fire. This jet is rising in vertical direction over the burning object and turn on the fast sprinkler which are located approximate over the engine of the car. In the first second the water from turn on sprinkler begin to extinguish the fire. Further the convective jet is spreading at the garage ceiling as one side wall confined jet that reaches the water sprinklers from the water curtain. The curtain is turn on and isolates the zone with burning vehicle and it prevent the spreading of fire in other direction.

* Lucrare inclusă în programul conferinței EENVIRO 2013

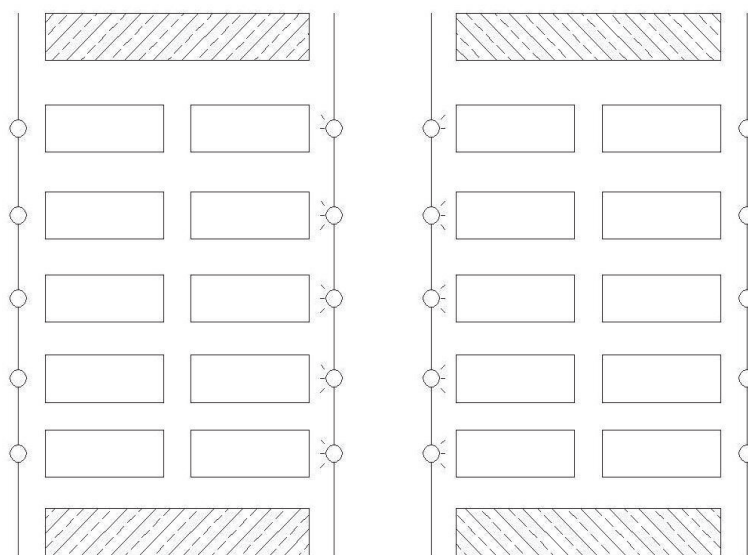


Fig.1

Simultaneously, the automation system is turn on over the relevant area of ventilation system. The system of aeration is operate on the following principle: sucks the smoke and heating air from the burning car and meanwhile not to create a gage pressure it is compressed air in the system.

According Drysdale [3] the velocity over a fire can approximately be determined by:

$$W_0 = 1,9Q^{1/5} \quad (1)$$

Where W_0 - initial velocity of the fire, m/s , Q - power of the fire, kW

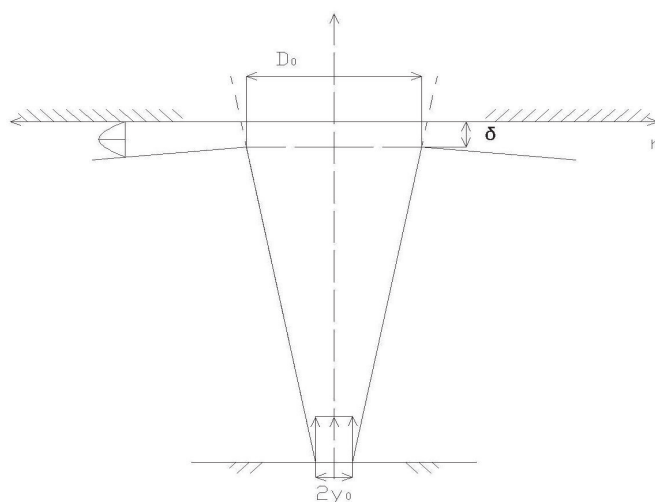


Fig.2

The possibility of replacing solid walls with water curtain applicable to a large underground garage

The parameters of convective upward jet (Fig. 2) according to [1] and [2] is calculated using the following relationships:

- The velocity of the upward jet:

$$u_m = B_u'' D_0^{1/3} \Delta T_{ni}^{4/9} \bar{x}^{-1/3} \quad (2)$$

- The temperature difference

$$\Delta T_m = T_m - T_{ok} = B_{\Delta T}'' D_0^{1/3} \Delta T^{8/9} \bar{x}^{-5/3} \quad (3)$$

Where D_0 - initial diameter of the heat source in case of the fire burning car,

m ; $\Delta T_1 = T_{ni} - T_{ok}$, K ; $\bar{x} = \frac{x}{D_0}$; constants B_u'' and $B_{\Delta T}''$ have values

$$B_u'' = 0,222 \left[m^3 K^{9/4} \right] \text{ and } B_{\Delta T}'' = 0,71 \left[m^{1/3} K^{9/8} \right].$$

These values satisfy the case when $\bar{x} = \frac{x}{D_0} \geq 3 \div 3,5$. The chosen size of the burning car which is create from the fire $D_0 = 0,5m$ and height of the garage $H = 3 \div 4,5m$, which means that \bar{x} will fulfill the above condition

In a relatively short distance to ceiling the high power of the fire (conditionally accepted for $Q = 1500W$ and temperature $T = 600K$) velocity and temperature of the rising convective jet did not significantly change

For obtaining initials velocities $W_0 = 8,2m/s$ at chosen power of fire, the convective stream reach the ceiling for different time at different heights of garage cells and this time is given in Table 1

Table 1

h,m	3	3,5	4	4,5
$\Delta t, s$	0,36	0,43	0,49	0,55

This means that for a time less than $\Delta t = 1s$ sprinklers over burning car will be activated and will turn on and extinguished process will started.

In next moment reaching the ceiling the convective jet is transformed into wall radial jet which is evolve at ceiling in all directions, steering to so-called "fast" sprinklers form the water curtain. Due to the short distance to the ceiling and high temperature of the flow the initial weight and velocity does not change. Because of the big difference in the densities of convective flow and the environment $\rho_{jet} < \rho_{env}$, the last "pressed" to the ceiling and don't allows her extension. It is assumed that the initial value of ring jet is determined according to fig.3 from the initial diameter $D_0 = 0,5m$ and thickness b_0 .

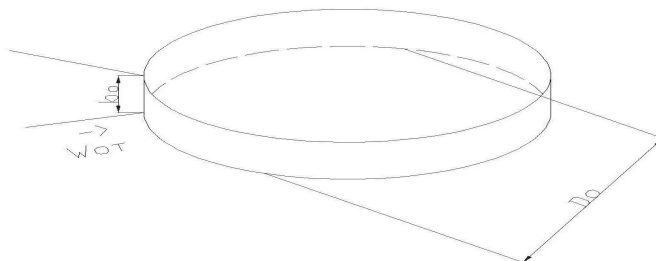


Fig.3

The initial parameters: diameter, thickness and velocity of the wall radial jet are defined as follows:

- The velocity at initial section after turning it on 90° is assuming equal to half of initial velocity of upward jet

$$W_{0T} = 0,5W_0 \quad (4)$$

For example when $W_0 = 8,2m/s$ then W_{0T} is equal to $4,1m/s$

- The initial width b_0 of the jet will be as following:

$$b_0 = \frac{V_0}{\pi D_0} \quad (5)$$

Where $V_0 = \frac{\pi D_0^2}{4} W_0$ is the initial volume of the flow

It is assuming that for the time of reaching of the ceiling the temperature and density are not changed

Using the above values for D_0 and W_0 for b_0 is getting:

$$b_0 = 10mm \quad (6)$$

The section at which the flow is expanded is determined by the expression:

$$S = 2\pi r b \quad (7)$$

If for b is accepted the equation according [1] then:

$$b = cr \quad (8)$$

Where: $c = 0,27$ is a constant and r is the distance from the center of the circle described above the flow (Fig. 3).

Replacing (8) in (7) is follow:

$$S = 2\pi cr^2 \quad (9)$$

Respectively.

$$S = 1,6959r^2 \quad (10)$$

Obtaining S it could be calculated the average velocity of the ceiling at current distance r from the center over the fire (Fig.3):

$$U_{pm} = \frac{W_{0T}}{S} \quad (11)$$

The possibility of replacing solid walls with water curtain applicable to a large underground garage

The calculation of $U_{pm} = f(r)$ at a different distance from the device is given in Table 2.

Table 2

$l = 1m$	$U_{PM1} = 2,41m / s$
$l = 2m$	$U_{PM1} = 0,604m / s$
$l = 3m$	$U_{PM1} = 0,268m / s$
$l = 4m$	$U_{PM1} = 0,15m / s$

If an average velocity to reach a current at distance l is assuming by:

$$\Delta U_{PM} = \frac{W_{OT} - W_{PM}}{2} + U_{PM} \quad (12)$$

It can be found the time that the wall jet is reach at current distances ie time of activation of so called „fast” sprinklers which is given in Table 3.

Table 3

l, m	$\Delta t, s$
$l = 1m$	$\Delta t \sum 0,55 + 0,35 = 0,9s$
$l = 2m$	$\Delta t \sum 0,55 + 0,855 = 1,4s$
$l = 3m$	$\Delta t \sum 0,55 + 3,27 = 3,82s$
$l = 4m$	$\Delta t \sum 0,55 + 4,155 = 4,7s$

This means that in the first two seconds will trigger on all sprinklers at distance 2 m from the burning car. For longer distances remote sprinklers will operate at condition that the temperature of the burning car do not fall too quick.

For maximum calculating time of 4,7 seconds could not be expected too much drop of the temperature, which leads to the conclusion that the ceiling temperature will be much greater than the starting temperature of "fast" sprinklers.

According to Figure 4, for time $\Delta t = 4,7s$ will be start from three to five fast-acting sprinklers standing at distance between them l_1 .

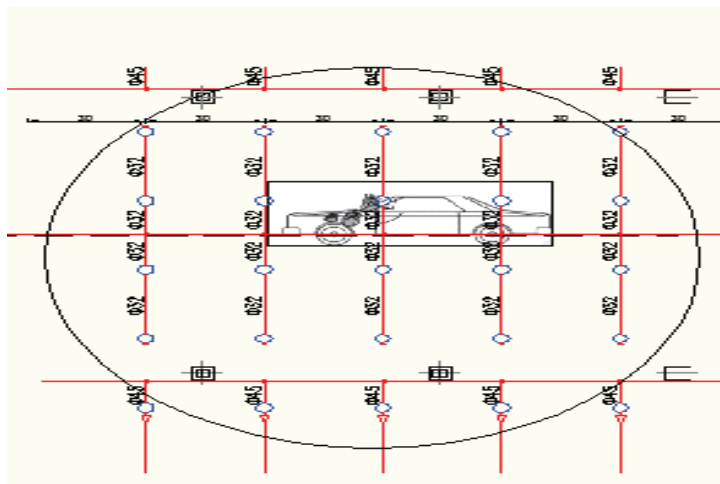


Fig.4

In the vicinity of the burning car to sprinkler curtain $l \leq 2m$ will trigger from 3 to 5 fast sprinklers. At a longer distance will trigger maximum of three quick sprinklers of water curtain plus this over the burning car and eventually this one which are lying in the range of $l = 4m$ ceiling sprinklers so that the number of activated sprinklers will be increase [5].

To create a smokeless zones under smoke floating layer according to[6] is design and install ventilation exhaust systems for smoke and hot gases. This ventilation systems for smoke and hot gases is a scheme of safety equipment designed to perform a positive role at unexpected fire. The smoke is drawn in the direction of the non carrier bulkhead from velocity of 2 m / s to 5 m / s. Quoted above standard allowed velocity from 5 m / s, but it should be take in mind that this velocity would affect negatively and lead to the merging of streams of pure air.

From [6] follows that the density of the thermal load in the rooms for the storage of combustible materials according to their purpose, is determined the heat capacity of the prevailing materials. Ventilation systems to remove smoke and heat systems(VSRSH) have to reach its design performance level within 60 seconds from receiving the command signal. Each VSRSH systems have to ensure the supplement of sufficient fresh air that enters the room for the expense of the flue products.

3. Thermal impact

Heat transfer by convection and radiation is define according to [5]. Thermal effects are expressed by the intensity of the heat flow $h_{nbt}, W / m^2$ to the surface of the element and is determined with taking into account the heat transfer by convection and radiation, such as:

$$h_{nbt} = h_{nbt,c} + h_{nbt,r}, W / m^2 \quad (12)$$

where: heat transfer by convection $h_{nbt,c}$ is given by the relationship

$$h_{nbt,c} = \alpha_c (\theta_g - \theta_m), W / m^2 \quad (13)$$

radiation heat transfer $h_{nbt,r}$ is given by the dependence:

The possibility of replacing solid walls with water curtain applicable to a large underground garage

$$h_{nbt,r} = \Phi \varepsilon_m \varepsilon_f \sigma \left[(\theta_r + 273)^2 - (\theta_m + 273)^4 \right], W / m^2 \quad (14)$$

Convection component of the intensity of the heat flow is determined by:

$$h_{nbt,t} = \alpha_c (\theta_g - \theta_m), W / m^2 \quad (15)$$

where: α_c is the heat transfer coefficient by convection $\left[\frac{W}{m^2} K \right]$; θ_g is the gas temperature near the exposed fire element [$^{\circ}C$], θ_m is the surface temperature of the element [$^{\circ}C$]

The coefficient of heat transfer by convection α_c is determined by the nominal curves "temperature-time". At indirectly heated surface elements the intensity of heat flow h_{nbt} is determined by the relationship (15) where $\alpha_c = 4 \left[\frac{W}{m^2} K \right]$. The coefficient of heat transfer by convection has value $\alpha_c = 9 \left[\frac{W}{m^2} K \right]$, considering that it is include the effects of heat transfer by radiation. Radiating components of net heat flux per unit surface area is defined as:

$$h_{nbt,r} = \Phi \varepsilon_m \varepsilon_f \sigma \left[(\theta_r + 273)^2 - (\theta_m + 273)^4 \right], W / m^2 \quad (16)$$

where: Φ factor of configuration, ε_m emitting surface element, ε_f transmission of fire, $\sigma = 5,67 \cdot 10^8 \left[\frac{WK^4}{m^2} \right]$ constant of Stefan - Boltzmann, θ_r is the effective temperature of the radiation environment [$^{\circ}C$], θ_m is the surface temperature of the element [$^{\circ}C$]. Transmission of fire is taking equals $\varepsilon_f = 1$

4. Determination of the intensity of the water curtain

Because of the difficulties associated with the construction of fire walls at normalization of fire stations and sections for that it is making experiments at these areas with aim to reduced such proportions that the primaryly split up do not disturb of the process. In many cases, such as in buildings of first degree of fire resistance, as already noted, firewalls did not provide the detriment of fire safety. In connection with this arise there is a need of using such fire barriers that could effectively limit the spread of fire and at the same time would give some freedom for internal layout of buildings with different functions which is the case of water curtain.

The effectiveness of water curtains is assessed according to the amount absorbed heat.

It is known that the dependence of the growing of the temperature of the source of radiation of maximum energy emission is moving to the side of the shorter waves. This follows from the law of Vin:

$$\lambda_{\max,T} T = 0,29 = const \quad (17)$$

where: λ is the wavelength in m, T - temperature at the surface of water curtain, $^{\circ}K$.

5. Required flow rate of the water curtain

The specific task is solved at given characteristics-density of the radiation heat flux, 1500 W/m^2 ; density of the irradiation protected material, 900 W/m^2 ; height of the hole -4 m; length of the hole - 6 m; pressure of water in sprinkler - 0.6 MPa (6 atm) and the radius of the water drops -0,0006 m ($600 \mu\text{m}$).

Optical density of the curtain:

$$\delta = \frac{2,303 \log q_{u3l}}{q_{kp}} = 0,51 \quad (18)$$

Thickness of the curtain:

$$R = \frac{\delta}{c} = \frac{0,51}{2,8} = 0,182 \text{ m} \quad (19)$$

Flow rate of the water curtain for 1 m^2 of lateral surface is defined by:

$$Q = 0,666 \mu \rho \frac{rR}{H} \sqrt{2gh} = 0,467 \frac{\text{l}}{\text{s}} \text{ m}^2 \quad (20)$$

For the whole surface of the water curtain:

$$Q^H = 11,2 \text{ l / s} \quad (21)$$

Water curtains are constructed so that the entire hole to be irrigate with finely dispersed water. For this purpose sprinklers are placed over the hole and next to it. When they are placed at the top of the hole it is possible to remain unprotected areas through which is possible a penetration of hot gases.

Sprinkler heads which are used to spray jets are spaced 0.5 m in protecting small holes and 1.25 - 1.5 m in protecting large holes. For sprinkler heads water curtain which are situated at a distance greater than 3 m, it is required head pressure of the water 4-6 mH_2O .

6. Conclusions:

It is made an approximate fast and easy to implement analysis and calculation of water curtain, which replacing the fire walls with water curtains.

It is possible to complicate the design task with the numerical simulation of the object, which could hamper by time the current work.

References:

1. Abramovich, Theory turbulentnyiy Strings, Moscow 1984
2. Antonov IC, Applied Fluid Mechanics, Sofia 2010
3. Drysdale D. An introduction to fire dynamics, John Wiley sons, 1999
4. Eurocode 1 - Impact on stoitelni structures, Part 1-2
5. EN-12845, Installation and Maintenance of fixed sprinkler systems in buildings and industrial plants
6. Annex № 9 of art. 122, para. 3 NSTPNOBP

Experimental Study Of Acoustic Barriers In Urban Environment*

Tiberiu Catalina, Vlad Iordache, George Craciunescu

Research Center CAMBI, Faculty of Building Services Engineering, Technical University of Civil Engineering
Pache Protopopescu street no. 66, District 2, Bucharest, Romania

E-mail: tiberiu.cattalina@gmail.com, viordach@yahoo.com, geo_mvp_2nite@yahoo.com

Rezumat. Acest articol prezintă un studiu experimental detaliat al unei bariere acustice proiectate pentru protecția la zgomot a ocupanților unui imobil de locuit. Studiul este bazat pe o situație de mediu urban reală în care măsurările nivelului de zgomot au fost realizate înainte și după implementarea acestei bariere acustice. Sursele de zgomot au fost unitățile exterioare ale unei pompe de caldură aer-apă. Începând cu protocolul de măsură până la concluzii, în acest articol sunt prezentate aspecte interesante privind protecția la zgomot a unei bariere acustice instalate în mediul urban. Atenuarea acustică maximă obținută în cadrul acestui studiu a avut valoarea de 18.96 dB pentru o frecvență de 125 Hz iar media a fost în jurul valorii de 15 dB. În cele din urmă, s-a putut constata că această barieră a fost o soluție bună iar confortul acustic a fost asigurat.

Cuvinte cheie: barieră acustică, studiu experimental, mediu urban.

Abstract. This article presents a detailed experimental study of the design and analysis of an acoustic barrier used to protect the occupants of a building from the noise produced by a HVAC system installed outdoors. The study is based on a real urban situation in which noise measurements were conducted before and after implementation of the noise barrier. In this case the noise sources are the four fans of an air-water heat pump. From measurement protocol to conclusions in this article are present interesting insights about a noise barrier installed in urban areas. The highest acoustic attenuation obtained in this study had a value of 18.96 dB at a frequency of 125 Hz and the average was around 15 dB. At the end, the use of the noise barrier was found a good solution and the acoustic comfort was achieved.

Key words: acoustic barrier, experimental study, urban environment.

1. Introduction

Nowadays, the general noise level has reached an alarmingly high level, as we are exposed to noise pollution not only by day but also at night time. Noise is among the most significant pollutants in the world and it can be generated by almost any sound source like road traffic, jet planes, loud music, construction equipment, manufacturing processes etc. The negative effects of noise pollution include hearing loss, high levels of stress, work inefficiency, sleep disorders, life quality alteration. As you can see, these unwanted sounds can affect human health and well-being and it is

* Lucrare inclusă în programul conferinței EENVIRO 2013

mandatory according to the current European noise pollution norms [1] and to the Romanian ones to try and rule them out from our daily routine in order to achieve acoustic comfort indoor [2] and outdoors [3]. Noise can derive from many sound sources and in this study we will focus on HVAC noise generating equipment's. The emergence of modern comfort systems like heat-pumps, chillers, etc., assumes that the noise generating equipment would be mounted outdoors, which decreases the indoor noise level and increases the outdoor one. HVAC (heating, ventilation, and air conditioning) systems represent the technology of which main purpose is to help maintain good indoor air quality through adequate ventilation with filtration and provide thermal comfort. The main problem with these HVAC systems is noise pollution that affects urban environments and indoor life quality [2] [4] [5]. Currently, there are only a few experimental studies on acoustic barriers in Romania, and even fewer projects based on the preliminary calculations of these acoustic barriers. The experimental study consists of measurements of the sound pressure levels of noise generating HVAC type equipment. The aim of this study is to demonstrate the practical aspect of implementing a professional acoustic barrier as a sound insulation solution for the urban environment and the nearby apartment buildings. Therefore, the main objective of the study will be the experimental comparison of sound pressure level before and after the installation of the acoustic barrier.

2. Experimental Study

The experimental study consists of acoustical sound pressure level measurements performed in order to establish the validity of the urban environment noise pollution norms. The measurement protocol has been accomplished before and after the implementation of the acoustic barrier solution. Noise is the main cause of this study, as its levels outweighed the legal outdoor noise pollution norm. In this case, noise is generated by four HVAC type equipment's (heat pump system) of which we will refer to as noise sources (NS). These sources are producing an important amount of noise pollution that affects an apartment building located near them. The noise generating sources as well as the noise polluted apartment building are presented in the following figure.

The sound pressure level measuring took place at night time to prevent high traffic noise levels and outdoor work-related unwanted sounds that could have interfered with the precision of the measurements. A professional Bruel & Kjaer class 1 sound level meter was used to perform the measurements. Background noise was measured in all the established measuring points before measuring the sound pressure levels of the operating noise sources. The upper limits of accepted sound levels for outdoor and indoor environments are shown in the next table according to the present European and Romanian noise pollution standards (NC=noise curve) [3].

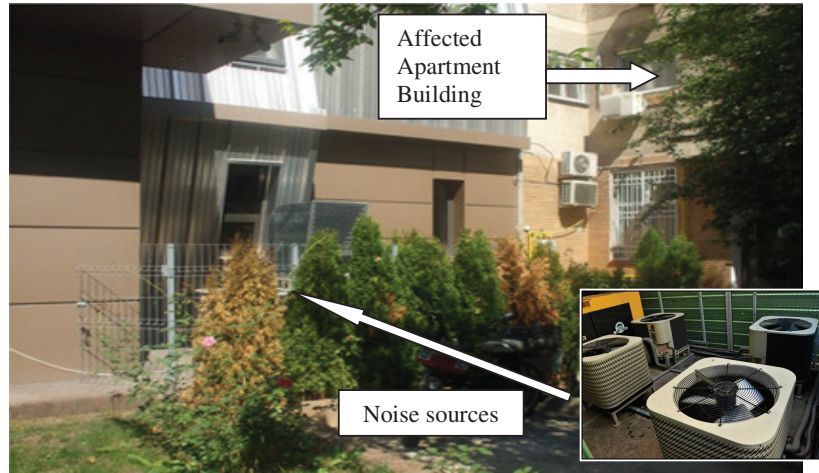


Fig.1 Noise sources and affected environment

Table 1 Outdoor Noise Pollution Norm for Urban Environments

Frequency [Hz]	31.5	63	125	250	500	1000	2000	4000	8000
NC30 [dB] indoor	75.8	59.2	48.1	39.9	34	30	26.9	24.7	22.9
NC45 [dB] outdoor	86	71	61.1	53.6	48.6	45	42.2	40	38.3

Measuring points were established before actually starting the measurements, resulting in a total of 6 measuring points located outdoors and indoors. The outdoors measuring points are located: in the center of the noise sources (**P1**), 0.5 m away from the noise source (**P2,P3**), 2 m away from the apartment building facade (**P4, P5**). The indoor measuring point is located inside the first floor apartment at 1 m away from the exterior window (**P6**) and were measured with the apartment windows closed. The measurements began after the heat-pumps started functioning in a nominal regime, to avoid any unwanted launching noise.

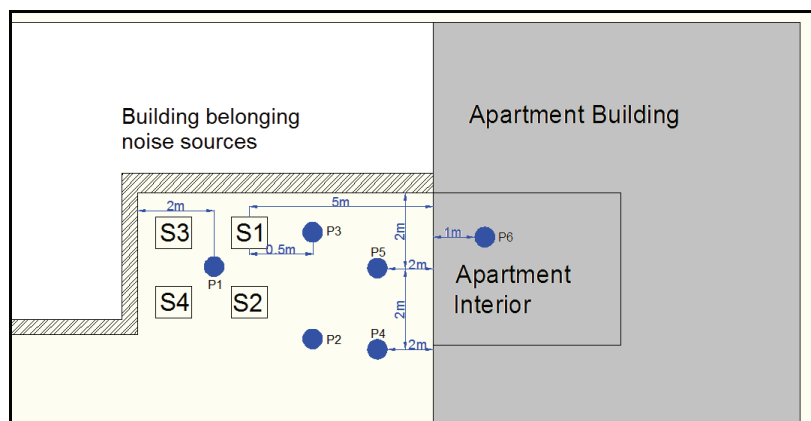


Fig.2 Outdoor and indoor measuring points;
S1, S2, S3, S4 are the four noise sources (outdoor units of the heat pump)

3. Initial noise measurements

The results of the both outdoor and indoor sound pressure level measurements have been obtained with the “BZ 5503” software, associated with the sound level meter and are selected and shown in the figures below and interpreted. The measured noise level for the outdoor points (P1,P2,P3,P4,P5) is compared with the outdoor noise curve CZ45 (NC45 - urban environment between apartment buildings), while the one measured indoor (P6) is compared with the indoor noise curve CZ30 (NC30 – indoor sleeping room). All comparisons were carried out for the spectra between 31.5 Hz and 8000 Hz. .

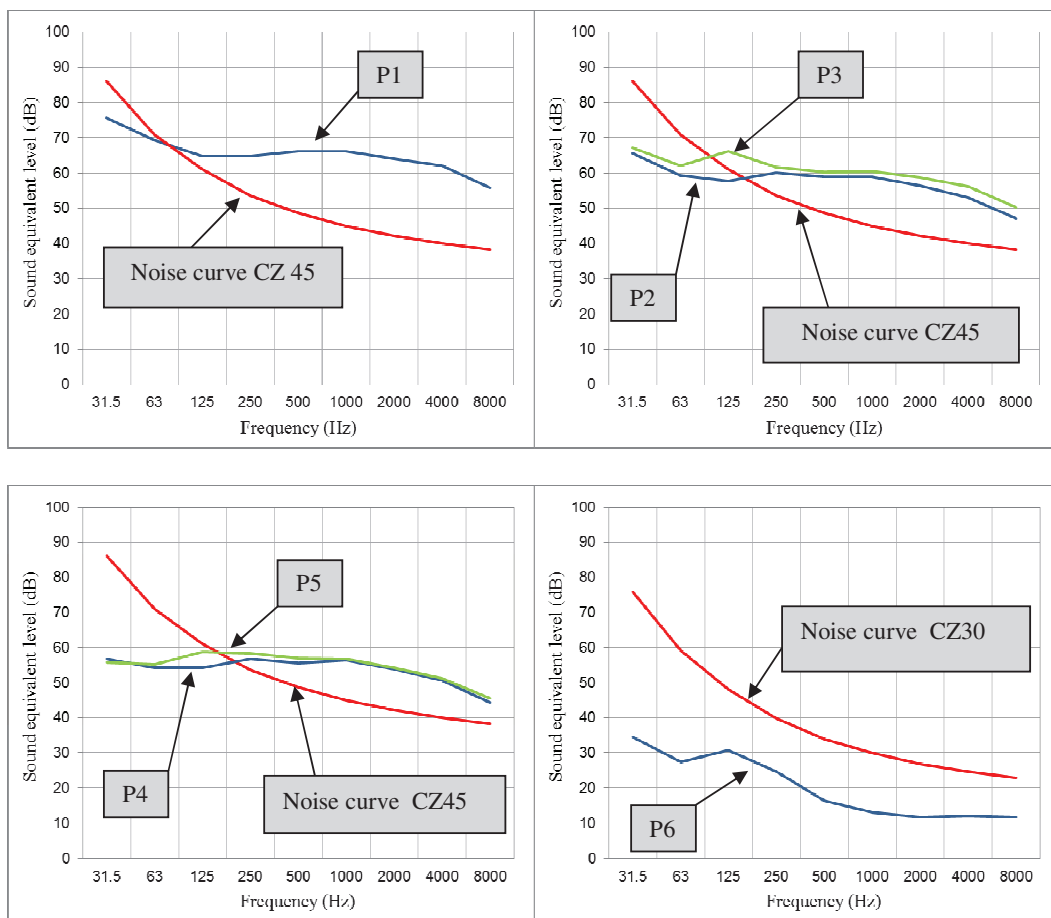


Fig.3 Sound equivalent levels for indoor and outdoor measured points (P1,P2,P3,P4,P5,P6) and comparison with the noise curves CZ45 and CZ30

As it can be noticed from Fig.3, the outdoor sound pressure levels are higher than the noise pollution norms from frequencies beginning with 125 Hz. The sound pressure level measured inside the apartment corresponds to the present noise

pollution norms, as the P6 curve has a lower value than the reference indoor NC30, but with the apartment windows open (ventilation purposes) we can notice that the exterior noise affects the acoustic comfort inside.

Thus, a sound insulation solution must be applied in order to obtain acceptable noise levels.

4. Noise protection solution

In most cases, the most adopted solution is represented by a simple acoustic barrier made from a sheet of metal which has near-zero noise absorption coefficients. This type of solution is cheap and quick, but in the end the results are not sufficient and the only key to this problem is adopting a high quality acoustic barrier. Another solution for keeping noise levels down is represented by placing the equipment on the building's roof. This solution is very expensive and can often be impossible to achieve due to architectural restraints. In conclusion, for this situation, the best sound insulating solution in this case is the installation of a quality acoustic barrier with a perforated metal sheet for best acoustic performances [6]. The acoustic barrier used in this experimental study is a high-performance acoustic multi-panel (Fig. 4), made out of two main materials:

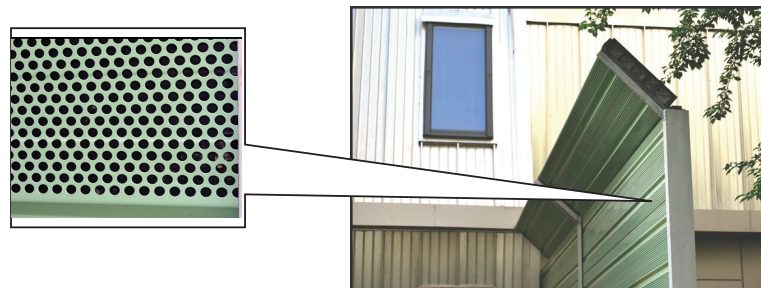


Fig.4 Acoustic barrier shape and model

- **Exterior:** 1mm thick perforated pre-painted zinked steel metal sheet on the front side of the barrier, that allows sound to be absorbed by the insulating material and 1mm thick Pre-painted zinked steel metal sheet on the back side of the barrier, that does not allow the sound to pass-through the acoustic barrier
- **Interior:** 60mm thick humidity-proof mineral wool with a density of 100 [kg/m²]. [9]

The barrier construction was designed to have a slight angular curvature at the top of its height, of which purpose is to stop and attenuate the sound propagation by diffraction phenomena [7,8]. The selected barrier represents a professional sound insulating solution that can reduce noise levels up to 25 dB, according to the manufacturer. The geometrical measures of the acoustic barrier are: height $H = 3.7$ m; length $L = 3.2$ m; width $W \sim 0.15$ m.



Fig.5 a) Photos of the acoustic barrier ; b) 3D model of the scene, recreated in 3Ds Studio Max

The next part of the paper presents the measured noise levels after the noise protection solution was installed between the outdoor units of the heat pumps and the nearby apartment building.

5. Noise measurements after the protection solution was mounted

The noise protection solution represented by the acoustic barrier has been installed between the noise sources (the heat pumps) and the receiver (the apartment building). Thus, it is important that a new series of measurements to be executed, in order to obtain the sound attenuation caused by the implementation of the acoustic barrier. The results of the both outdoor and indoor sound pressure level measurements **after implementing the acoustic barrier** have been obtained, as it was previously mentioned, with the software associated with the usage of the sound level meter and then imported in excel format. Results have afterwards been selected and compared to the initial measurement results along with the noise curves NC45 and NC30 that must be respected.

The comparison was done between the sound pressure levels before and after the installation of the acoustic barrier, only for the following measurement points:

- A) 0.5 meters away from the noise source (P2, P3)
- B) 2 meters away from the apartment building facade (P4, P5)

The results for the other measuring points were not taken into consideration due to their inconclusive character. At the end of the comparison, the **global sound pressure levels** will be shown for all sound frequencies and the results will appear in tabular form. The sound pressure levels before the installation of the acoustic barrier were higher than the noise curves NC45 from the frequency of 125 Hz. The sound level after the implementation of the acoustic barrier was estimated to correspond with the current noise pollution norms, as it can be seen in the following figure.

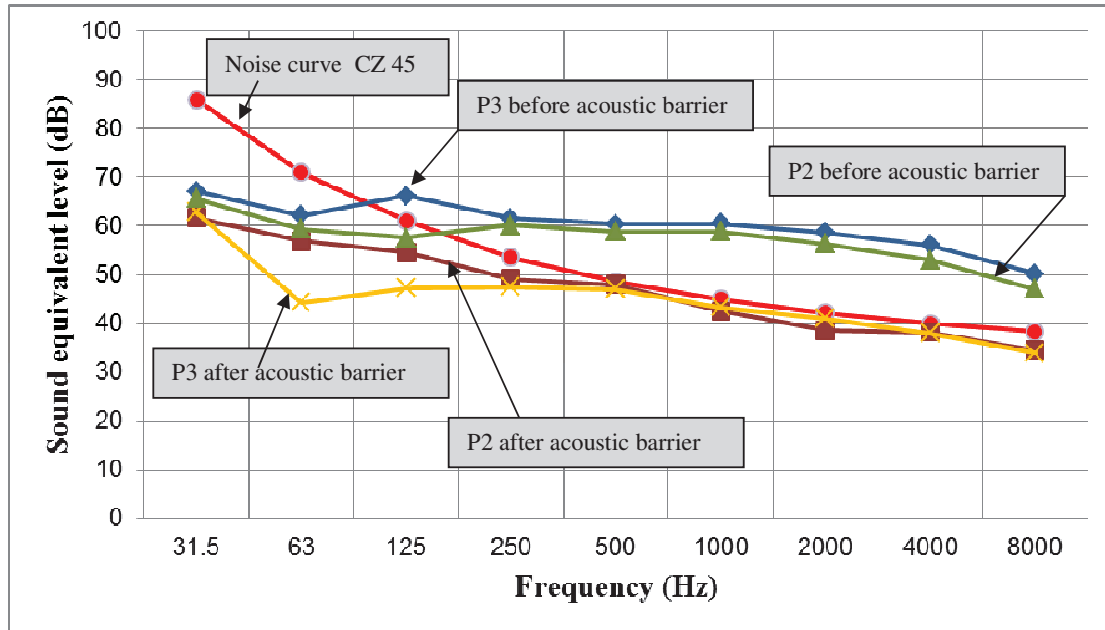


Fig.6 Comparison of the sound pressure levels of P2,P3 before and after the implementation of the acoustic barrier

As it can be observed from Fig.6 there is a visible sound attenuation after the installation of the acoustic barrier, and looking at the noise curves chart, the noise pollution norms are respected even if for some frequencies (500 to 4000 Hz) the results were on the edge. The following table is a numeric representation and shows the sound attenuation of the P2 and P3 measured points before and after the installation of the acoustic barrier.

Table 2 Noise attenuation in P2 and P3 due to implementation of the acoustic barrier

Frequency (Hz)	31.5	63	125	250	500	1000	2000	4000	8000
P2 before (dB)	65.64	59.37	57.63	60.13	58.92	58.87	56.36	52.99	46.99
P2 after (dB)	61.64	56.93	54.59	49.18	47.91	42.52	38.59	38.21	34.45
Attenuation ΔL_p (dB)	4.00	2.44	3.04	10.95	11.01	16.35	17.77	14.78	12.54
P3 before (dB)	67.13	62.09	66.23	61.56	60.37	60.48	58.63	56.11	50.21
P3 after (dB)	62.79	44.27	47.27	47.53	47.03	43.35	40.94	37.95	33.88
Attenuation ΔL_p (dB)	4.34	17.82	18.96	14.03	13.34	17.13	17.69	18.16	16.33

The maximum sound attenuation (18.96 dB) was obtained for the 125 Hz frequency in the case of the P3 measuring point. The minimum sound attenuation was

obtained for the P2 measuring point (2.44 dB) at the frequency of 63 Hz. The same comparison was carried out for the measuring points P4 and P5 where the sound pressure levels before and after the mounting of the acoustic barrier (Fig 7). The sound level after the implementation of the acoustic barrier was estimated to correspond with the current noise pollution norms, as it can be seen in the following figure. As it can be observed from Fig.7 there is a visible sound attenuation after the installation of the acoustic barrier, and looking at the noise curves chart, the noise pollution norms are respected exactly like in the previous case. For the 1000 to 4000 Hz frequencies the sound attenuation, corresponding to the P4 and P5 measuring points, barely corresponds to the present noise pollution norms.

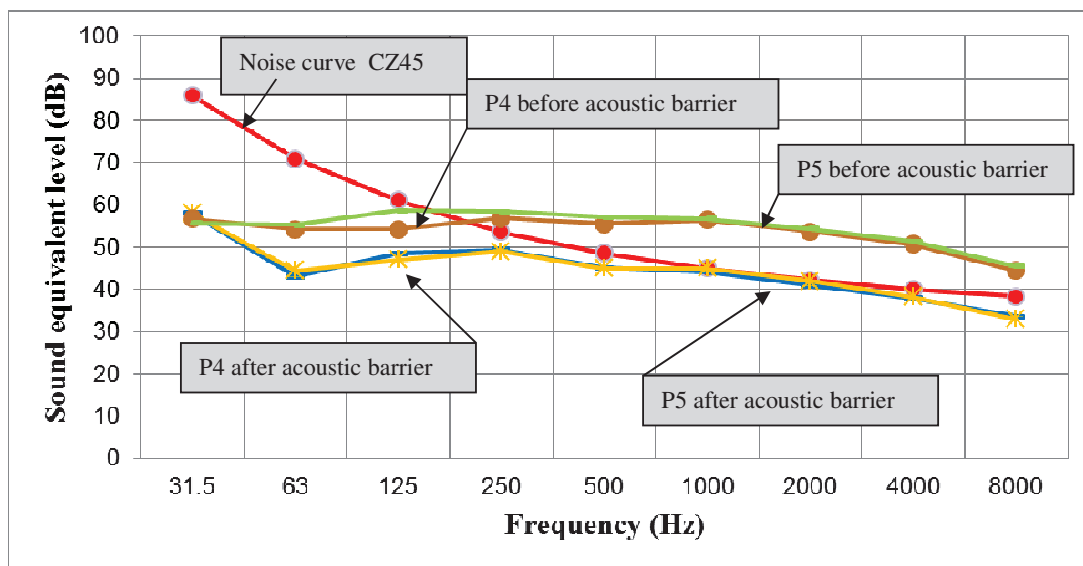


Fig.7 Comparison of the sound pressure levels of P4, P5 before and after the implementation of the acoustic barrier

The following table is a numeric representation and shows the sound attenuation of the P4 and P5 measured points before and after the installation of the acoustic barrier.

Table 2 Noise attenuation in P4 and P5 due to implementation of the acoustic barrier

Frequency (Hz)	31.5	63	125	250	500	1000	2000	4000	8000
P4 before (dB)	56.76	54.19	54.25	56.81	55.58	56.47	53.76	50.66	44.4
P4 after (dB)	58	44.5	47	49	45	45	42	38.2	33
Attenuation ΔL_p (dB)	-1.24	9.69	7.25	7.81	10.58	11.47	11.76	12.46	11.40
P5 before (dB)	55.69	55.27	58.64	58.35	57.05	56.69	54.3	51.33	45.49
P5 after (dB)	58.06	43.06	48.49	49.43	45.14	44.24	40.91	37.87	33.57
Attenuation ΔL_p (dB)	-2.37	12.21	10.15	8.92	11.91	12.45	13.39	13.46	11.92

The maximum sound attenuation (13.46 dB) was obtained for the 4000 Hz frequency in the case of the P5 measuring point. The minimum sound attenuation was obtained for the P4 measuring point (7.25 dB) at the frequency of 125 Hz. The sound attenuation for the P2 and P3 measuring points was greater than that of the P4 and P5 points because the P2, P3 points were located behind and in the proximity of the acoustic barrier, while the P4 and P5 points were located further away from the barrier thus resulting in the possibility of sound waves reflection to occur and amplify the sound pressure level. Using the measured data we were able to show the global sound pressure level for all the frequencies of each measured point before and after the implementation of the acoustic barrier as well as the sound attenuation regarding each measured point. The results are listed below in Table 4.

Table 4 Effect of the acoustic barrier with respect to the global sound pressure levels

	Sound pressure level [dB(A)]			LIMIT according to [2,3]
	Before	After	Sound attenuation ΔL_p (dB)	
P1	71	71.8	-0.8	50
P2	63.4	49.2	14.2	50
P3	65.4	48.92	16.48	50
P4	60.7	49.53	11.17	50
P5	61.4	49.14	12.26	50
P6	21.6	15.22	6.38	35

As it can be seen from the previous table, the noise levels diminished considerable. For the case of the P1 measuring point, the sound pressure level was amplified by 0.8 dB(A) because of the resulting reflections after the installation of the acoustic barrier.

6. Conclusion

The present study set out to determine the effect of an acoustical barrier installed between a noise source - the four fans of the heat pump system) and a receiver - the apartment).

The necessity of installing an acoustic barrier came from the excessive noise level in relation to present noise pollution norms [1, 2]. The noise levels at 2 m away from the building's facade were above the noise curve NC45 before the installation of the acoustic barrier. After the implementation of the barrier, the noise levels dropped considerably and the noise pollution norms were respected. The noise levels at 0.5 m away from the sound source also diminished after the installation of the acoustic barrier and the noise pollution norms were also respected.

The maximum sound attenuation obtained during the measurements was 18.96 dB and it was obtained for the P3 measuring point (0.5 meters away from the sound source) on the frequency of 125 Hz.

The maximum global sound attenuation was also obtained for the P3 point (0.5 meters away from the sound source) with a value of 16.48 dB(A).

This study has gone some way towards enhancing our understanding of how noise insulation solutions work and makes several noteworthy contributions to the apprehension of acoustic barriers.

In conclusion, this study has found that in general, a quality acoustic barrier is an almost flawless solution when it comes to diminishing noise pollution.

Acknowledgment

This work was supported by the grants of the Romanian National Authority for Scientific Research, CNCS – UEFISCDI, project number PN-II-RU-TE-2011-3-0209 and PN-II-RU-TE-2012-3-0108.

References

- [1] Directive 2002/49/EC of the European Parliament and of the Council of 25 June 2002 relating to the assessment and management of environmental noise - Declaration by the Commission in the Conciliation Committee on the Directive relating to the assessment and management of environmental noise
(<http://eur-lex.europa.eu/LexUriServ/LexUriServ.do?uri=OJ:L:2002:189:0012:0025:EN:PDF>)
- [2] STAS 6156-86 Protecția împotriva zgomotului în construcții civile și social-culturale. Limite admisibile și parametri de izolare acustică. (in Romanian)
- [3] STAS 10009-88 Acustica urbană. Limite admisibile ale nivelului de zgomot urban (in Romanian)
- [4] Vlad Iordache, Tiberiu Catalina, Acustica clădirii și instalațiilor: Aplicații Proiectare, ISBN: 978-973-755-909-8, Seria Complemente Ingineresti, Editura MATRIX Rom, 2013
- [5] Vlad Iordache, Protecție la Zgomot. Acustica clădirilor și instalațiilor, Editura MATRIX ROM, București, 2007, ISBN 978-973-755-224-2
- [6] M. Naderzadeh, M. R. Monazzam. „Application of perforated sheets to improve the efficiency of reactive profiled noise barriers”. Applied Acoustics, vol. 72, Issue 6, May 2011, Pages 393-398.
- [7] T. Okubo, K. Yamamoto. „Procedures for determining the acoustic efficiency of edge-modified noise barriers”. Applied Acoustics, vol. 68, Issue 7, July 2007, Pages 797-819.
- [8] Ishizuka T, Fujiwara K. “Performance of noise barriers with various edge shapes and acoustical conditions” Applied Acoustics 2004;65:125–41.
- [9] G.R. Watts, N.S. Godfrey. „Effects on roadside noise levels of sound absorptive materials in noise barriers”. Applied Acoustics, vol. 58, Issue 4, December 1999, Pages 385-402

The influence of different flow velocities on the heat transfer inside a ventilated façade*

Monica Chereches¹, Nelu-Cristian Chereches^{2#}, Sebastian Hudisteanu²

¹National Institute for Research and Development in Construction, Urban Planning and Sustainable Spatial Development, NR&DI URBAN-INCERC Iași Branch

37 Anton Sesan street, 700048, Romania

E-mail: putina_monica@yahoo.com

²Technical University "Gheorghe Asachi" of Iasi, Faculty of Civil Engineering and Building Services, Department of Building Services Engineering

13, bd Dimitrie Mangeron, 700050, Iasi, Romania

E-mail: chereches@tuiasi.ro, seby_hudisteanu@yahoo.com

Abstract. *In this paper, a comparative numerical study has been conducted in order to analyze the thermodynamic behavior inside a channel of a double skin ventilated façade in cold season with air supply ventilation mode. The study was performed in forced convection with CFD software Ansys-Fluent. A parametric investigation concerning the fluid inlet velocity has been conducted to study its influence on both fluid flow and heat transfer. The obtained results show the temperature and the velocity profiles, for different air velocities at the inlet section in order to calculate the heat losses through the surface of the interior glazing.*

Key words: numerical simulation, forced convection, air velocity, heat flux

1. Introduction

Double skin facades (DSF) are building envelopes composed of two layers of glass separated by a ventilated air channel. Due to the transient and complex air flow in the façade channel, the influence on the indoor environment and energy consumption are very difficult to evaluate. Computational Fluid Dynamics (CFD) can play an important role in evaluating and improving the thermodynamic behavior of a double skin facade. At the moment, there are more than 240 software products for simulations, available for over 20 years. The most known and used of these are: CAPSOL, ANSYS, TRNSYS, ESP-r, TAS, ENERGYPLUS, Ecotect. The performed simulations can be grouped into the following categories [1]: simulations for real buildings and simulation without any connection with these. Among these, Saelens [2] analyzed the energy efficiency of various types of single-storey facades; Balocco [3] used a computer model to study the steady state energy performance of a naturally ventilated façade; Li Hao Yin Chiu et al. [4] investigated the energy savings that

* Lucrare inclusă în programul conferinței EENVIRO 2013

correspondent author: chereches@tuiasi.ro

resulting from the preheating ventilation air by means of a double naturally ventilated facades. Kalyanova et al. [5] performed an empirical validation of building models with DSF, with various building simulation tools (ESP-r, IDA ICE 3.0, VA114, TRNSYS-TUD and BSim). In the literature there are also several examples of using CFD to evaluate energy efficiency and thermal performance of naturally or mechanically ventilated facades [6, 7, 8].

It was concluded that none of the models was consistent enough when comparing simulation results with experimental data for the ventilated cavity and only some models showed reasonable agreement with the experimental results for the thermal buffer mode.

Safer [9] realized a comprehensive modelling of a compact double-skin facade equipped with a venetian blind and forced ventilation. It was concluded that the distance between the blind and the external glazing have a major impact on the velocity profiles inside the double-skin facade channel.

In this study a comparative numerical analysis was made for thermodynamic behavior of a double skin façade. The façade channel with 45 cm thickness is composed of a single glazing to the exterior and a double glazing to the interior.

The parametric investigation concerning the fluid inlet velocity has been conducted in order to study its influence on both fluid flow and heat transfer.

2. Case description

The simulations were performed in forced convection for the following hypothesis and boundary conditions:

- channel geometry: 2,8m height, 2 m width and 0,45m channel thickness (fig.1);
- exterior glazing: 2,8m height, 2 m width;
- interior glazing: 1.85m height, 2 m width.

The façade channel is subjected to a uniform solar flux on the external glazing which is refracted to the interior one:

- constant heat flux density of solar radiation on the exterior glazing: $\varphi_e = 56 \text{ W/m}^2$;
- constant heat flux density of solar radiation on the interior glazing: $\varphi_i = 45 \text{ W/m}^2$;
- air temperature at inlet section of the channel corresponding to the cold season: $T_e = -18^\circ\text{C}$;
- velocity at inlet section of the channel: $v_i = 0,1\text{m/s}$, $0,3\text{m/s}$ and $0,5\text{m/s}$ (table1);

Table 1

Velocity \ Cases	1	2	3
v_i (m/s)	0,1	0,3	0,5

The influence of different flow velocities on the heat transfer inside a ventilated façade

- air supply ventilation mode (ascendant air circulation between exterior inlet and interior outlet sections).

3. Fluid Dynamic Modeling

The analysis was made using CFD software ANSYS-Fluent in turbulent flow using the $k-\epsilon$ RNG turbulence model and the control volume method in order to resolve the continuity, the momentum and the energy equations in the steady state on a three-dimensional model (fig. 2). Moreover, a uniform rectangular network of nodes was performed for fluid domain. The calculation is an iterative one, the chosen convergence criteria are 10^{-6} for the temperature and 10^{-4} for both the pressure and the velocities. The geometry and the mesh for channel were made with Ansys-DesignModeler.

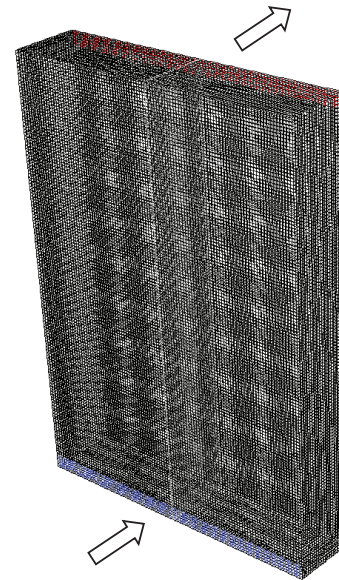
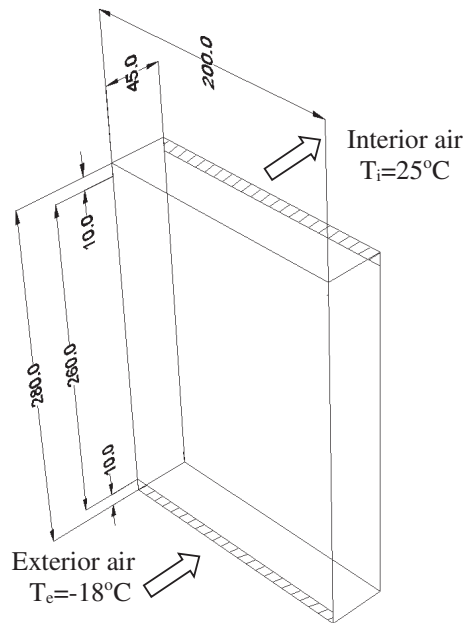


Fig. 1. The 3D configuration of air flow channel Fig. 2. The meshing of three-dimensional model

The obtained results show the temperature and the velocity profiles inside the channel (fig. 3-5), for different air velocities at the inlet section in order to evaluate the heat losses through the surface of the interior glazing.

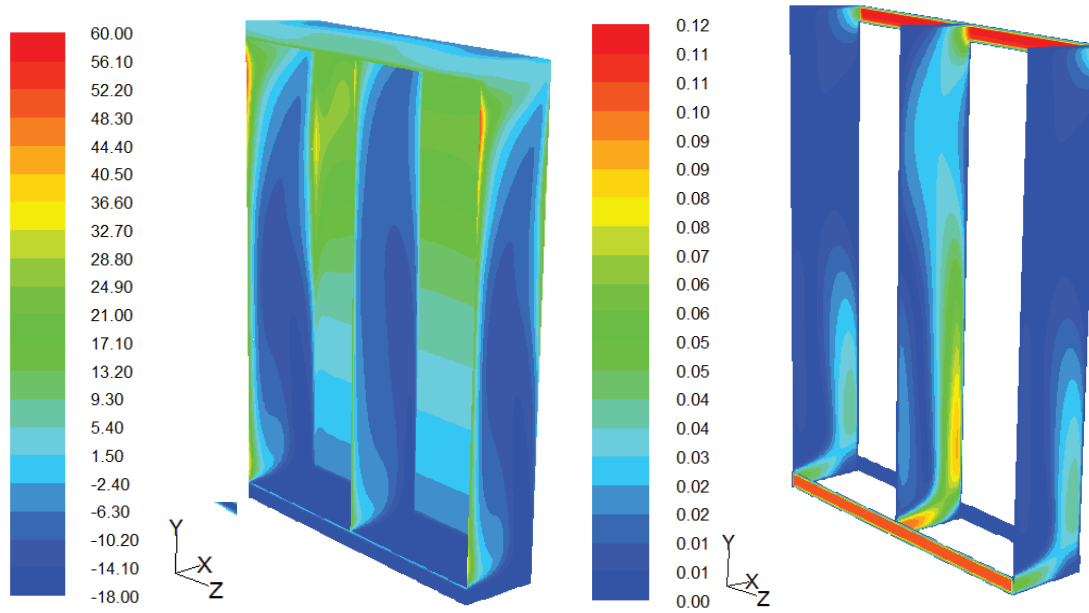


Fig. 3. Temperature and velocity fields inside the channel for case 1

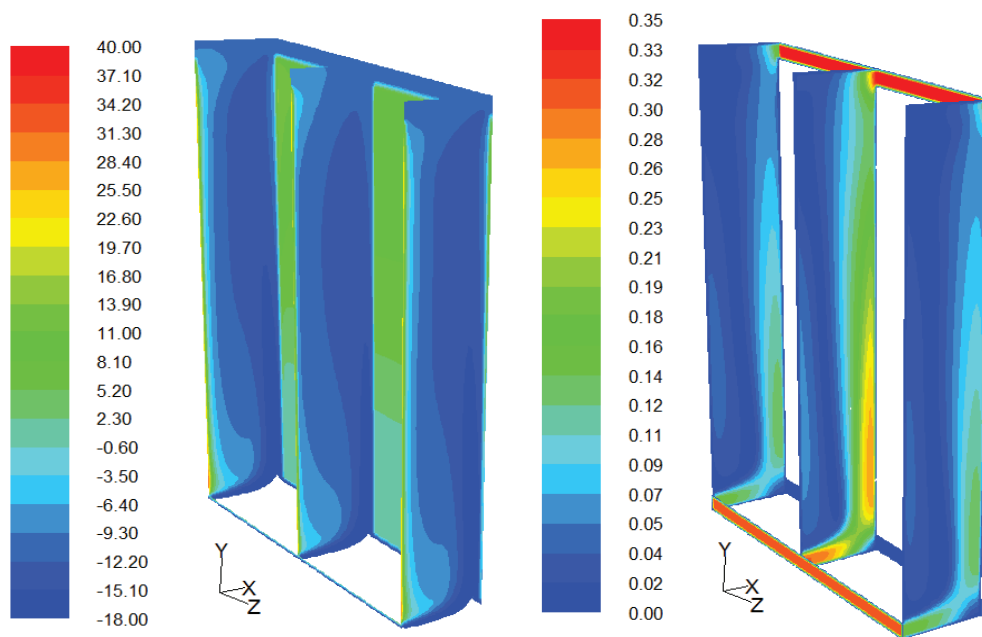


Fig. 4. Temperature and velocity fields inside the channel for case 2

The influence of different flow velocities on the heat transfer inside a ventilated façade

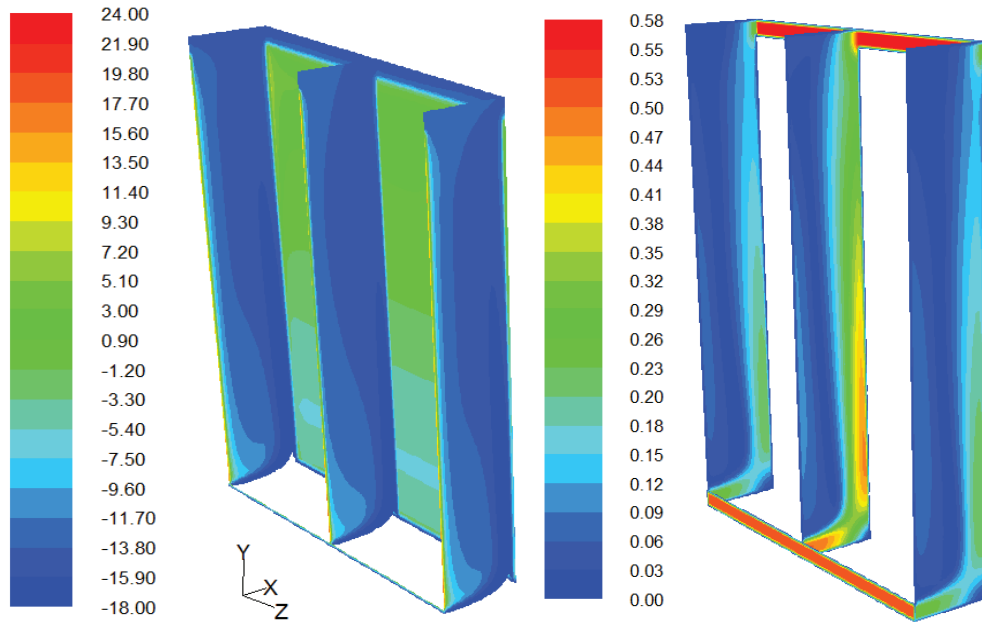


Fig. 5. Temperature and velocity fields inside the channel for case 3

The temperature and velocity profiles in median zone of the channel are presented in fig. 6 - 8 for the three cases.

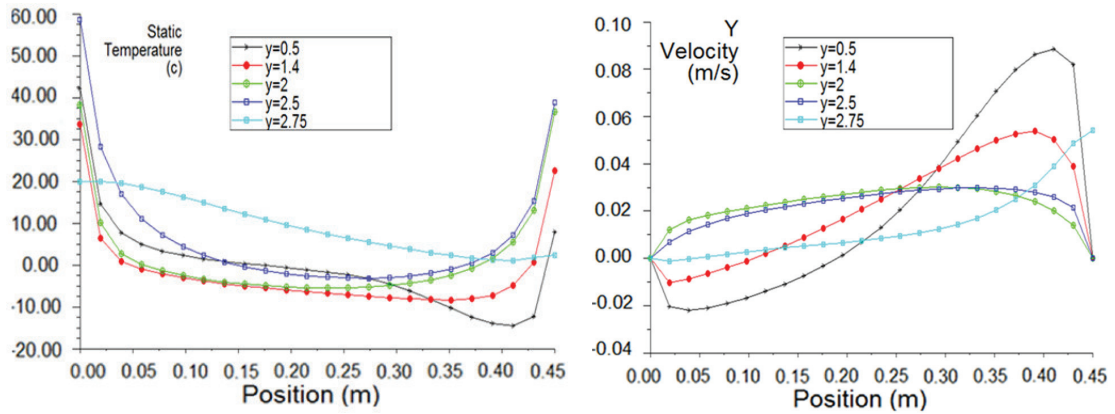


Fig. 6. Temperature and velocity profiles inside the channel for case 1

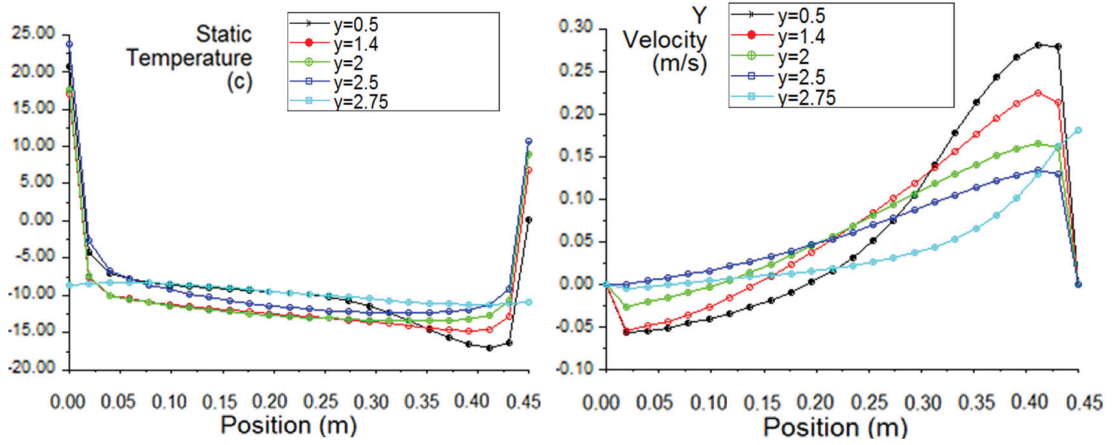


Fig. 7. Temperature and velocity profiles inside the channel for case 2

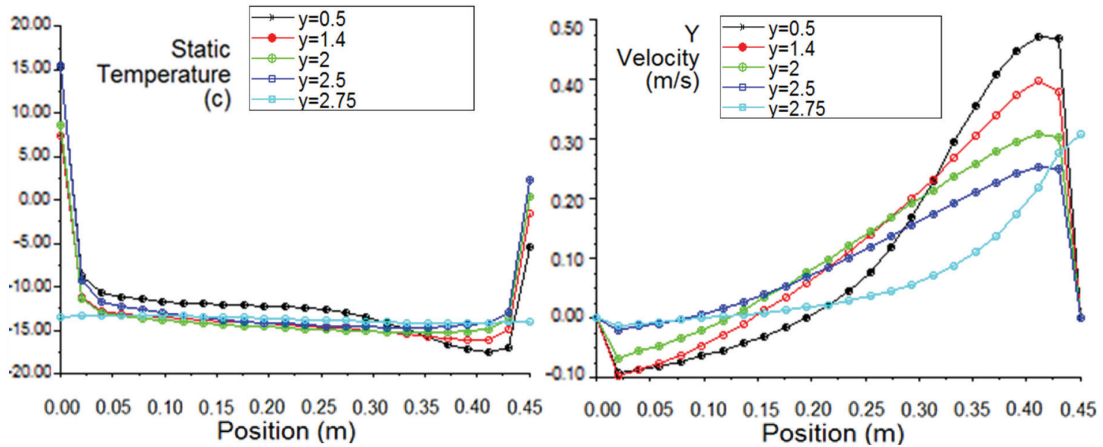


Fig. 8. Temperature and velocity profiles inside the channel for case 3

4. Results and discussion

In table 2, we evaluated the heat flux Q (W) (eq.1) transferred from interior chamber with temperature $T_i = 20^\circ\text{C}$ into the double skin channel, through the inner glass with properties: surface $S = 3,7 \text{ m}^2$ and thermal resistance $R = 0,6 \text{ m}^2\text{C}/\text{W}$ ($K=1/R$). The temperature of the air channel (T_c) was calculated from numerical simulations as averaged temperature (table 2). Thus, it was observed an increase of heat flux transferred through interior glazing (in terms of recovered heat) with increasing of the air flow velocity (table 2) due to the decrease in air temperature inside the channel.

$$Q = SK(T_i - T_c) \text{ (W)} \quad (1)$$

Table 2

Heat losses through the surface of the interior glazing			
	Case 1	Case 2	Case 3
	$v_i = 0,1$	$v_i = 0,3$	$v_i = 0,5$
T_c (°C)	-1,85	-11,39	-13,80
Q (W)	134,7	193,6	208,4

The numerical results obtained by iteration in ANSYS-Fluent software highlighted the velocities and temperatures profiles and the fluid recirculation phenomena near exterior glass inside the channel which increases with air velocity. (fig. 6-8). Also, it was observed an ascending flow inside the channel near the inner glass surface where velocities are higher values. Consequently, the values of air temperature are higher near the inner glass surface and lower near the exterior glass (fig. 3-5).

5. Conclusions

In this paper, numerical simulation of a double skin façade channel has been conducted in cold season in order to observe the influence of air velocity on the heat transfer through the interior glass surface. After analyzing the results it was found that the flow regime depends on the air velocity inside the channel and the solar flux on glazing. Thus, the spectrum of non-isothermal flows (including the velocity and the temperature) is characterized by the severe impact of the boundary conditions. The numerical simulations reveal that for lower velocities, the air temperature increases inside the channel and the heat losses decreases leading to better energy saving.

Finally, the CFD analyses are important tools to predict the behavior of these facades for the design processes, leading to more simulations in order to take into account different parameters and to propose optimal functional configuration.

Acknowledgement

We gratefully acknowledge the financial support of the Ministry of Regional Development and Public Administration through contract no. 493/2011.

References

- [1] *M. Perino et al.*, „State of the Art Review of Responsive Building Elements”, Volume 2A, International Energy Agency (IEA), 2008
- [2] *D. Saelens, J. Carmeliet, H. Hens*, „Energy performance assessment of multiple skin facades”, Int. Journal of HVAC&Research, vol. 9, no. 2, 2003, pp.167-186
- [3] *C. Balocco*, „A non-dimensional analysis of a ventilated double façade energy performance”, Energy and Buildings, vol. 36, 2004, pp. 35-40
- [4] *Y. Chiu, L. Shao*, „A parametric study of solar double skin façade on energy saving effect”, Proceedings of the 7th Clima 2001 World Congress, Napoli, Italy, 2001

- [5] *O. Kalyanova, P. Heiselberg, C. Felsman, H. Poirazis, P. Strachan*, „An empirical validation of building simulation software for modeling of double skin façade (DSF)”, Eleventh International IBPSA Conference Glasgow, Scotland, July 27-30, 2009, pp. 1107 – 1114
- [6] *H. Manz, A. Schaelin, H. Simmler*, „Airflow patterns and thermal behavior of mechanically ventilated glass facades”, *Building and Environment* 39, 2004, pp. 1023–1033
- [7] *H. Manz*, „Total solar energy transmittance of glass double facades with free convection”, *Energy and Buildings* 36, 2004, pp. 127–136
- [8] *A. Zoller, E.R.F. Winter, R. Viskanta*, „Experimental studies of combined heat transfer in turbulent mixed convection fluid flows in double-skin facades”, *International Journal of Heat and Mass Transfer* 45, 2002, pp. 4401–4408
- [9] *N. Safer, M. Woloszyn, J.J. Roux*, „Three-dimensional simulation with a CFD tool of the airflow phenomena in single floor double-skin façade equipped with a venetian blind”, *Solar Energy* 79, 2005, pp. 193-203
- [10] *D. Constantinescu*, „Contribuții la calculul și optimizarea sistemelor pasive și mixte de încălzire solară”, PhD Thesis, ICB, 1988.

Conception of a simplified seated thermal manikin for CFD validation purposes*

Angel Dogeanu¹, Bode Florin^{1,2}, Alexandru Iatan¹, Cristiana Croitoru¹, Ilinca Nastase¹

¹ CAMBI, Technical University of Civil Engineering in Bucharest, Building Services Department, 66 Avenue Pache Protopopescu, 020396, Bucharest, Romania,
E-mail: angel.dogeanu@cambi.ro, cristiana.croitoru@cambi.ro,

²Technical University Of Cluj-Napoca, Mechanical Engineering Department, 103-105 Muncii , D03, Cluj-Napoca, Romania
E-mail: florin.bode@termo.utcluj.ro

Rezumat. *Aceasta lucrare prezinta unul dintre cele cinci prototipuri de manechine termice concepute la Facultatea de Inginerie a Instalatiilor de la Universitatea Tehnica de Constructii. Acest prototip a fost conceput pentru a avea o forma simplificata cu unghiuri drepte pentru validarea modelelor numerice în cadrul unor studii de tip CFD. Toate testele sunt coerente si indica posibilitatea utilizarii acestui prototip în cadrul unor studii viitoare. Modelul este funcțional si temperatura fiecărei zone a corpului poate fi usor modificata în conformitate conditiile la limita dorite de utilizator. Forma geometrica a manechinului are un rol important în generarea curgerilor convective din jurul lui, de aceea acest prototip nu este potrivit pentru studii experimentale de rezolutie fina a micro-climatului corpului uman. El poate fi utilizat în cadrul unor studii globale de confort atât pentru cladiri cât si pentru vehicule.*

Cuvinte cheie: manechin termic, confort termic, validare CFD

Abstract. *This paper is presenting one among the five prototypes of thermal manikins conceived at the Building Services Faculty (Thermal-Hydraulic Systems Laboratory) at the Technical University of Civil Engineering. This particular prototype was chosen to have a simplified square angled shape in order to be used for validation in CFD studies. We designed a seated thermal manikin that can simulate the human presence in a room. All the tests are coherent and this manikin can be further used to validate our CFD models. The model is fully functional and the temperatures of each body zone can be easily modified in accordance to our needs. The shape have an important role in the air movement o around the human body and this manikin is not suitable for local and high resolution measurements around the human body but can be used for global measurement in a room or inside a vehicle.*

Key words: thermal manikin, thermal comfort, CFD validation

1. Introduction

Thermal manikins were used for more than 70 years. At the beginning they were used for testing clothing for soldiers by the US Army [1]. The shape and heating system were very simple at that stage. Since then the shape and complexity of the thermal manikin raised and start to approach the complexity of the human body. The number of independently controlled zones increased from a single zone corresponding to the entire surface up to 120 individually controlled zones [2]. The material used for developing the thermal manikin have diversified, from copper to plastic and carbon fiber to skin like silicon. If at the beginning the purpose of the thermal manikin was limited to clothing testing, in time, the range of applications become wider. The use of thermal manikin in the field of thermal comfort research become more and more active. The technology used to create thermal manikin had different approach. Most of them try to simulate the human body and the heat emission in the environment, while others are more or less complex measurement devices for assessing thermal environment quality by simulating the human body thermal regulation mechanisms and measuring its heat loss towards its environment [1]. The most advanced of them can also simulate body sweating and heat exchange through evaporation [1-4].

This paper is presenting one among the five prototypes of thermal manikins conceived at the Building Services Faculty (Thermal-Hydraulic Systems Laboratory) at the Technical University of Civil Engineering. This particular prototype was chosen to have a simplified square angled shape in order to be used for validation in CFD studies. Further evaluations of the importance of the shape in modelling hypothesis were also taken into account when the manikin was designed.

2. Building the manikin

The thermal manikin was designed in a seated position and is divided in 9 body parts (head, neck and shoulders, two hands, upper leg, lower leg, torso, back, seat) as displayed in Fig. 1 The size of the manikin is a standard human size with a total surface of 1.8mp (Fig.2). The base structure of the manikin was manufactured from extruded polystyrene. The body parts were welded with polyurethane foam and screws.

Conception of a simplified seated thermal manikin for CFD validation purposes

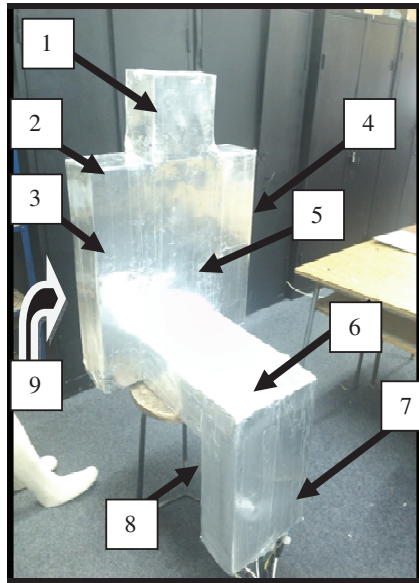


Fig.1 – Independent controlled body parts. 1 – Head; 2 – shoulders; 3,4 – Right/Left hand; 5 – torso; 6- upper legs; 7 – lower legs; 8 – seated part; 9 – back);

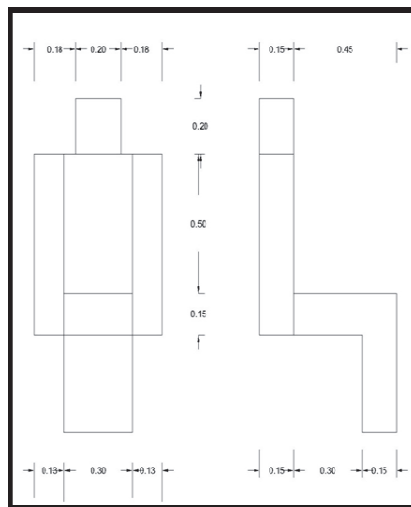


Fig.2 – Dimensions of the manikin



Fig. 3 a) Photograph of the heating film used for the thermal manikin, b) Sketch of the composition of the heated film.

Several types of films from different producers were tested. During these tests heating film from one of the manufacturers was found to produce non uniform surface temperature distribution, with a gradient of 7°C on across its width of 30cm (Fig. 4).

The heating film patches were placed on the polystyrene base using with double side adhesive tape. After covering a body zone the electrical connections and circuits were created. Every electrical connection was tested for leakage for safety reasons. The electrical wire was embedded in the polystyrene basis. In order to ensure that the thermal load of the film mounted over the wires is not influencing the cable stability we selected special wire that works at temperatures above 70grd .

During a preliminary test, without any control of the circuits, the temperature of each zone stabilized at 45°C when the room temperature was stable at $^{\circ}\text{C}$, a rather encouraging result offering a wide range to control the temperature of each zone and the possibility to simulate different cases of body heat release.

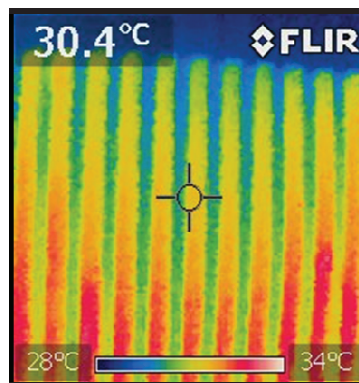


Fig. 4 Problematic surface temperature on one of the tested heating films

Using this kind of heating element has also some disadvantages. Because of the space between the electrical elements (i.e. carbon film stripes – see Fig. 3) it appear a zebra phenomenon, an alternation of hot– cold stripes and therefore an non-uniform temperature of the surface, phenomenon that need to be avoided [5]. As a solution we decide to cover the entire manikin surface with adhesive aluminium foil to ensure enhanced conduction heat transfer and thus better surface temperature uniformity. Finally, in order to facilitate further investigations with a thermal (IR) camera the entire manikin surface was covered with light black textile.

3. Electrical power consumption

In order to validate the manikin prototype we performed several tests.

a) Infrared surface temperature

For this test we used an infrared camera FLIR E60. The air temperature was stable at 26°C. Each zone was electrically powered. The surface temperature control of each zone was performed using a dedicated electrical dimmer (Fig.5). The temperature for each body zone was set using the measurements with IR camera and contact sensors and compared with human body temperature and with literature. Given that the air temperature of the room was constant and considering the simulated activity of the human body reaching the desired zone temperature was easy to reach and was similar to human body in the same conditions (fig.6).



Fig 5. Electrical dimmer installed on every circuit.

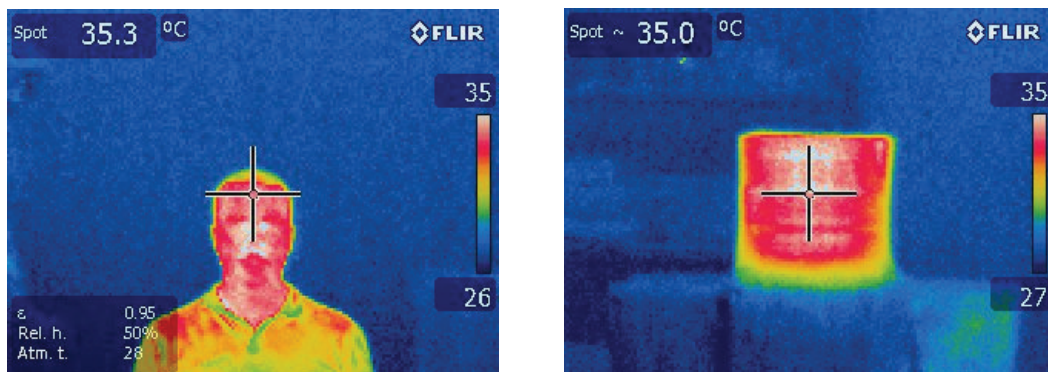


Fig. 6a. Comparing the surface temperature of the human body and of the thermal manikin using the IR camera

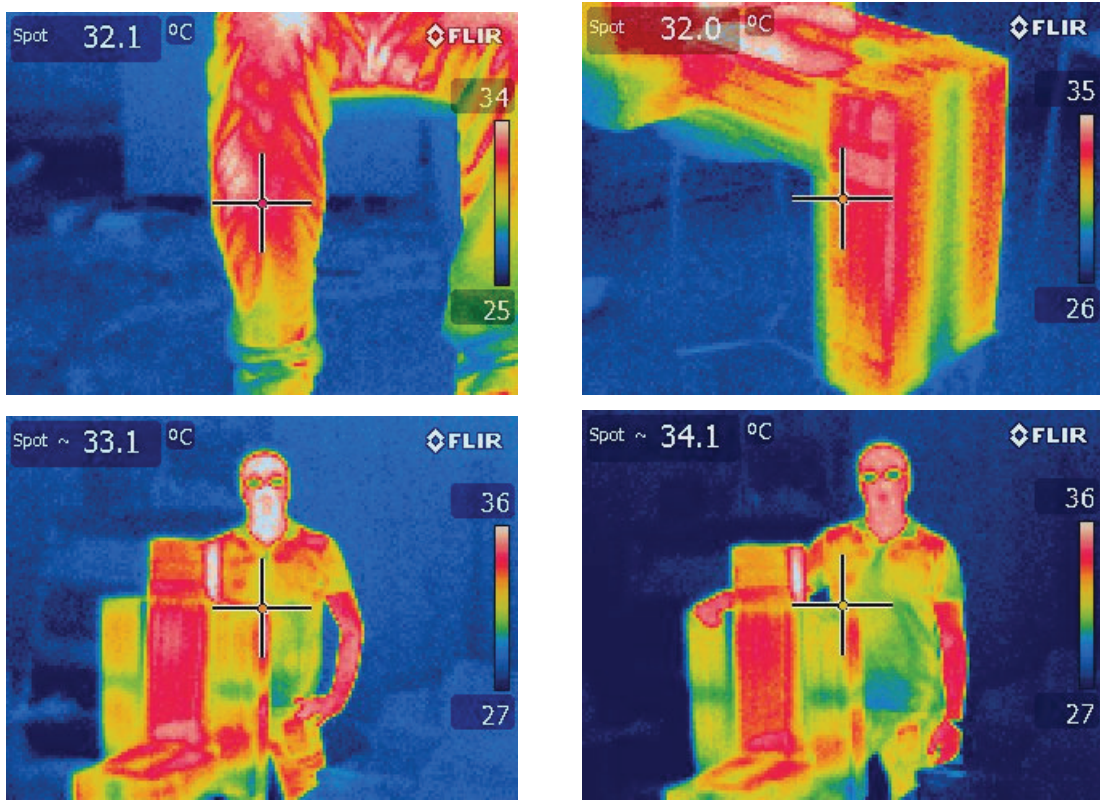


Fig. 6b. Comparing the surface temperature of the human body and of the thermal manikin using the IR camera

b) Contact temperature sensors

In order to eliminate eventual errors introduced by the IR camera calibration we used contact thermal sensors [6]. For each zone we used two sensors to measure the temperature uniformity of the surface. In Table 1 we centralized the temperature measured with the contact sensors on every thermal zone. The thermometer used was a Lutron device model TM939 type with 2 thermocouples of type J (fig.7).



Fig 7. Thermometer TM 946 with contact sensor

c) Electrical power consumption

The electrical power is the only power source that is converted in heat 100%. We aimed to measure the electrical consumption of the thermal manikin [1]. In order to do this we used an EU socket wattmeter (fig.8). We measured the power consumed by the wattmeter without any consumer and found that it consume 2W running without connecting any power consuming source. In table 2 we centralized the power consumed by every circuit of heating film. As a design condition the manikin surface is 1.8m² which is the equivalent surface of standardized human body [6]. After the electrical power measurements we find the power generated by the thermal manikin to have a coherent value equal with the dry heat generated by a human body in the sitting position, performing office activity.



Fig.8 – Employed wattmeter

Table 1 – Measured surface temperature with the contact sensors

Zone/temp	Right down		Left down		Left up		Right up	
Shoulders	34.5	32.6	33.5	33.5	35	35.1	34.2	34.4
Head	Face		Top of the head				Neck	
	34.1	33.9	34.3	33.7	33.8	33.8	34.2	34.5
Torso front	Right down		Left down		Left up		Right up	
	32.7		33.1		33.4		32.2	
Torso back	Right down		Left down		Left up		Right up	
	33.1		33.4		32.6		32.2	
Upper legs	Right down		Left down		Left up		Right up	
	32		31.6		32		32.2	
Lower legs	Right down		Left down		Left up		Right up	
	32		32.1		32		30.6	
Left hand	Front		Lateral		back			
	33.1	32.8	32	32.4	32	32.2		
Left hand	Front		Lateral		back			
Right hand	32	32.5	32.9	32.7	33.2	32.1		

Table 2 – electrical power consumed on each circuit

Zone	Head	Torso front	Torso back	Left Hand	Right Hand	Upper legs	Lower legs	Shoulders	Total [W]
Power[W]	6	8	9	10	12	9	18	9	81

4. Convective flow around manikin around the manikin

We wanted to check also the convective flow around the body of the manikin using IR measurement following a method described in [7]. The measurements show that the natural thermal flow around our manikin body (fig.10) is not completely similar to the one generated by a humanoid shaped thermal manikin. However this was not the primary goal in manufacturing this prototype. The thermal plume was expected to be not similar with the one produced by with a thermal manikin with anatomic shape given our previous CFD studies [7] (Fig 10).

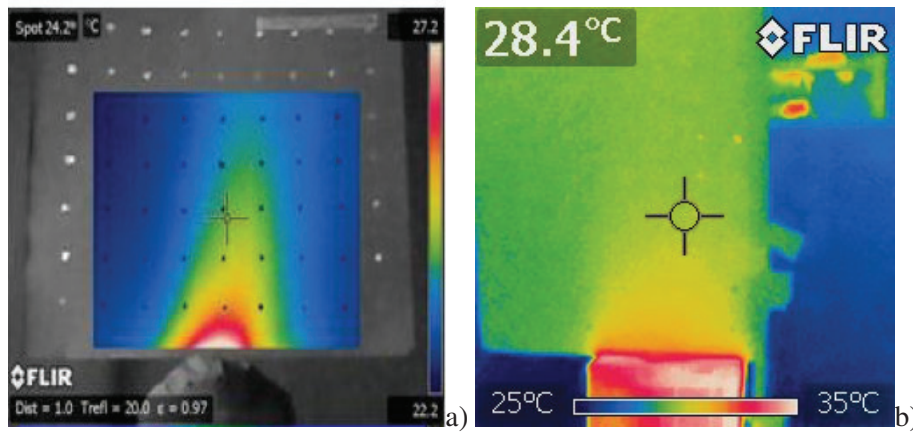


Fig. 9 – a) Convective plume of a humanoid shape thermal manikin [7], b) Fig 9 – b) Convective plume of our manikin

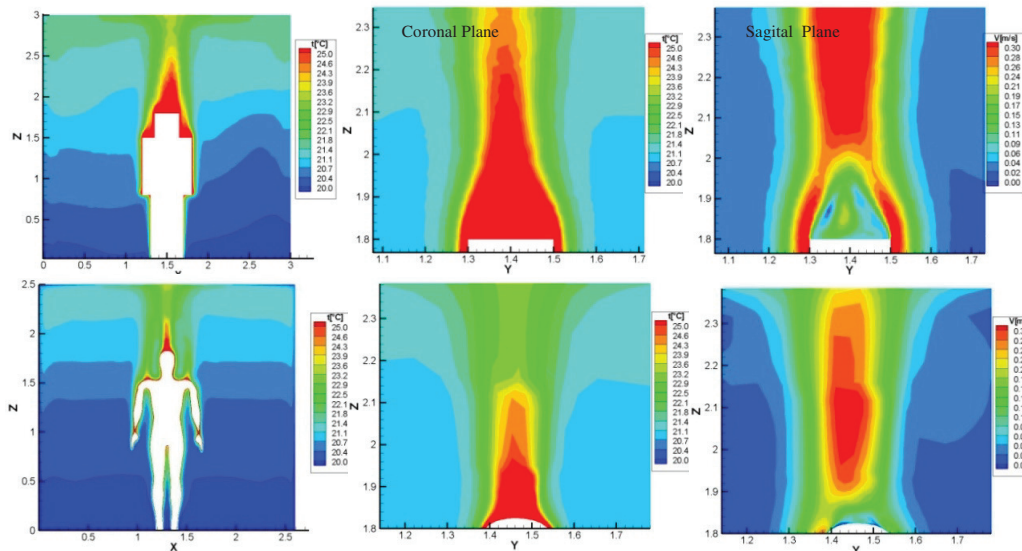


Fig. 10 – Comparison between the temperature distributions in the convective plume of a simplified and of an anatomic model of human body. CFD results from our previous study [7]

5. Conclusions

Our goal was met and we manage to create a sitting thermal manikin that can simulate the human presence in a room. All the tests are coherent and this manikin can be further used to validate our CFD models. The model is fully functional and the temperatures of each body zone can be easily modified in accordance to our needs. The shape have an important role in the air movement of the air around the human body and this manikin is not suitable for local and high resolution measurements around the human body but can be used for global measurement in a room or inside a vehicle.

6. References

1. Holmér, I., Thermal manikin history and applications. *European Journal of Applied Physiology*, 2004. **92** p. 614-618.
2. Rugh, J.P. and D. Bharathan. Predicting Human Thermal Comfort in Automobiles in Vehicle Thermal Management Systems Conference and Exhibition,. 2005. Toronto, Canada
3. Alahmer, A., et al., Vehicular thermal comfort models; a comprehensive review. *Applied Thermal Engineering*, 2011. **31**(6–7): p. 995-1002.
4. Sakoi, T., et al., Thermal comfort, skin temperature distribution, and sensible heat loss distribution in the sitting posture in various asymmetric radiant fields. *Building and Environment*, 2007. **42**(12): p. 3984-3999.
5. Melikov, A.K., Breathing thermal manikins for indoor environment assessment: important characteristics and requirements. *European Journal of Applied Physiology*, 2004. **92**(6): p. 710-713.
6. Wang, J. and E. Hihara, Human body surface area: a theoretical approach. *European Journal of Applied Physiology*, 2004. **91**: p. 425-428.
7. Croitoru, C., I. Nastase, and F. Bode, The Influence of the Geometric Form of the Virtual Thermal Manikin on Convective Flow. *Mathematical Modelling*, 2011. **7**(4).

Experimental and theoretical study regarding the thermal performances of the heat exchangers with steel panels and extended surfaces

Anica Ilie¹, Răzvan Calotă²

^{1,2}Technical University of Civil Engineering,
66, Pache Protopopescu Bd., Bucharest, Romania
e-mail: anica_59@yahoo.com; razvan.calota@yahoo.com

Abstract: *The present paper refers to the thermal performances of the heat exchangers with steel panels, used in the buildings' heating installations. The heat exchanger was set up in a thermostatic test room, built in conformity with SR EN 442-2:2002/A2:2004 and was tested in standard functioning conditions. The experimental were compared with those obtained by applying the correlations that characterize the heat transfer for the flow of liquids through narrow vertical spaces and the flow of air by natural convection in different situations.*

Keywords: heat exchanger; thermal performances

Nomenclature			
c_p	specific heat capacity, [kJ/kgK]	<i>Greek letters</i>	
D_h	hydraulic diameter, [m]		
Gr	Grashof adimensional criteria	α	convective coef. [W/m ² K]
k	global heat transfer, [W/m ² K]	ε	emissivity [-]
L	length [m]	λ	conductivity coef. [W/mK]
\dot{m}	water flow, [kg/s]	ρ	water density [kg/m ³]
Nu	Nusselt adimensional criteria	ν	kinematic viscosity [m ² /s]
Pr	Prandtl adimensional criteria	σ	Stefan-Boltzmann constant
Re	Reynolds adimensional criteria	δ	thickness [m]
\dot{Q}	heat flux, [W]		
$S_{transfer}$	heat transfer surface, [-]	<i>Subscripts</i>	
S	flowing section, [m ²]		
w	water velocity, [m/s]	w	water

1. Introduction

Radiators are part of the family of heat exchangers used for living spaces heating. These can be made in several variants and by using different materials of which the most common are steel, cast iron, and aluminum. Among all types of heaters, the most currently used are the steel panels.

The authors analyze how heat transfer occurs from the surface of a radiator to the environment air, using relationships Criteria and ultimately determining the heat flux transmitted. The tested radiator is a steel panels type PKKP 1000x600 mm with the following dimensional characteristics measured and calculated by the authors.

- The hydraulic diameter of the flow of the water through vertical channels is 0.0138 m;
- Total heat transfer surface, corresponding to a length of 1 m, is 6.1 m², of which 2,564 m² is the panels' surface (4 x 0.641 m²) and 3.54 m² is represented by the extended surface;
- Hexagonal section flow of the heating water is 0.000183 m². In total, an 1 m radiator has 54 such sections flow, resulting a total flow section of 0.009882 m².

The total heat transfer area is the sum of the exterior surface of the panel and the total area of the extended surfaces corresponding to an 1 m radiator length.

The outer surface of the panel resulted by applying a finning coefficient given by the producer to the value of the plane surface of the panel.

Extended surface area was calculated as the product of length corresponding to 1 m linear radiator and its height. The measured height of the sheet forming the extended surface has a value of 0.4 m from the total radiator's total height of 0.6 m.

Experimental research in order to determine the thermal power of the radiator were held in a specially thermostatic test room built in the Laboratory of Thermotechnics from Technical University of Civil Engineering, Bucharest.

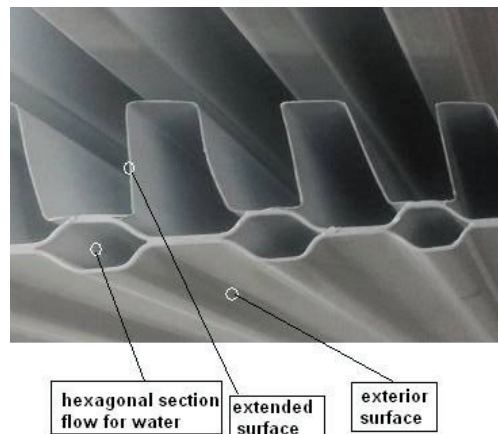


Figure 1. Hexagonal sections of the heat flow

The testing room was built in accordance with European Standard EN 442-2 for the experimental determination of heat power of radiators and convectors.

2. Experimental study for the determination of radiator's heat power

2.1 Experimental stand

The test room is an unventilated space where the tested radiator was mounted. The walls, ceiling and floor of this room are made of sandwich panels containing a copper coil $\Phi 12 \times 1$. Inside this coil circulates cooling water as a medium to stabilize the room internal temperature regardless of the heat generated inside and regardless of the temperature outside the room. Cooling water is circulated by a group of five pumps located on the top of the test chamber. Schematically, the camera is shown in Figure 2.

Air temperature in the test chamber is maintained at 20 ± 0.5 °C by adjusting the parameters (flow and temperature) of the cooling water that circulates through coils in the walls of the test chamber. Room air temperature is measured with thermocouples NiCr-Ni, type T190-0 in 4 points on the vertical axis located in the geometric center of the room.

The circulating fluid through the radiator is hot water, prepared in a boiler that feeds a tank first and then by freefall the tested radiator. This mode is used for maintaining constant the hot water flow and is a standard requirement.

To adjust the hot water temperature, an electrical resistance heater is provided into the tank, which start in steps, depending on the water temperature. Heat flow is measured by a Corriollis flowmeter mounted at the output of the radiator heating circuit. Water temperature at the inlet and the outlet of the radiator is measured by two Pt100 temperature sensors.

Radiator surface temperature was determined as an average of 12 thermocouples indications, mounted at equal distances.

Temperature of the air inside the radiator was determined as an average of the medium of five thermocouples mounted on the top of the radiator and the test chamber air temperature at the enter on the bottom of the radiator.

Sensors to measure air and water temperature were connected to a data acquisition device.

The experiments were carried out to an average temperature of the hot water at about 70 °C (water temperature at the radiator inlet: 75 °C and the water temperature at the exit of the radiator: 65 °C) and the temperature of the air in the test chamber at about 20 °C. In Figure 1 it can be seen the feeding scheme of the coils inside the chamber walls and the radiator mount mode for testing.

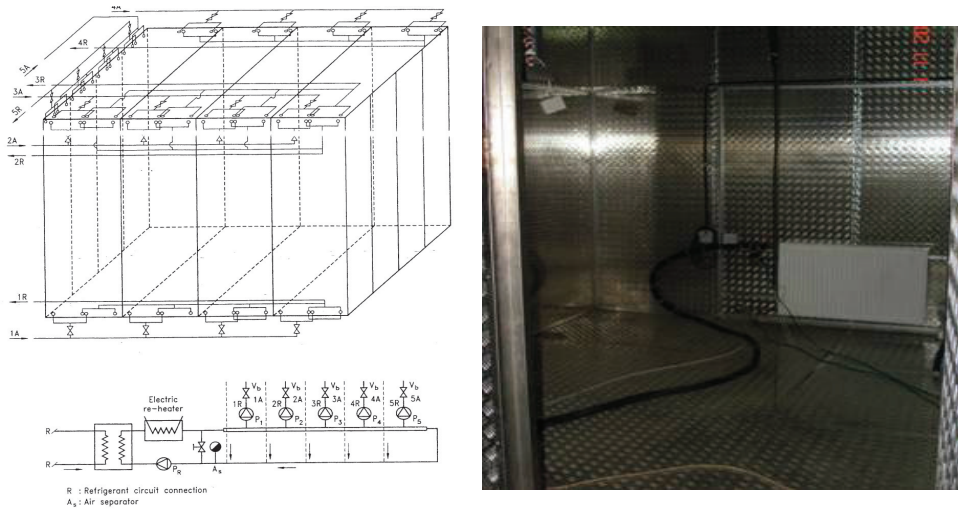


Figure 2. Test chamber scheme

2.2 The testing methodology

Measurements for the determination of the heat power were made after installation of a quasi-stationary regime of operation.

It was considered that the quasi-stationary operating regime is installed when:

- Temperature of water flow and the test chamber air temperature did not vary during 30 minutes with more than ± 0.1 K;
- Water flow did not vary during 30 minutes with more than $\pm 1\%$.

2.3 Results obtained by direct measurement

In Table 1 are presented the measured values of the parameters of interest, after installing the quasi-stationary regime.

Table 1

Date and hour of the test	H.E. type	Testing room temp. [°C]	Water Flow [kg/s]	Air medium temp. at the exit from the H.E. [°C]	Inlet water temp. [°C]	Outlet water temp. [°C]	H.E. surface medium temperature [°C]
30.05.13 10:06	0.6 x 1 m	20.5	0.0298	43.1	75.5	65	69.3
30.05.13 10:16	0.6 x 1 m	20.5	0.0298	43.2	75.4	64.9	69.2
30.05.13 10:26	0.6 x 1 m	20.4	0.0298	43.1	75.5	65	69.2
30.05.13 10:36	0.6 x 1 m	20.4	0.0298	43.1	75.5	64.9	69.2
30.05.13 10:46	0.6 x 1 m	20.4	0.0298	43.2	75.6	64.9	69.3

3. Theoretic study for determination of thermal power of the radiator

Theoretical study sought to determine the heat power of a radiator with geometric and functional characteristics of corresponding test criteria.

3.1 Methodology

The input data for theoretical study are the measured values of water flow and medium temperature (hot water and room air).

Using the equation of continuity and having known volume flow and flow section we could determine the speed of the water inside the hexagonal channels of the radiator. Reynolds criteria values obtained indicates that the flow is laminar.

3.2. Calculation of the heat flow

Heat transfer in the case studied is complex. Thus we have 3 situations:

- **From the front panel of the radiator to the test chamber air- free convection and radiation in large spaces;**

- *The water heat convection coefficient*

For water flow in canals and pipelines we have the following relationship, [1]:

$$Nu = 3.66 + \frac{0.065 \cdot (D/L) \cdot Re \cdot Pr}{1 + 0.04 \cdot [(D/L) \cdot Re \cdot Pr]^{2/3}} \quad (1)$$

It will be used the thermophysical properties of water at a temperature of 70.2 ° C calculated as an average between the inlet and outlet of the radiator.

In order to determine the dimensionless Reynolds criteria, velocity of water in the radiator is obtained from the equation of continuity, depending on the mass flow rate, flow section and density of water at ambient temperature.

$$w = \frac{\dot{m}}{S \cdot \rho} = \frac{0,0298}{0,009882 \cdot 974,8} = 0,0031 m/s \quad (2)$$

$$Re = \frac{w \cdot l_c}{\nu} = \frac{w \cdot D_h}{\nu} = \frac{0,0031 \cdot 0,0138}{0,39 \cdot 10^{-6}} = 109,7 \quad (3)$$

$$Nu = 3.66 + \frac{0.065 \cdot (D/L) \cdot Re \cdot Pr}{1 + 0.04 \cdot [(D/L) \cdot Re \cdot Pr]^{2/3}} = 4.005 \quad (4)$$

With this value known we can determine the coefficient of heat transfer from the water.

$$Nu = \frac{\alpha_1 \cdot l_c}{\lambda} \Rightarrow \alpha_1 = \frac{Nu \cdot \lambda}{D_h} = \frac{4.005 \cdot 0.671}{0.0138} = 194.74 \text{ W / m}^2 \text{ K} \quad (5)$$

- *The heat transfer coefficient from the air*

The free convection flow regime type is determined by the product $Gr \cdot Pr$.

The medium temperature has a value of 44.9 °C, given by the average surface temperature of the radiator and the air temperature inside the test chamber. Depending on the temperature we could determine the physical properties of air.

Characteristic length is given by the dimension in the direction of air flow, respectively the radiator height of 0.6 m

$$Gr \cdot Pr = \beta \cdot \frac{g \cdot l_c^3}{\nu^2} \cdot \Delta T \cdot \frac{\nu}{a}; \quad \beta = \frac{1}{T_m} = \frac{1}{318.05} \quad (6)$$

$$Gr \cdot Pr = 3.67 \cdot 10^8 > 2 \cdot 10^7 \quad (7)$$

According to the obtained results, the air flow regime is turbulent one.

In calculating the heat transfer coefficient by convection was chosen an appropriate criteria equation corresponding to a free convection for a vertical plate in turbulent flow. We use the following equation given by Miheev.

$$Nu = 0,135 \cdot (Gr \cdot Pr)^{0,33} = 90.5 \quad (8)$$

$$Nu = \frac{\alpha \cdot l_c}{\lambda} \Rightarrow \alpha_2 = \frac{Nu \cdot \lambda}{h} = 4.18 \text{ W / m}^2 \text{ K} \quad (9)$$

The heat transfer from the hot water to the air in the test chamber takes place simultaneously by convection and radiation, and therefore it will be calculated also the heat transfer coefficient of radiation from the radiator surface to the air.

Coefficient of heat transfer by radiation is determined by the empirical relationship, [1]:

$$\alpha_3 = \varepsilon \cdot \sigma_0 \cdot \frac{T_s^4 - T_{aer}^4}{T_s - T_{aer}} = 6.92 \text{ W / m}^2 \text{ K} \quad (10)$$

The overall coefficient of heat transfer from the radiator to the air in the room will be:

$$\alpha_{total} = \alpha_2 + \alpha_3 = 11.1 \text{ W / m}^2 \text{ K} \quad (11)$$

The heat flux transferred in this specific case will be:

$$\dot{Q}_1 = \alpha \cdot S \cdot \Delta t = 11.1 \cdot 0.641 \cdot 48.8 = 347.2 \text{ W} \quad (12)$$

- **From the front panel of the radiator placed towards the wall of the test chamber, to the air**

We have free convection and radiation in limited spaces between flat wall surface of the radiator and indoor air.

In order to determine the convective heat transfer coefficient will be used Berkovska relations referring to free convection in space bounded by two plates of different temperatures. This relationship is valid for $Pr < 10$ and $Gr \cdot Pr < 10^{10}$, [3]. Characteristic length is considered to be the height of the radiator face, along which there is air circulation.

$$\overline{Nu}_\delta = 0.22 \cdot \left(\frac{L}{\delta}\right)^{-1/4} \cdot \left(\frac{Pr}{0.2 + Pr} \cdot Gr \cdot Pr\right)^{0.28} = 73.87 \quad (13)$$

Using thermophysical properties of air at average ambient temperature we could determine convective heat transfer coefficient:

$$\overline{Nu}_\delta = \frac{\bar{\alpha} \cdot l_c}{\lambda} \Rightarrow \alpha_4 = \frac{\overline{Nu}_\delta \cdot \lambda}{h} = 3.398 \text{ W / m}^2 \text{ K} \quad (14)$$

The heat flux transferred in this case is:

$$\dot{Q}_{2,cv} = \alpha_4 \cdot S \cdot \Delta t = 3.398 \cdot 0.641 \cdot 48.8 = 106.3 \text{ W} \quad (15)$$

To analyze the flow component related to radiation, we consider flux transmitted to be equal to the heat flow exchanged by radiation between two parallel walls, [4].

$$\dot{Q}_{2,rad} = \varepsilon \cdot \varphi \cdot S \cdot C_0 \cdot \left[\left(\frac{T_{S1}}{100}\right)^4 - \left(\frac{T_{S2}}{100}\right)^4 \right] = 133.09 \text{ W} \quad (16)$$

The reduced emissivity is depending on the emissivities of the two surfaces which exchange heat by radiation. Emissivity of the steel sheet, has a value of 0.95, and the emissivity value of stainless steel sheet from which is made the test chamber wall has a value of 0.75. For the reduced emissivity result a value of $\varepsilon = 0.58$.

We make the simplifying assumption that the factor of mutual irradiation has value $\varphi = 1$ for the two flat parallel surfaces.

Finally, the total flux transmitted to the air is calculated as a sum of convective and radiative component.

$$\dot{Q}_2 = \dot{Q}_{2,cv} + \dot{Q}_{2,rad} = 239.4 \text{ W} \quad (17)$$

- **From the inner sides of the radiator and extended surface to the air that circulates through the inside of the radiator**

We have heat transfer by conduction through extended surfaces between the inner walls of the radiator and extended surface, heat transfer by free convection between the radiator inner flat walls including extended surface, and air;

- *Determining the plane inner surface of the radiator*

To determine the plane surface of the radiator in contact with indoor air will be subtracted from the total area of the inner face of the radiator surface the area occupied by the base of the extended surface, which have a thickness of 0.5 mm.

$$S_{plane} = S_{tot} - S_{base,ext.surfaces} = 1.282 - 0.5 \cdot 10^{-3} \cdot 0.4 \cdot 54 \cdot 2 = 1.271 m^2 \quad (18)$$

The total area of the extended surface in contact with air is $S_{ext.surfaces} = 3.542 m^2$.

- *The total heat flux transferred in this case*

$$\dot{Q}_3 = \dot{Q}_{plane,surfaces} + \dot{Q}_{ext,surfaces} \quad (19)$$

Initially, we calculate the heat flux transmitted to the air inside the radiator, without considering the extended surface. Flux transmitted by the inner plane surface of the radiator is determined by the average surface temperature and the air inside the radiator's temperature measured as a media between inlet and outlet from radiator, 31.8 °C.

Coefficient of heat transfer by convection is determined by applying the same methodology as the first point, because the distance between the two radiator panels is large enough to no longer stay within limited space situation. It results a total convection heat transfer coefficient: $\alpha_{4,cv} = 4,15 W / m^2 K$

$$\dot{Q}_4 = \alpha_{4,cv} \cdot S \cdot \Delta t_{int} = 4.15 \cdot 0.641 \cdot 2 \cdot 37.5 = 199.51 W \quad (20)$$

The purpose of this calculation is to demonstrate further the usefulness of applying extended surfaces.

Next, using the above data, it will be determined the heat flux transmitted through the inner plane surface of the radiator where it is applied the base of the extended surfaces.

$$\dot{Q}_{plane,surfaces} = \alpha_{4,cv} \cdot S_{plane} \cdot \Delta t_{int} = 4.15 \cdot 1.271 \cdot 37.5 = 197.8 W \quad (21)$$

To obtain the heat flux transmitted through extended surface we calculate the average temperature of the sheet from which is made that area. Since U-shaped extended surface has a total length of 0.082 m, to simplify the calculation we will consider it composed of two rectangular fins of equal length joined at an end, and will determine the temperature at mid, which we will consider further the medium temperature of the extended surfaces.

$$t(x) = t_f + (t_0 - t_f) \frac{\cosh m \cdot (L - x) + \frac{\alpha}{\lambda_{OL} \cdot m} \sinh m \cdot (L - x)}{\cosh m \cdot L + \frac{\alpha}{\lambda_{OL} \cdot m} \sinh m \cdot L} \quad (22)$$

In this equation the factor m is calculated according to the area and perimeter of the fin section. After calculation resulted in a value $m = 19.5 \text{ [m}^{-1}\text{]}$. Distance x , for which the calculation is done at the mid of the fin was measured and has a value of 0.0205 m. It results an average extended surface temperature $t_{m, \text{ ext surface}} = 63.7 \text{ }^\circ\text{C}$.

The heat flux transmitted from the extended surface to the air inside the radiator will be:

$$\dot{Q}_{\text{ext, surface}} = \alpha_{\text{total, 2}} \cdot S_{\text{ext, surface}} \cdot \Delta t_{\text{ext surface-air}} = 4.15 \cdot 3.542 \cdot 31.9 = 468.91 \text{ W} \quad (23)$$

The total heat flux transmitted to the air from the interior of the testing room is calculated as a sum of the four components calculated above. It has a value of 1253 W.

4. Analysis of the results

The analysis of data obtained from mathematical modeling of heat transfer processes taking place between the body surface of the radiator and the air from testing room have highlighted the following:

- Heat transfer area of the radiator was calculated as a sum between the heating panel plane surface, corrected by a factor of finning and the extended surface area represented by the corrugated sheet. Note that the heat transfer surface grows about 2.4 times with this expansion;
- The coefficient of heat transfer from the radiator to the air in the enclosure is a complex one that takes into account both the coefficient of convection and radiation at the surface of the radiator to the air from the test chamber. Of the total heat transfer coefficient, 38% is the contribution of heat transfer by convection and the radiation contribution is represented by the remaining 62%;
- When considering the situation in which additional radiator area was not extended with corrugated sheet, we obtained a total heat flux transferred to the indoor

air with 37% down as compared to the situation when those extended surfaces would have been applied;

- The radiator heat power can be determined according to European Standard EN 442, [2], as the product of mass flow rate of the heating fluid, specific heat of water and the temperature difference between inlet and outlet of the water.

$$\dot{Q} = \dot{m} \cdot c_p \cdot \Delta t_w = 1310 \text{ W} \quad (24)$$

- By adding all the flows obtained from the mathematical modeling of the heat transfer processes we obtain a value with 57 W lower as compared to the application of the standard formula.

5. Conclusions

The study made in the present paper highlights the usefulness of extending the surface of heat transfer, the heat flux transmitted by this additional area representing 37% of the total flux transmitted in the analysed situation.

By comparing the result of the mathematical modelling with the value obtained for the total flux transmitted by the radiator surface to the air inside the testing room resulting from applying the formula given in the relevant European Standard for heaters, results a deviation of 4.3%, which is lower than that allowed in the literature. Thus, by applying appropriate formulas for each heat transfer situation, we get a validation of the standard calculation formula.

6. Bibliography

- [1] *ASHRAE Handbook- Fundamentals*, Ch. 4, 2009.
- [2] *SR EN 442:2-2002 Radiatoare si convectoare. Metode de incercare si evaluare.*
- [3] *Kreith F., Manglik R.- Principles of Heat Transfer*, Ch. 5, 2011, Cengage Learning Inc.
- [4] *Dumitrescu R., Chiriac F. – Lectii de termotehnica si transfer de caldura*, Ch.13, 2010, Editura Conspress

Consecințe energetice ale încălzirii intermitente a clădirilor

Energetic consequences of intermittent heating of buildings

Florin Iordache¹, Vlad Iordache²

¹Universitatea Tehnică de Construcții București
Facultatea de Inginerie a Instalațiilor
Bdul. Pache Protopopescu, 66, România
fliord@yahoo.com

²Universitatea Tehnică de Construcții București
Facultatea de Inginerie a Instalațiilor
Bdul. Pache Protopopescu, 66, România
viordach@yahoo.com

Rezumat: Reducerea consumului de energie în domeniul consumatorilor civili este un deziderat intens urmărit în contextul preocupărilor actuale europene și internaționale. Încalzirea spațiilor reprezintă un domeniu caracterizat de un consum considerabil de energie și preocuparea pentru reducerea acestora stă în atenția specializatorilor de pretutindeni. Adoptarea regimului de încălzire intermitentă în locul regimului de încălzire continuă poate fi o soluție în anumite situații arhitecturale constructive de clădiri. Lucrarea are ca obiectiv tocmai identificarea unor criterii de urmărit, utile în adoptarea regimului intermitent de încălzire în locul celui continuu, în vederea reducerii consumurilor energetice. Sunt vizati parametrii constructivi de natură termică cum ar fi rezistența termică medie și masivitatea clădirii. Se au de asemenea în vedere și capacitatea instalată a sistemului de încălzire care face apel la investițiile necesare alături de consumurile energetice.

Cuvinte cheie: reducere consum energie, încălzire intermitentă

Abstract: Reduction of energy consumption in the consumer civilians is a goal pursued extensively in European and international context of current concerns. Space heating is an area characterized by a considerable energy consumption and reduce their concern lies in attention specializatorilor everywhere. Adoption heating regime in place intermittent continuous heating regime can be a solution in some situations constructive architectural buildings. This paper aims to identify just watched criteria useful in adopting intermittent instead of continuous heating, to reduce energy consumption. It covers the nature of design parameters such as thermal resistance thermal medium and massive building. We have also taken into account the installed capacity of the heating system that appeals to the investments required with energy consumption.

Key words: reducing energy consumption, intermittent heating

1. Introducere

Obiectivul lucrării de față este cel de identificarea situațiilor în care este oportuna, din punct de vedere energetic, utilizarea programului intermitent de alimentare cu căldură a unei clădiri. De exemplu se considera ca o clădire caracterizată de o capacitate termică C și o rezistență termică R și având un program de utilizare a spațiilor interioare mai mic decât 24h, este profitabil din punct de vedere energetic să adopte un program de încălzire intermitent în locul programului de încălzire continuă. Concluziile acestui studiu vor fi influențate și de programul de intermitență necesar a fi adoptat.

2. Descrierea sistemului analizat și programului de exploatare

Primul tip de regim intermitent de încălzire.

Așa cum s-a menționat clădirea se considera caracterizată de o capacitate termică C (kWh/K) și de o rezistență termică medie R (K/kW) și deci de o constantă de timp $C_T = C \cdot R$ (h).

Alimentarea continuă cu căldură a clădirii presupune menținerea în permanență a temperaturii interioare de utilizare normate t_u (°C). Puterea termică livrată de către sursa este constantă, valoarea ei fiind P_u (kW). Alimentarea cu intermitență cu căldură a clădirii vizează asigurarea temperaturii interioare de utilizare normate numai pe perioada de utilizare efectivă a clădirii τ_u (h). În consecință, pe această perioadă (τ_u) sursa de alimentare cu căldură se considera că furnizează o putere termică corespunzătoare acestei situații P_u (kW), (fig. A).

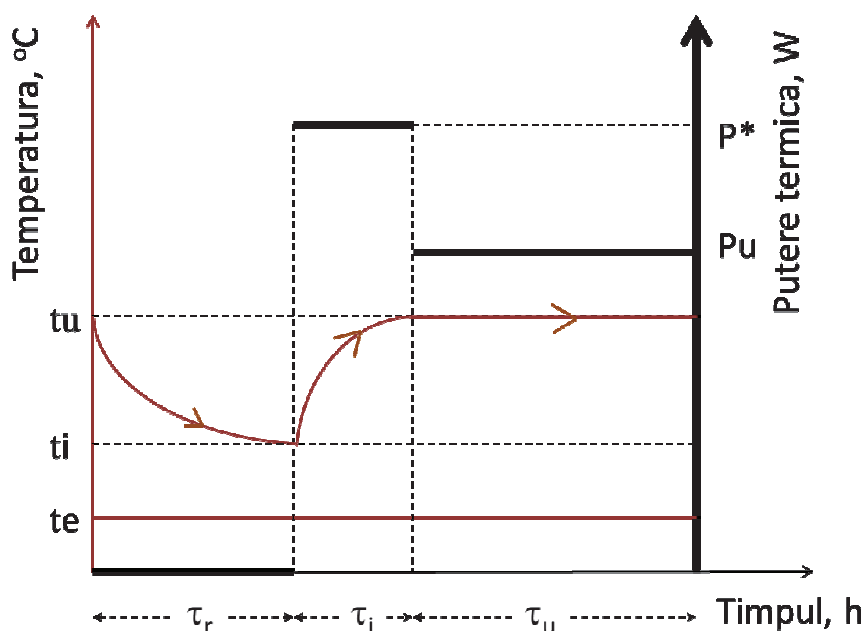


Fig. A

Dupa expirarea perioadei de utilizare sursa se opreste, puterea termica livrata fiind nula. Aceasta etapa dureaza o perioada de timp τ_r (h), evident mai mica ca durata decat $24 - \tau_u$. In aceasta perioada cladirea intra intr-o perioada de racire temperatura ei atingand la sfarsitul acestei perioade o temperatura minima t_i ($^{\circ}\text{C}$), situata intre temperatura mediului exterior t_e ($^{\circ}\text{C}$) si temperatura interioara de utilizare t_u ($^{\circ}\text{C}$). Urmeaza in continuare etapa a treia de functionare, in care sursa reporneste, furnizand insa o putere termica P^* (kW) sensibil mai mare decat puterea de utilizare P_u (kW), pentru a putea incalzi in aceasta perioada cladirea, de la temperatura minima t_i ($^{\circ}\text{C}$) la temperatura de utilizare t_u ($^{\circ}\text{C}$). Durata acestei perioade va fi $\tau_i = 24 - \tau_u - \tau_r$ (h). Valoarea puterii termice necesar a fi furnizata de catre sursa depinde in consecinta de : valoarea temperaturii intermediare t_i ($^{\circ}\text{C}$), de durata perioadei de reincalzire intensiva τ_i (h) si de valoarea temperaturii de utilizare t_u ($^{\circ}\text{C}$).

Al doilea tip de regim intermitent de incalzire.

In continuare se pune problema unui al doilea regim de incalzire intermitenta. In cadrul acestui regim de incalzire intermitenta, zilnic, sunt numai din doua etape, una in care sursa furnizeaza putere termica constanta in perioada de incalzire intensiva si o a doua etapa de racire libera a cladiri, (fig. B). Astfel in prima parte a perioadei de utilizare, sursa functioneaza, iar in a doua parte cladirea se afla in regim de racire libera. In prima parte a perioadei de neutilizare a cladirii regimul este de racire libera iar in a doua etapa sursa functioneaza si furnizeaza putere termica.

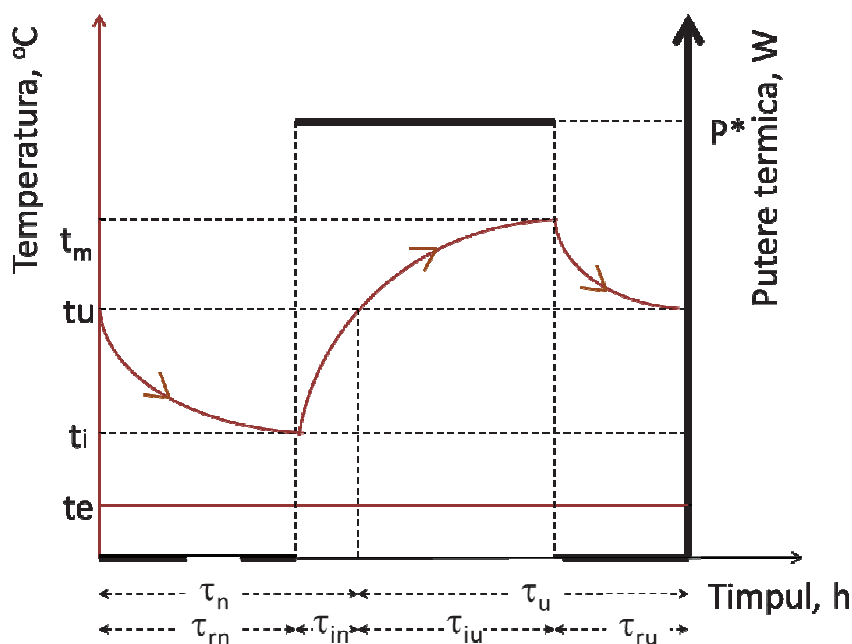


Fig. B

3. Bilanturi termice. Modelarea matematica a regimurilor termice nestationare

Primul tip de regim intermitent de incalzire.

Se incepe analiza cu tratarea etapei de racire libera a cladirii. Bilantul termic in regim nestationar al cladirii in aceasta etapa se poate scrie astfel :

$$\frac{t_e - t}{R} = C \cdot \frac{dt}{d\tau} \quad (1)$$

sau :

$$\frac{dt}{d\tau} = -\frac{1}{C_T} \cdot t + \frac{1}{C_T} \cdot t_e \quad (2)$$

Unde : $C_T = C \cdot R$ – constanta de timp a cladirii (h)

S-a considerat ca ipoteza simplificatoare de lucru, regimul regulat, in care masivitatea cladirii este caracterizata de o temperatura uniforma t (τ), iar temperatura exterioara (t_e) este constanta. Se vor face analize pentru diverse valori ale temperaturii exterioare, caracteristice sezonului rece al anului.

Solutia ecuatiei diferentiale liniare (2), cu conditia initiala $t(\tau)|_{\tau=0} = t_u$, este :

$$t = t_e + (t_u - t_e) \cdot \exp\left(-\frac{\tau}{C_T}\right) \quad (3)$$

Relatia (3) permite stabilirea temperaturii intermediare la care ajunge masivitatea cladirii dupa o perioada de racire libera cu durata τ_r :

$$t_i = t_e + (t_u - t_e) \cdot \exp\left(-\frac{\tau_r}{C_T}\right) = t_e + (t_u - t_e) \cdot E_r \quad (4)$$

$$\text{unde } E_r = \exp\left(-\frac{\tau_r}{C_T}\right)$$

Urmatoarea etapa analizata este etapa de incalzire intensiva a cladirii in care sursa trebuie sa pompeze o putere termica mare pentru a reusi sa aduca cladirea la nivelul temperaturii de utilizare, tu, intr-un timp destul de scurt, τ_i . Se urmareste determinarea valorii acestei puteri termice pentru a calcula consumul energetic in aceasta perioada. Bilantul in regim nestationar in aceasta perioada este:

$$P^* + \frac{t_e - t}{R} = C \cdot \frac{dt}{d\tau} \quad (5)$$

de unde rezulta ecuatia diferentiale liniara :

$$\frac{d\theta}{d\tau} = -\frac{1}{C_T} \cdot t + \frac{1}{C_T} \cdot (t_e + R \cdot P^*) = -\frac{1}{C_T} \cdot t + \frac{1}{C_T} \cdot t_e^* \quad (6)$$

unde $t_e^* = t_e + R \cdot P^*$

Ca și în ecuația diferențială (2) considerând de această dată și puterea livrată de sursă în această etapă constantă în timp, și de condiția inițială $\theta(\tau)|_{\tau=0} = t_i$, rezultă soluția :

$$t = t_e^* + (t_i - t_e^*) \cdot \exp\left(-\frac{\tau}{C_T}\right) \quad (7)$$

În continuare impunem condiția finală $\theta(\tau)|_{\tau=\bar{\alpha}} = t_u$, și se obține :

$$t_u = t_e^* + (t_i - t_e^*) \cdot \exp\left(-\frac{\tau_i}{C_T}\right) = t_e^* + (t_i - t_e^*) \cdot E_i \quad (8)$$

unde $E_i = \exp\left(-\frac{\tau_i}{C_T}\right)$

Din relația (8) se determină puterea pe care trebuie să o livreze sursa în perioada de încălzire intensivă, $P^*(W)$, rezultă că fiind :

$$P^* = \frac{1}{R} \cdot \frac{t_u - t_e - (t_i - t_e) \cdot E_i}{1 - E_i} \quad (9)$$

Înlocuind (4) în (9) se obține :

$$P^* = \frac{1 - E_r \cdot E_i}{1 - E_i} \cdot \frac{(t_u - t_e)}{R} = \frac{1 - E_r \cdot E_i}{1 - E_i} \cdot P_u \quad (10)$$

Rezultă în concluzie destul de simplu de înțeles că energia consumată de sursă pentru alimentarea zilnică a clădirii este în cazul încălzirii intermitente :

$$Q_{\text{int}} = P^* \cdot \tau_i + P_u \cdot \tau_u = \frac{1 - E_r \cdot E_i}{1 - E_i} \cdot \frac{(t_u - t_e)}{R} \cdot \tau_i + \frac{(t_u - t_e)}{R} \cdot \tau_u \quad (11)$$

În regim de încălzire continuă avem un consum zilnic energetic de :

$$Q_{\text{cont}} = P_u \cdot 24 = \frac{(t_u - t_e)}{R} \cdot 24 \quad (12)$$

Raportand consumul energetic pentru incalzirea cladirii in regim de alimentare intermitenta la cel de regim de alimentare continua rezulta :

$$\eta = \frac{Q_{int}}{Q_{cont}} = \frac{1 - E_r \cdot E_i}{1 - E_i} \cdot \frac{\tau_i}{24} + \frac{\tau_u}{24} \quad (13)$$

$$\text{Trebuie sa tinem seama de faptul ca : } \tau_r + \tau_i + \tau_u = 24 \quad (14)$$

Puterea termica livrata de sursa in etapa de incalzire intensiva raportata la puterea termica livrata in regim de incalzire continua are expresia :

$$\frac{P^*}{P_u} = \frac{1 - E_r \cdot E_i}{1 - E_i} \quad (15)$$

Modul in care am pus problema incalzirii intermitente are in vedere o sursa reglabila care furnizeaza putere termica la o valoare ridicata, P^* , in perioada incalzirii intensive, τ_i , si apoi o putere mai scazuta, P_u , in perioada de utilizare a cladirii, τ_u .

Se prezinta in continuare cateva rezultate obtinute in situatia in care etapa de utilizare a cladirii dureaza : $\tau_u = 10h$, iar etapa de racire libera ia diferite valori in domeniul 0 – 14 h.

Tabel 1 : Raportul - Qintemitent / Qcontinuu

τ_r / C_T	1	2	4	8	16	24
2	0,916669	0,917452	0,926975	0,948433	0,969264	0,978292
5	0,791713	0,795534	0,82319	0,875445	0,924961	0,946667
9	0,626413	0,643423	0,699839	0,787048	0,869327	0,906267
12	0,513043	0,548378	0,622062	0,727934	0,830229	0,877302

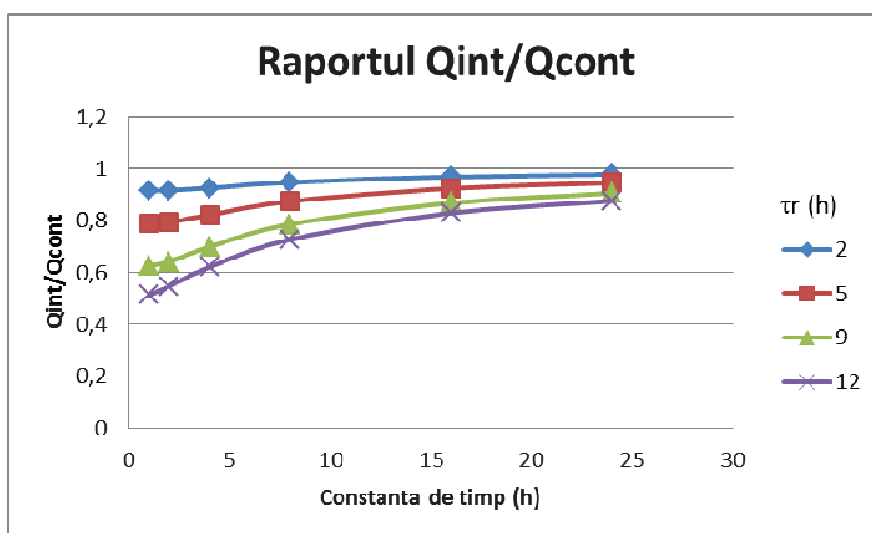


Fig. 1

În tabelul 1 și fig. 1 se prezintă raportul dintre consumul de energie aferent regimului intermitent de încălzire și cel aferent regimului continuu. Se observă că sunt posibile reduceri de până la 50% în diferite situații de clădiri și de durate de întrerupere a alimentării cu căldură. Reducerile energetice importante rezultate prin aplicarea programului de încălzire intermitentă se obțin în special în cazul clădirilor caracterizate de constante de timp mici adică de masivități reduse și de rezistențe termice de asemenea reduse. În cazul clădirilor caracterizate de constante de timp mai ridicate reducerile de consumuri energetice sunt mai scăzute 10% – 15% și chiar mai mici. Sigur că nici aceste valori nu sunt neglijabile însă trebuie văzute ce implică aceste valori. Un alt parametru important este timpul de oprire al alimentării cu căldură al clădirii și se observă că dacă acest timp este mai mare atunci și reducerea de consum energetic este mai mare. Dar și de această dată trebuie văzute ce implică acest lucru.

Tabel 2 - Raport - P*/Pu

τ_r / C_T	1	2	4	8	16	24
2	1,000005	1,001571	1,020616	1,063532	1,105195	1,123251
5	1,000123	1,010312	1,084062	1,223409	1,35545	1,413335
9	1,006783	1,088432	1,359228	1,77783	2,172772	2,350081
12	1,156517	1,580534	2,464748	3,735212	4,962746	5,52763

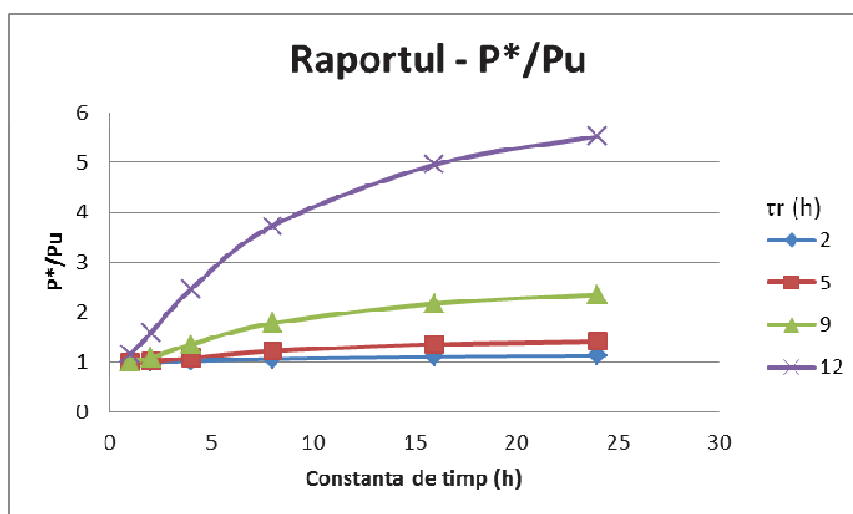


Fig. 2

În tabelul 2 și fig. 2 se prezintă raportul dintre puterea necesară a fi furnizată de sursa de încălzire în regim intensiv și puterea furnizată de sursa în regim continuu de încălzire. După cum era de așteptat, în regim de încălzire intermitent, în cadrul etapei de încălzire intensivă sursa trebuie să aibă capacitatea să furnizeze o putere termică sensibil mai mare decât cea din cadrul regimului continuu. Cu cât clădirea este caracterizată de o constantă de timp mai mare și cu cât perioada de racire liberă a fost mai mare cu atât pentru readucerea în regim este necesară o putere mai mare, de chiar câteva ori mai mare decât cea de regim continuu.

Al doilea tip de regim intermitent de incalzire.

Fara a mai scrie bilanturile termice in regim nestationar ale cladirii in diversele perioade mentionate, ne rezumam la a prezenta direct relatiile operationale rezultate ca solutii a acestor ecuatii de bilant termic. Pentru perioadele de racire :

$$t_u = t_e + (t_m - t_e) \cdot E_{ru} \quad \text{- racirea libera a cladirii in cadrul etapei de utilizare} \quad (16)$$

$$t_i = t_e + (t_u - t_e) \cdot E_{ri} \quad \text{- racirea libera in cadrul etapei de neutilizare} \quad (17)$$

$$t_i = t_e + (t_m - t_e) \cdot E_r \quad \text{- racirea libera - intreaga perioada} \quad (18)$$

Pentru perioada de incalzire intensiva :

$$t_u = t_e^* + (t_i - t_e^*) \cdot E_{iu} \quad \text{- incalzirea intensiva - in cadrul etapei de neutilizare} \quad (19)$$

$$t_m = t_e^* + (t_u - t_e^*) \cdot E_{im} \quad \text{- incalzirea intensiva - in cadrul etapei de utilizare} \quad (20)$$

$$t_m = t_e^* + (t_i - t_e^*) \cdot E_i \quad \text{- incalzire intensiva - intreaga perioada} \quad (21)$$

unde :

$$t_e^* = t_e + R \cdot P^* \quad \text{- temperatura exterioara corectata} \quad (22)$$

$$E_{ru} = \exp\left(-\frac{\tau_{ru}}{C_T}\right); \quad E_{ri} = \exp\left(-\frac{\tau_{ri}}{C_T}\right); \quad E_r = \exp\left(-\frac{\tau_r}{C_T}\right);$$

$$E_{iu} = \exp\left(-\frac{\tau_{iu}}{C_T}\right); \quad E_{im} = \exp\left(-\frac{\tau_{im}}{C_T}\right); \quad E_i = \exp\left(-\frac{\tau_i}{C_T}\right);$$

Prelucrand relatiile (17) si (19) rezulta valoarea puterii termice necesare a fi furnizate in perioada de incalzire :

$$P^* = \frac{1 - E_{iu} \cdot E_{im}}{1 - E_{iu}} \cdot P_u \quad (23)$$

unde :

$$P_u = \frac{(t_u - t_e)}{R}$$

In continuare se urmareste determinarea perioadei de timp in care are loc incalzirea, adica τ_i .

Prelucrarea relatiilor (18) si (21) conduce la :

$$\tau_r = C_T \cdot \ln \frac{t_m - t_e}{t_i - t_e} \quad (24)$$

$$\tau_i = C_T \cdot \ln \frac{t_i - t_e^*}{t_m - t_e^*} \quad (25)$$

Relatia (25) permite acest lucru, insa este necesar sa cunoastem in prealabil temperaturile t_i si t_m . Prelucrand relatia (25) o putem aduce la forma :

$$\tau_i = C_T \cdot \ln \frac{P_i - P^*}{P_m - P^*} \quad (26)$$

unde :

$$P_i = \frac{(t_i - t_e)}{R} \quad (27)$$

$$P_m = \frac{(t_m - t_e)}{R}$$

Parametrul P_i este destul de ușor de stabilit utilizând relația (17) :

$$P_i = E_m \cdot P_u \quad (28)$$

Mai dificil este de stabilit P_m , și pentru asta se va proceda astfel :

Prelucrând relațiile (16) și (20) se obține :

$$\tau_{ru} = C_T \cdot \ln \frac{t_m - t_e}{t_u - t_e} \quad (29)$$

$$\tau_{iu} = C_T \cdot \ln \frac{t_u - t_e^*}{t_m - t_e^*} \quad (30)$$

Adunând relațiile (29) și (30) rezultă :

$$C_T \cdot \ln \left(\frac{t_m - t_e}{t_u - t_e} \cdot \frac{t_u - t_e^*}{t_m - t_e^*} \right) = \tau_u \quad (31)$$

Sau :

$$\frac{P_u \cdot (P_m - P^*)}{P_m \cdot (P_u - P^*)} = E_u \quad (32)$$

Rezultă :

$$P_m = \frac{1 - E_{in} \cdot E_m}{1 - E_{in} [1 - E_u \cdot (1 - E_m)]} \cdot P_u \quad (33)$$

Și în final se compară consumul de energie în cazul regimului intermitent de încălzire cu cel din regimul continuu.

$$\eta = \frac{Q_{int}}{Q_{cont}} = \frac{P^* \cdot \tau_i}{P_u \cdot 24} = \frac{P^*}{P_u} \cdot \frac{C_T}{24} \cdot \ln \frac{P_i - P^*}{P_m - P^*} = \frac{P^*}{P_u} \cdot \frac{C_T}{24} \cdot \ln \frac{P_i/P_u - P^*/P_u}{P_m/P_u - P^*/P_u} \quad (34)$$

unde :

$$\frac{P^*}{P_u} = \frac{1 - E_{in} \cdot E_m}{1 - E_{in}}$$

$$\frac{P_i}{P_u} = E_m$$

$$\frac{P_m}{P_u} = \frac{1 - E_{in} \cdot E_m}{1 - E_{in} [1 - E_u \cdot (1 - E_m)]}$$
(35)

Se prezinta in continuare cateva rezultate obtinute in situatia in care etapa de utilizare a cladirii dureaza: $\tau_u = 10h$, iar etapa de racire libera ia diferite valori in domeniul 0 – 14 h.

Tabel 3 - Raport - Qintemitent / Qcontinuu

τ_r / C_T	1	2	4	8	16	24
2	0,916671	0,917976	0,932381	0,959463	0,979761	0,986843
5	0,791759	0,798972	0,844875	0,911603	0,955626	0,97052
9	0,628956	0,672638	0,786573	0,889384	0,939635	0,956817
12	0,571252	0,730489	0,908444	0,947322	0,946984	0,954773

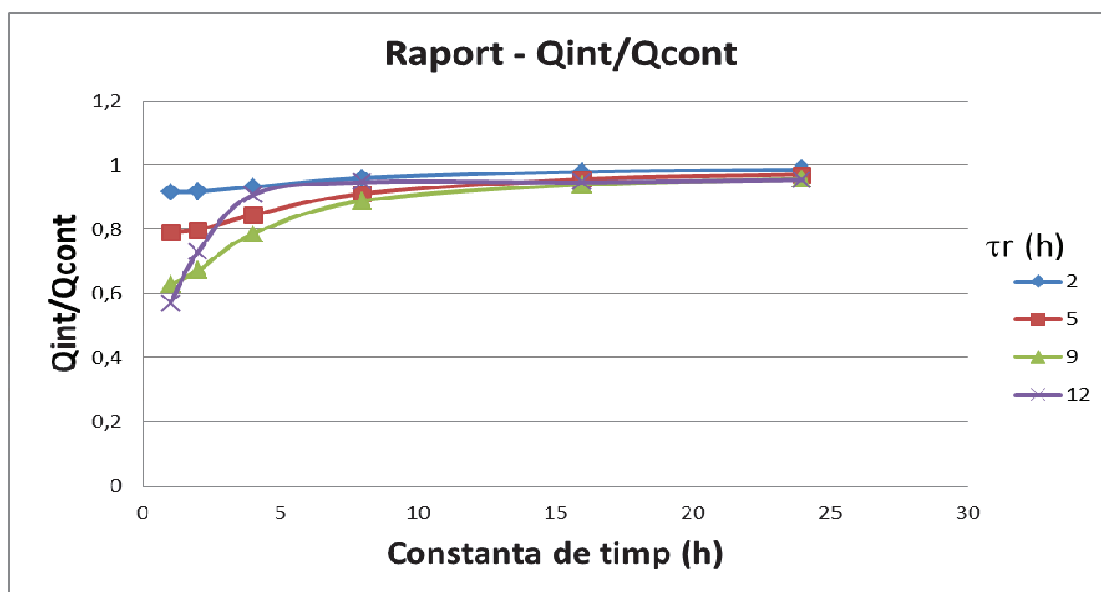


Fig 3

In tabelul 3 si fig. 3 se prezinta pentru al doilea tip de regim intermitent raportul dintre consumul de energie aferent regimului intermitent de incalzire si cel aferent regimului continuu. Se observa ca sunt posibile reduceri de pana la 60% in direrite situatii de cladiri si de durate de intrerupere a alimentarii cu caldura. Reducerile energetice importante rezultate prin aplicarea programului de incalzire intermitenta se

obtin, de asemenea, în special în cazul clădirilor caracterizate de constante de timp mici adică de masivități reduse și de rezistențe termice de asemenea reduse. În cazul clădirilor caracterizate de constante de timp mai ridicate reducerile de consumuri energetice sunt mai scăzute 10% și chiar mai mici. Sigur că nici aceste valori nu sunt neglijabile însă trebuie văzut ce implică aceste valori. Un alt parametru important este timpul de oprire al alimentării cu căldură al clădirii și se observă, la fel, că dacă acest timp este mai mare atunci și reducerea de consum energetic este mai mare. Dar și de această dată trebuie văzut ce implică acest lucru.

Tabel 4 - Raportarea - P*/Pu

τ_r / C_T	1	2	4	8	16	24
2	1,000005	1,001571	1,020616	1,063532	1,105195	1,123251
5	1,000123	1,010312	1,084062	1,223409	1,35545	1,413335
9	1,006783	1,088432	1,359228	1,77783	2,172772	2,350081
12	1,156517	1,580534	2,464748	3,735212	4,962746	5,52763

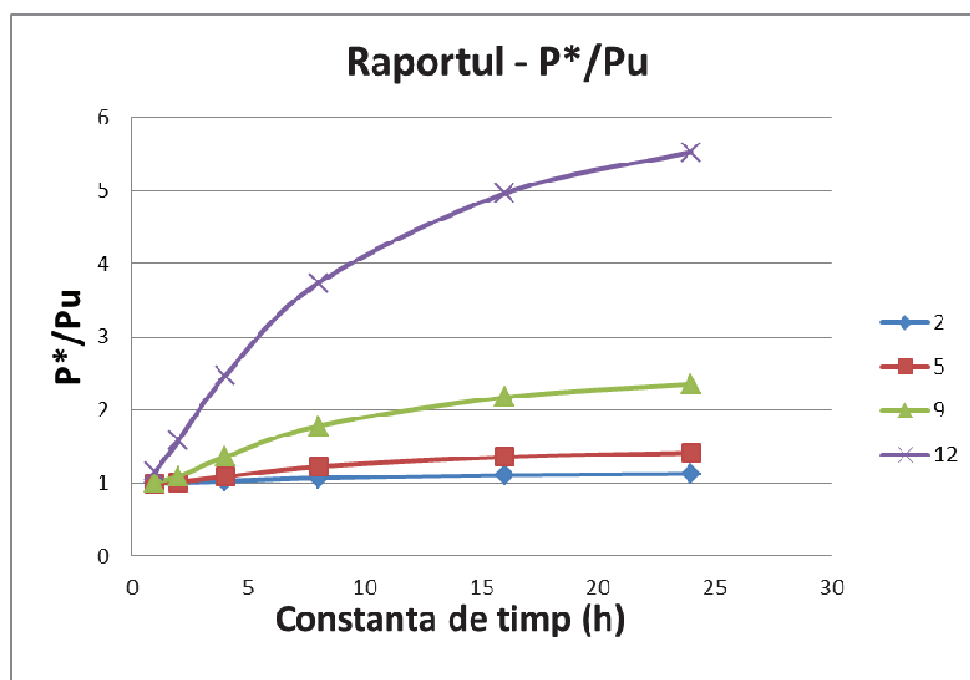


Fig. 4

În tabelul 4 și fig. 4 se prezintă raportul dintre puterea necesară a fi furnizată de sursa de încălzire în regim intensiv și puterea furnizată de sursa în regim continuu de încălzire. După cum era de așteptat, în regim de încălzire intermitent, în cadrul etapei de încălzire intensivă sursa trebuie să aibă capacitatea să furnizeze o putere termică sensibil mai mare decât cea din cadrul regimului continuu. Cu cât clădirea este caracterizată de o constantă de timp mai mare și cu cât perioada de racire liberă a fost

mai mare cu atat pentru readucerea in regim este necesara o putere mai mare, de chiar cateva ori mai mare decat cea de regim continuu.

Facand acum o comparatie intre cele tipuri de regimuri de incalzire intermitenta putem spune ca cel de al doilea are performante energetice mai scazute. Este explicabil acest lucru dat fiind ca exista o perioada in care temperatura interioara depaseste temperatura de utilizare, acest lucru nefiind necesar din punct de vedere al utilizarii spatiului ci numai in vederea functionarii acestui al doilea tip de regim intermitent.

4. Concluzii

Reducerile energetice oferite de adoptarea regimului de incalzire intermitenta presupun insa o etapa de incalzire intensiva a cladirii, etapa in care sursa de caldura trebuie sa furnizeze o putere termica apreciabila, sensibil mai mare decat puterea in regim curent de utilizare a cladirii. Este deci necesar ca sursa sa fie dimensionata la o capacitate de cca. 4-5 ori necesarul de calcul al consumatorului.

Se poate totusi adopta o dimensionare ceva mai lejera a sursei de caldura la numai cca. de 2 ori necesarul de caldura de calcul al consumatorului, insa nu trebuie vizate economii energetice (adica nu trebuie adoptat regimul de incalzire intermitent) in perioadele de solicitare climatica apropiate ca intensitate de situatia de calcul. Perioadele foarte reci ale sezonului de incalzire nu au durata mare si deci in consecinta nu se prejudiciaza mult realizarea economiilor energetice prin adoptarea regimului de incalzire intermitent. Frecventa cea mai mare de aparitie o au solicitarile medii de iarna ($t_e = 1-3$ oC) si in aceste perioade se poate adopta regimul de incalzire intermitent si ne putem astepta la economii energetice de luat in considerare.

Un studiu de fezabilitate este insa cel mai in masura sa raspunda clar la problema rentabilitatii implementarii unei surse supradimensionate in vederea realizarii unor economii energetice pe parcursul intregului sezon de incalzire

Notatii

t – temperatura curenta a cladirii, °C;

t_e – temperatura exterioara, °C;

t_u – temperatura interioara in perioada de utilizare, °C;

t_i – temperatura interioara minima la care se raceste cladirea, °C;

t_m – temperatura interioara maxima la care se incalzeste cladirea, °C;

τ - timpul curent, h;

τ_u – durata perioadei de utilizare a cladirii, h;

τ_r – durata perioadei de racire a cladirii, h;

τ_i – durata perioadei de incalzire a cladirii, h;

τ_{iu} – durata perioadei de incalzire intensiva din cadrul etapei de utilizare, h;

τ_{ru} – durata perioadei de racire libera din cadrul etapei de utilizare, h;

τ_m – durata perioadei de racire libera din cadrul perioadei de neutilizare, h;

τ_{in} – durata perioadei de incalzire intensiva din cadrul perioadei de neutilizare, h;

Consecințe energetice ale încălzirii intermitente a clădirilor

P_u – puterea termica necesar a fi livrata de sursa in regim de incalzire continua, W;
 P^* - puterea termica necesar a fi livrata de sursa in regim de incalzire intensiva, W;
 Q_{int} – consumul zilnic de energie in regim de incalzire intermitenta, J;
 Q_{cont} – consumul zilnic de energie in regim de incalzire continua, J;
 R – rezistenta termica a cladirii, K/kW;
 C – capacitatea termica a cladirii, kWh/K;
 C_T – constanta de timp a cladirii, h;
 η - raportul Q_{int}/ Q_{cont} , -;

Bibliografie

1. Florin Iordache – Termotehnica Constructiilor – ed. 3 – editura Matrix Rom - 2010;
2. Florin Iordache – Energetica echipamentelor si sistemelor termice din instalatii – editura Conspress – 2010;
3. Horia Asanache – Higrotermica cladirilor – editura Matrix Rom – 1999;
4. Frank Kreith, et al. - Heat and mass transfer – ed. Frank Kreith, 1999;
5. Holman J.P. – Heat Transfer – McGraw-Hill – 2010;

Analiza performanței energetice a unei instalații solare de preparare a apei calde de consum în diverse condiții de utilizare

Analysis of the energy performance of a thermal solar system for DHW production, under different operating conditions

Răzvan Popescu¹, Lelia Popescu², Andrei Damian³

¹ Universitatea Tehnică de Construcții București
B-dul Lacul Tei nr.122-124, sector 2, București, Romania
E-mail: razvan22@yahoo.com

² Universitatea Tehnică de Construcții București
B-dul Lacul Tei nr.122-124, sector 2, București, Romania
E-mail: lelialetitia@yahoo.com

³ Universitatea Tehnică de Construcții București
B-dul Lacul Tei nr.122-124, sector 2, București, Romania
E-mail: adamian7@yahoo.com

Rezumat. În lucrarea de față se prezintă un studiu parametric aplicat unei instalații de preparare a apei calde de consum ce deservește o clădire de tip hotel situată în România. Studiul urmărește evidențierea anumitor factori de influență precum: climatul local, tipul de panou, tipul de profil de consum, orientarea cardinală a panourilor solare sau înclinarea acestora față de orizontală, asupra performanței energetice a instalației. Metoda de analiză este numerică, în regim dinamic și face apel la simulări pe un an de zile, realizate cu ajutorul programului de calcul SimSol. Rezultatele obținute, în termeni de factori de acoperire solară, permit câteva recomandări practice privind dimensionarea acestor sisteme pentru diferite tipuri de clădiri.

Cuvinte cheie: panouri solare, factor de acoperire solară, profil de consum apă caldă

Abstract. In the present paper is presented a parametric study regarding the operation of a solar thermal system for DHW preparation, equipping a small hotel located in Romania. The study main goal is to outline the influence that several parameters, such as: local climate, solar panel type, solar panels orientation and slope, could have on the system energy performance. The method of analysis is numerical one, it is made under dynamic operational conditions, and it is performed by using the software SimSol, especially designed for the simulation of solar thermal installations. The results obtained by numerical simulations over one-year period could mean to practical recommendations regarding the design of this type of systems for different buildings.

Key words: solar panels, solar cover factor, DHW consumption

1. Introducere

Unul dintre obiectivele actuale majore ale Uniunii Europene este reducerea cu 20%, până în 2020, a emisiilor de gaze cu efect de seră (GES), în condițiile creșterii producției de energie din surse regenerabile tot cu un procent de 20% [1].

În prezent, pe plan mondial, energia consumată în sectorul rezidențial depășește cu peste 40% energia totală consumată în sectorul construcțiilor, pentru utilități precum: încălzire, preparare apă caldă de consum, climatizare și iluminat. În viitor, se preconizează ca aportul energetic adus de sursele de energie regenerabile să crească procentual semnificativ, înlocuind astfel, contribuția energetică adusă de combustibilii fosili, în contextul epuizării continue a acestor resurse la nivel mondial.

Prezentul articol tratează oportunitatea utilizării energiei solare, ca parte integrantă a ansamblului surselor de energie regenerabile disponibile pe Glob, pentru prepararea apei calde de consum (a.c.c.), în diferite condiții climatice de utilizare. Sunt realizate câteva studii parametrice cu scopul evidențierii factorilor semnificativi de influență asupra performanței unei instalații de producere a a.c.c. dotată cu panouri solare.

În România, există la ora actuală date certe privind distribuția gradului de însorire a teritoriului național în patru zone distincte, după cum este prezentat în figura 1. Din acest motiv, apare justificată încercarea de a compara aceeași instalație cu panouri solare, din punct de vedere a performanței sale energetice, plasând-o în zone climatice diferite din punct de vedere al intensității radiației solare. În plus, este analizată tehnologia de preparare a a.c.c. relativ la tipul de panou solar utilizat (plan sau cu tuburi vidate), cunoscând modul diferit de captare a energiei solare al acestora.

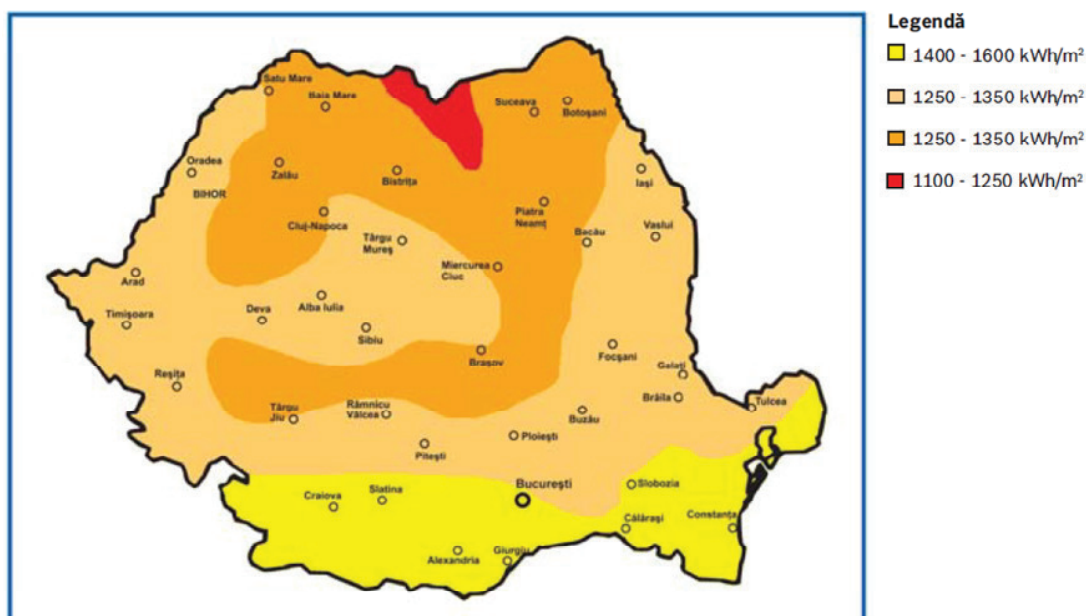


Figura 1: Repartiția intensității radiației solare pe teritoriul României

În prezent, captarea energiei solare se realizează cu două categorii de panouri solare, diferite prin modul de conversie în alte forme de energie [2] :

- Panouri solare "termice", care convertesc radiația solară absorbită în energie termică, cu ajutorul unui debit circulant de apă caldă, și
- Panouri solare "fotovoltaice" (abrev.PV) [3], ce convertesc energia solară captată în energie electrică, utilizată în diverse scopuri casnice sau, la puteri electrice mari, de ordinul sutelor de kW, în scopuri industriale

Din punct de vedere al performanței energetice, s-a demonstrat că panourile solare termice prezintă randamente de conversie apropiate de 80%, mult superioare panourilor PV, motiv pentru care volumul de comercializare al sistemelor aferente "solarului termic" este mult superior celui corespunzător "solarului fotovoltaic". Acest fenomen este amplificat de costul mai redus al panourilor solare termice față de modulele fotovoltaice, la caracteristici de conversie energetică apropiate.

Scopul principal al utilizării de panouri solare termice este prepararea apei calde de consum (a.c.c.) pentru nevoi menajere curente în sectorul rezidențial sau ne-rezidențial (spălat, gătit) și, mai rar, pentru consumuri tehnologice, în sectorul industrial. Oportunitatea implementării acestor sisteme este dependentă de intensitatea și durata anuală de persistență a radiației solare în locul geografic respectiv, la nivel european fiind favorizate țările mediteraneene cu grad de însorire ridicat și relativ uniform. Odată cu apariția panourilor solare cu tuburi vidate, care captează radiație solară directă și difuză cu eficiențe ridicate, aria geografică de utilizare a panourilor solare termice s-a extins foarte mult, iar țări precum Austria și Germania, au devenit exemple de implementare a sistemelor solare termice pe diferite tipuri de clădiri.

În cazul clădirilor cu grad ridicat de izolare termică, se pot utiliza sisteme "hibride" cu panouri solare termice, la care apă caldă preparată la 50-60 °C poate fi destinată atât consumului menajer (a.c.c.), cât și pentru necesități de încălzire, prin introducerea în rezervorul de acumulare (boiler) a unei serpentine suplimentare pentru circuitul de încălzire. Acest lucru presupune dimensionarea instalației de încălzire interioare (corpuri de încălzire, planșeu radiant) în concordanță cu temperaturi mai reduse ale agentului încălzitor pe circuitul-tur (40-45 °C), în raport cu cele obținute la centralele termice clasice (80-90 °C).

Aplicațiile sistemelor cu panouri solare termice devin și mai interesante în cazul "climatizării solare", atunci când energia solară captată este dirijată către o mașină frigorifică cu absorbție (chiller cu absorbție). Această soluție de producere a frigului este mult mai ecologică în raport cu cele bazate pe compresia mecanică, prin reducerea semnificativă a emisiilor de CO₂ în atmosferă, însă utilizarea sa este limitată datorită costului ridicat al acestor echipamente. În prezent, la nivel european există doar aproximativ 50 de instalații de climatizare funcționale bazate pe energia solară [4], [5], [6], [7].

Recent, odată cu intrarea în vigoare a Directivei 31/2010 a Consiliului European, privind creșterea performanței energetice a clădirilor la orizontul anilor 2020, cu mărirea aportului din surse de energie regenerabile, a apărut tot mai interesantă integrarea energiei solare în clădiri noi, pentru aducerea acestora cât mai aproape de

conceptele de "casă pasivă", "clădire zero-energie" sau chiar "clădire cu energie pozitivă", la care energia anuală produsă din surse regenerabile depășește ca valoare energia consumată pentru utilități (încălzire, apă caldă de consum, iluminat, ventilare și climatizare). Aceste concepte necesită în mod obligatoriu implementarea tehnologiilor performante de producere a apei calde pentru nevoi menajere și încălzire, prin utilizarea energiei solare [8], [9]. Se poate concluziona că domeniul "solarului termic" trece în mod gradual, de la etapa de "Opțional" la cea de "Obligatoriu", în contextul proiectării, la nivelul anului 2020, doar a clădirilor cu atributul "aproape zero-energie" sau nZEB (nearly Zero Energy Buildings).

2. Descrierea metodei de analiză

Metoda de analiză abordată în prezenta lucrare este eminent numerică, și face apel la utilizarea unui program de calcul cu licență gratuită (SimSol), descărcabil de pe internet. Acest program are în componența sa câteva sisteme de preparare a apei calde de consum ce utilizează panouri solare termice, ale căror componente (module) pot fi configurate de utilizator prin intermediul unei interfețe grafice sugestive (fig.2). Aceste componente reproduc destul de fidel schema tehnologică a funcționare a sistemelor cu panouri solare termice, bazată pe circuitul panourilor (panouri solare-pompă de circulație-primar schimbător de căldură în plăci/boiler) sau pe circuitul apei calde de consum (secundar schimbător de căldură-boiler-consumatori-pompă de reirculare-vană cu trei căi). La modulul de panou solar este conectat un modul "Meteo", care preia dintr-un fișier de date meteo pre-definit (din baza de date internă a SimSol) valorile de temperatură exterioră și radiație solară necesare simulării instalației într-o anumită locație geografică.

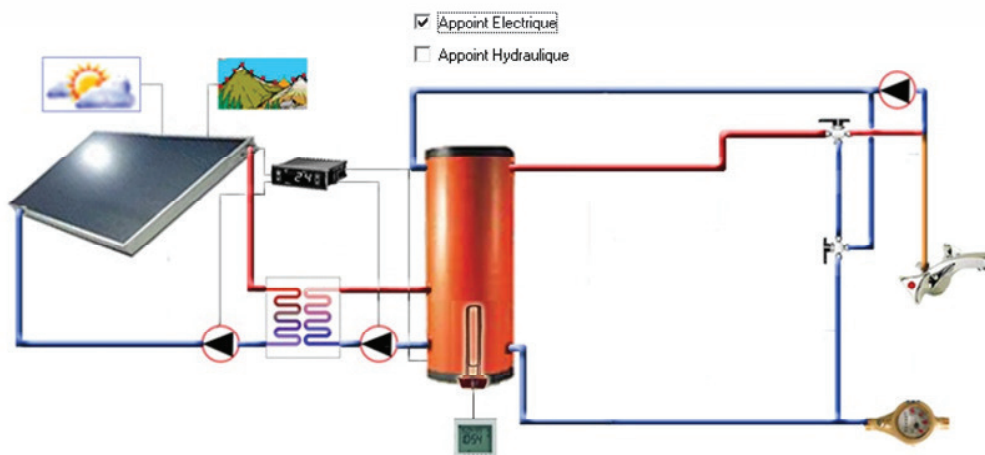


Fig.2: Reprezentarea în SimSol a unei instalații solare de preparare a a.c.c. cu boiler bivalent, schimbător de căldură intermediar și pompă de recirculare

Datele de ieșire ale programului de simulare a funcționării instalației cu panouri solare termice sunt:

Analiza performanței energetice a unei instalații solare de preparare a apei calde de consum în diverse condiții de utilizare

- Factorul anual de acoperire solară a necesităților pentru prepararea a.c.c.;
- Consumurile energetice anuale ale echipamentelor auxiliare (rezistență electrică boiler, pompe de circulație, consum de gaz natural în cazul aportului suplimentar de energie la boiler de la o centrală termică);
- Nivelurile de temperatură ale apei atinse pe înălțimea boilerului (stratificarea termică verticală în boiler)

În urma simulării pe un an de zile, se obțin pentru mărimile de ieșire mai sus enunțate, câte 12 valori globale, aferente celor 12 luni ale anului, oferind astfel o imagine concretă asupra variației performanței energetice a sistemului în funcție de sezon și de intensitatea radiației solare incidente asupra panourilor.

Programul de calcul SimSol permite introducerea unor date foarte variate privind consumul de a.c.c. în funcție de destinația și modul de utilizare al clădirii. Profilurile de consum "zilnic" și "anual" diferă foarte mult în funcție de acești factori și influențează în mod semnificativ consumurile de energie auxiliare ale sistemului. În studiul de caz prezentat în cadrul prezentului articol, s-au utilizat, pentru o clădire cu destinația hotel/pensiune, două profiluri de consum anuale de tip: "constant" și "hotelier" și respectiv, un profil de consum zilnic de tip "european" (fig.3).

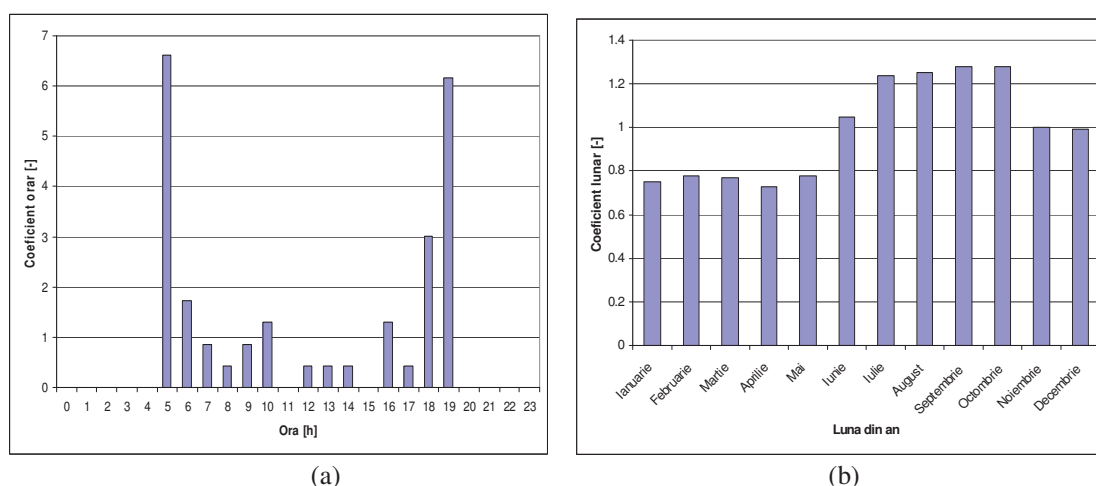


Fig.3: Profilurile de consum de a.c.c. utilizate în studiile de caz: a) zilnic și b) anual

3. Studii de caz și rezultate obținute

Simulările numerice privind performanța energetică a instalațiilor de preparare a a.c.c. cu panouri solare termice, ce fac obiectul prezentului articol, au fost realizate pentru situația unei clădiri reale, de tip hotel/pensiune, amplasat în zona Deltei Dunării. Această clădire este compusă din trei module de cazare și un restaurant, iar instalația de încălzire și producere a apei calde este amplasată la subsolul tehnic. Panourile solare utilizate în simulări sunt de două tipuri: cu tuburi vidate (tip tub termic de înaltă performanță), și respectiv plane, ambele având o suprafață totală de captare de 15 m².

Datele meteo utilizate în simulări, pentru situația reală, sunt cele aferente municipiului Galați (zona climatică III), orașul cel mai apropiat de locul geografic al clădirii analizate. În vederea comparării influenței climei asupra randamentului energetic al instalației, s-au realizat, pentru aceeași clădire și același sistem, și simulări pentru orașele Constanța (zona climatică I), București (zona climatică II) și Brașov (zona climatică III). Fișierele meteo pentru aceste localități au fost create de către autori și introduse în baza de date meteo a SimSol, în vederea unor comparații cât mai apropiate de realitate.

În figura 4 sunt reprezentate valorile anuale ale: factorului de acoperire solară (a) și, respectiv, energiei incidente și utile (b), pentru două tipuri diferite de panouri solare: cu tuburi vidate și plane, și pentru cele patru orașe mai sus menționate, aparținând celor 4 zone climatice diferite de pe teritoriul României.

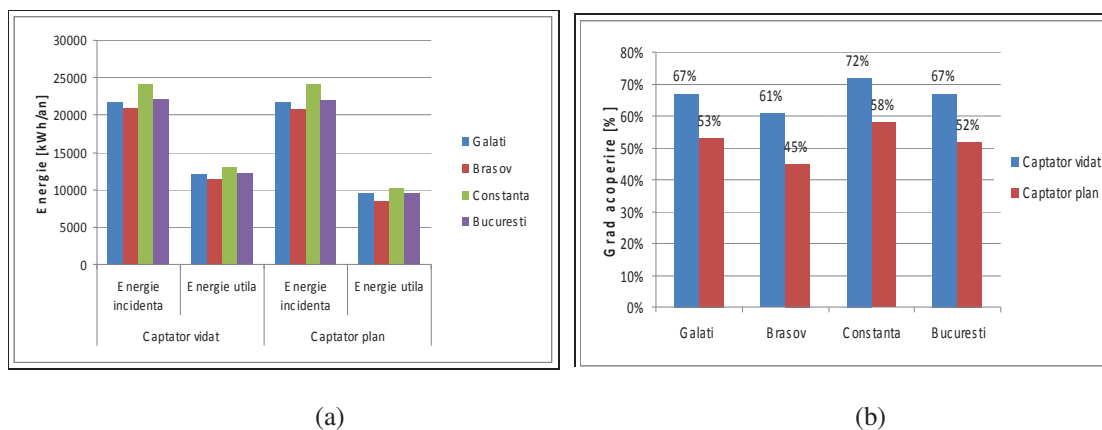


Fig.4: Factorul anual de acoperire solară (a) și energia anuală incidentă/utilă (b) obținute în urma simulărilor cu două tipuri de panouri solare și pentru patru zone climatice

Se pot remarca, din figura 4, valorile mai mari ale factorului de acoperire solară și energiei utile captate de panourile solare cu tuburi vidate, în raport cu captatoarele plane. Acest fenomen se datorează în mod direct tehnologiei de captare a radiației solare, mult mai performantă în cazul tuburilor vidate. Diferențele relative între factorii de acoperire solară corespunzători celor două tipuri de panouri se situează între 14% (Galați și Constanța) și 16% (Brașov). În ceea ce privește valorile absolute ale factorilor de acoperire solară obținute în urma simulărilor, cea mai ridicată se obține în cazul orașului Constanța, pentru captatorul cu tuburi vidate (72%), iar cea mai scăzută pentru cazul orașului Brașov, pentru captatorul plan (45%), situații ce corespund cu situațiile extreme de însorire, combinate cu performanțele de captare ale celor două tipuri de panouri.

Ținând cont de costul important al panourilor cu tuburi vidate în raport cu cel al panourilor plane, dar și de diferențele reduse între factorii de acoperire solară obținuți pentru cele două tipuri de captatoare (13-15%), pentru fiecare oraș analizat, rezultă că, pentru aplicația studiată, nu este indicată implementarea unor panouri cu

tuburi vidate, datorită timpului mai lung de amortizare a investiției inițiale, în contextul unor debite de a.c.c. relativ reduse.

În figura 5 sunt reprezentați factorii anuali de acoperire solară pentru cele două profiluri de consum a a.c.c. considerate: constant și hotelier și pentru patru unghiuri diferite de înclinare a panourilor solare cu tuburi vidate: 0, 30, 45, 60 și 90°. Se poate observa că tipul profilului de consum nu are, în cazul considerat, o influență importantă asupra factorului de acoperire solară, însă unghiul de înclinare este un factor de influență semnificativ. Astfel, unghiul de înclinare optim obținut este de 45°, însă diferența între 30° și 45° este foarte redusă. De obicei, în practica curentă de proiectare a instalațiilor solare termice, unghiul de înclinare a panourilor solare se consideră numeric egal cu latitudinea geografică a localității unde se proiectează instalația.

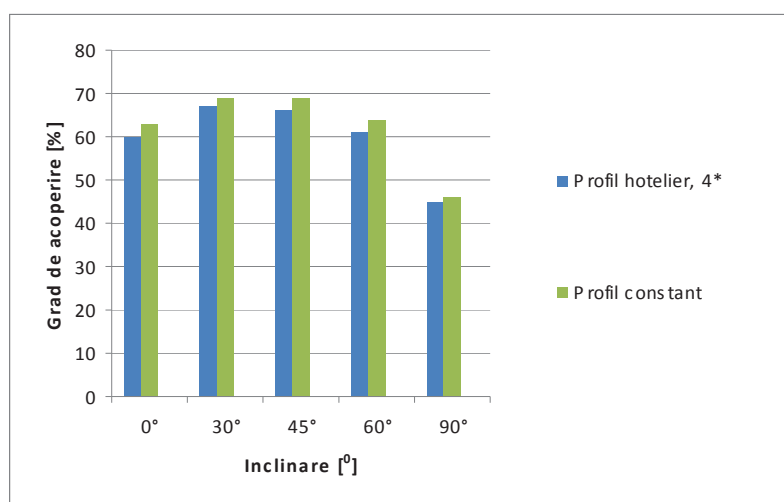


Fig.5: Factorul anual de acoperire solară obținut în urma simulărilor cu două tipuri de profil de consum al a.c.c. și pentru patru unghiuri de înclinare față de orizontală a panourilor solare

În figura 6 este reprezentată variația factorului anual de acoperire solară, pentru cazul sistemului cu panouri plane, în funcție de volumul boilerului de acumulare (fig.6a) și, respectiv, de orientarea cardinală a panourilor solare (fig.6b), fiind considerate toate orientările cardinale posibile, mai puțin Nordul. Volumul boilerului a fost variat în plaja de valori 500 litri – 5000 litri, căutându-se volumul optim al vasului de acumulare a apei calde pentru un sistem de producere a a.c.c. a-priori cunoscut, din punct de vedere al debitului de apă caldă ce trebuie preparat și al suprafeței de captare a energiei solare.

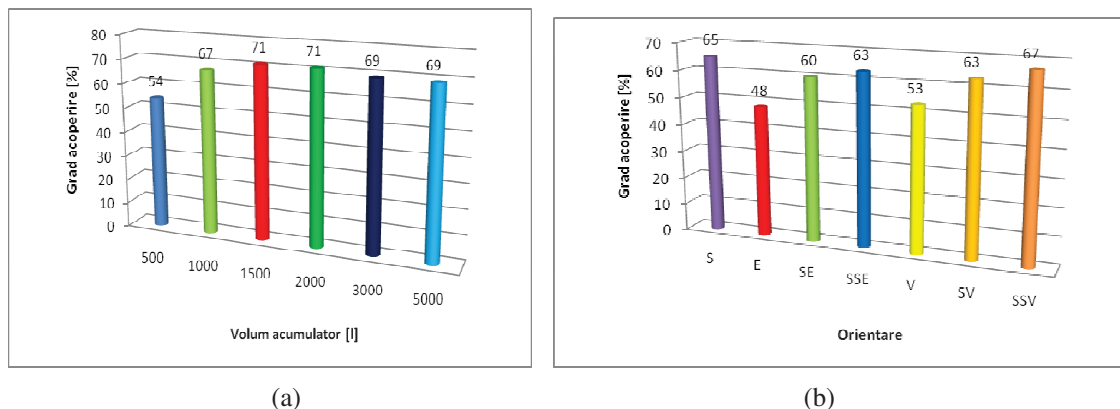


Fig.6: Factorul anual de acoperire solară obținut în urma simulărilor cu mai multe capacități ale boilerului de acumulare a a.c.c. (a) și pentru șapte orientări cardinale ale panourilor solare (b)

Se poate observa din figura 6a că factorul de acoperire solară crește odată cu mărirea volumului boilerului în intervalul 500-200 litri și scade apoi, în intervalul 2500-5000 litri, datorită creșterii pierderilor energetice prin mantaua boilerului, direct proporțională cu suprafața exterioară a acestuia. În cazul studiat, alegerea unui boiler de acumulare cu volumul de 1000 litri pare un bun compromis, ținând cont de investiția inițială mult mai redusă în raport cu boilerul de 2000 litri (având factorul de acoperire maxim), combinată cu o scădere nesemnificativă a factorului anual de acoperire solară (67% față de 71%). În ceea ce privește influența orientării cardinale a panourilor, se poate remarca (fig. 6b) un maxim al factorului de acoperire solară pentru orientările Sud (S) și Sud-Sud-Vest (SSV), cele mai avantajate din punct de vedere al intensității și duratei de persistență a radiației solare.

În finalul lucrării prezentăm influența obstacolelor exterioare clădirii, cu rol de umbră a acesteia, asupra factorului de acoperire solară al sistemului analizat. În acest scop, cu ajutorul SimSol, am putut configura mai multe obstacole adiacente clădirii, după cum urmează:

- O clădire cu 3 etaje, având înălțimea totală $h_{tot}=17$ m,
- O pădure, cu înălțimea totală $h_{tot}=70$ m și, respectiv,
- Un munte cu înălțimea totală $h_{tot}=1000$ m

Rezultatele obținute denotă o reducere a factorului de acoperire solară în situația umbririi clădirii, de la valoarea de 67% (fără nicio umbră, caz de referință) la valoarea de 30% (un munte ca obstacol). Această observație ne conduce la ideea de a studia atent peisajul în care este amplasată o clădire pe care se dorește implementarea unui sistem ce utilizează panouri solare.

4. Concluzii

În cadrul articolului a fost realizat un studiu parametric privind oportunitatea implementării unor sisteme de preparare a apei calde de consum ce utilizează panouri solare termice, în condițiile climatice din România. Studiile de caz, realizate cu ajutorul programului de calcul SimSol, au evidențiat următoarele aspecte :

Analiza performanței energetice a unei instalații solare de preparare a apei calde de consum în diverse condiții de utilizare

- Captatoarele cu tuburi vidate prezintă eficiențe energetice superioare în raport cu captatoarele plane, însă, datorită costului lor ridicat, nu se justifică decât pentru aplicații care necesită prepararea unor debite foarte mari de apă caldă pentru consum menajer și eventual, încălzire;
- Unghiul optim de înclinare față de orizontală al panourilor solare termice poate fi cuprins între 30° și 45°, alegându-se de obicei o valoare egală numeric cu latitudinea geografică a locului considerat;
- Volumul optim al rezervorului de acumulare (boilerului) se alege de la caz la caz, în funcție de suprafața panourilor și de debitul de apă caldă ce trebuie preparat, ținând cont de faptul că, peste o anumită valoare, nu se justifică investiția într-un echipament de volum prea mare, comparativ cu câștigurile energetice aduse instalației;
- Orientările cardinale optime ale panourilor solare sunt Sud și Sud-Sud-Vest
- Eventualele obstacole prezente în vecinătatea clădirii echipate cu panouri solare pot reduce semnificativ energia solară utilă captată de acestea și, implicit, factorul anual de acoperire solară

Toate aceste observații pot fi utile proiectanților de instalații solare termice, în vederea optimizării costului de investiție și exploatare a acestora. Acest tip de analiză poate fi extins și în cazuri mai complexe de instalații solare, ca de exemplu cele utilizate la încălzirea piscinelor de mari dimensiuni sau chiar pentru aplicații de tip ”climatizare solară”.

Referințe

- [1] Memo: EU energy security and solidarity action plan: 2nd strategic energy review, reference online : <http://ec.europa.eu/energy/strategies/2008>.
- [2] Clean energy project analysis. Solar water heating – Retscreen International, site online: www.etscreen.ca
- [3] Photovoltaic systems – Viessmann Co, site online: www.viessmann.com
- [4] Reference online : <http://www.actu-environnement.com/ae/news/tecsol-climatisation-solaire-installations-techniques-10729.php4>
- [5] Kim D.S., Infante Ferreira C.A. - Solar absorption cooling. 1st progress report – Delft University of Technology, 2003
- [6] Kim D.S., Infante Ferreira C.A. - Air-cooled solar absorption air conditioning. Final Report -Delft University of Technology, 2005
- [7] Kelemen G., Ursa D. – Alternative energetique. Principe de fonctionnement du capteur plan, Rev. Tehnica instalatiilor nr. 1/2004
- [8] Nazif G. and Altan H., Zero energy house design for cyprus: enhancing energy efficiency with vernacular techniques, Proceedings of Building Simulation 2013 conference, August 2013, pp. 2978-2984.
- [9] Pagliano L. and Zangheri P., Design of nearly zero energy buildings coupled with an earth to air heat exchanger in mediterranean climate: development of an analytic model and validation against a monitored case study, Proceedings of Building Simulation 2013 conference, August 2013, pp. 3705-3711.

The behaviour analysis of an anaerobic sludge digester exposed on thermic action*

Sorohan Lucian Valentin

Universitary Assistant, PhD, Technical University of Civil Engineering – Bucharest, Romania
 Faculty of Hydrotechnics, Hydraulic Engineering Department.
e-mail: sorohan@utcb.ro

Abstract: The anaerobic sludge digesters existing in wastewater treatment plants are exposed to temperature variations, due to permanent sludge heating at 35°C - 37°C and external weather temperature variation. This work presents the behaviour in time, as well as the calculation analysis of thermic effects action diminution for that kind of things, taking into account a small energetic balance.

Keywords: rigidity, thermoelasticity, thermal action.

List of variables and constants

E - elasticity module;

μ - Poisson coefficient;

α_t - coefficient of thermal dilatation;

α_i , α_e - coefficient of thermal transfer at the exterior surface, respectively at the interior surface of the tank;

λ_b , λ_p - coefficient of thermal conduction of concrete, respectively of thermal insulation;

h - thickness of the plate;

$D = \frac{E \cdot h}{1 - \mu^2}$ - stretching stiffness of the plate in elastic state;

$B = \frac{E \cdot h^3}{12(1 - \mu^2)}$ - bending stiffness of the plate in elastic state;

R_i , R_s - the rays of the inferior contour, respectively the superior one of the tronconical plate;

$T_i(r)$, $T_i(x)$ -temperature function on the interior face of the plate;

$T_e(r)$, $T_e(x)$ -temperature function on the exterior face of the plate;

$T_0(r)$, $T_0(x)$ - the uniform component of temperature field upon the thickness of the plate;

$\Delta T_0(r)$, $\Delta T_0(x)$ - the linear component of temperature field upon the thickness of the plate;

$X(r)$, $X(x)$ - the component of the external loads on radius direction, respectively on the generating line direction;

$Z(r)$, $Z(x)$ - the component of the external loads on plate surface;

*Lucrare inclusă în programul conferinței EENVIRO 2013

α - the angle between the generating line of the tronconical plate and the horizontal plane;

k - the amortization factor of the cylindrical plate;

a - the medium ray of the cylindrical plate;

$u(r)$, $u(x)$ - the plate deformation on the ray direction, respectively on the generating line direction of the plate;

$w(r)$, $w(x)$ - the plate deformation on normal direction on the surface of the plate;

$\Delta_r(x)$ - the curved plate deformation on radius direction;

$\chi_r(r)$, $\chi_x(x)$ - plate rotation on radius direction, respectively on the generating line direction;

$N_r(r)$, $N_\theta(r)$, $N_x(x)$ - axial force on circular and curved plates;

$M_r(r)$, $M_\theta(r)$, $M_x(x)$ - bending moment on circular and curved plates;

$Q_r(r)$, $Q_x(x)$ - shearing force on circular and curved plates.

1. Introduction

The water treatment and purifying technique made necessary the accomplishment of numberless structures with different forms: cylindrical, tronconical, spherical, rectangular or combinations between them, for example cylindrical-tronconical or ovoidal form, as in case of the anaerobic sludge digester tanks.

In practice, the achievement of hydroedilitary constructions in Romania's last 100 years showed a generally corresponding behaviour of the structures, registering quite frequently the necessity of rehabilitation of the structures from the structural point of view, resulting from damages due to lapse of time, which jeopardise the tightness and durability.

The damage causes are multiple, but one of the most important, that produce fissuration and deterioration in time of the hydroedilitary constructions structures, is the temperature variations action, determined both by seasonal variation of the exterior air temperature, the accumulated fluids temperature variation, as well as a series of other factors like: the degree of thermoisolation and the quality of the thermoinsulating materials, the presence of underground waters. For that we can name numberless deteriorations due to temperature variation as:

- fissuration above the admisible limits of circular foundation plates, immediately after placing the concrete, due to the thermal gradient produced by hidratation heat, on unprotected and untreated structures;

- fissuration and cracking of the tronconical reinforced concrete domes on anaerobic sludge digester tanks, where the thermal action is significative, because the sludge stored is heated permanently at +35 °C, while the exterior temperatures can vary from -25 to +40 °C.

In tehcnical literature, the establishment of the state of efforts from the action of temperature variation, for different structural elements, was made in the hypothesis of

the ideal-elastic working stage of reinforced concrete, not taking into account the damages of the rigidities in time, which provoke implicitly modifications of the state of efforts, especially due to thermal action, taking into account that the efforts produced by the thermal sollicitation depend on rigidity.

So in this work we present an analysis of the effect produced in time by the temperature variation, in the structure of an anaerobic sludge digester tank, with a stiffness degradation coefficient variable in time.

2. Determination of the effort state produced in the tank's structure from the simultaneously action of charges and temperature variations.

We shall study the case of anaerobic sludge digesters tanks from reinforced concrete (C25/30), with a capacity of 4000 m³, with a classical cylindro-tronconical form, presented in figure 1 with the following characteristics:

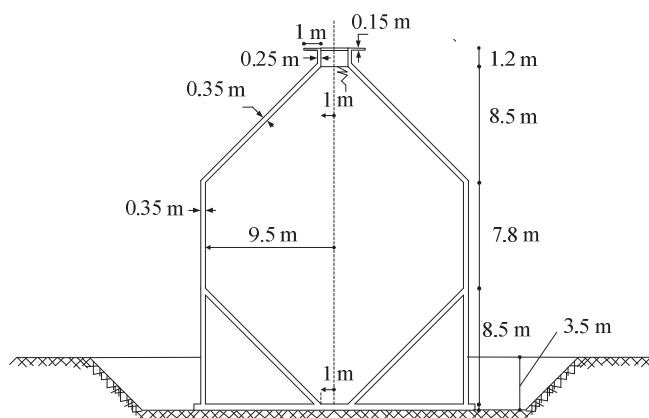


Fig. 1 The anaerobic sludge digester tank. Vertical section.

2.1. Calculus hypothesis

This state of efforts and deformations analysis has the following basic hypothesis:

- simplifying hypothesis from the linear-elastic theory for plane and curved bending plates, stated by Kirchhoff [1],[2];
- linear temperature variation on the thickness of the plate;
- temperature functions on the interior face T_i and the exterior face T_e are defined by thermal transfer calculations, in a stationary regime.

In order to obtain calculations facilities, the thermal field which take action upon the plate may be split into two components (figure 2) as follows:

- a uniform component on the thickness of the plate, T_0 which lead to the development of sectional axial efforts;

- a linear component on the thickness of the plate T_0 , with zero value in the median surface, which produce sectional bending efforts.

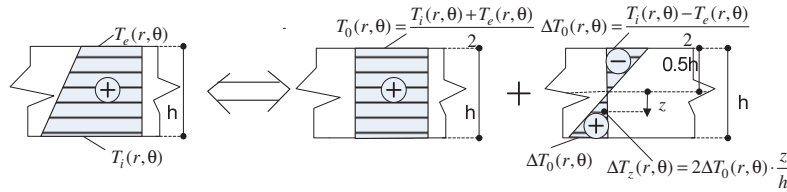


Fig. 2 The decomposing of the thermic field in elementary components when the circular plane plate is concerned

In order to establish the state of efforts produced by the permanent charges and by the temperature variation, we shall use the general efforts method. We must state that due to the fact that the efforts resulted from the permanent or cvasi-permanent actions do not depend on the stiffness, we shall consider that the structure works in the elastic stage. In same time, we shall consider that, as is described in technical literature, it is produced a degradation of stiffness and a variation in time of values of efforts state produced by thermal action.

From the analysis of numberless damages produced at the anaerobic sludge digester tanks made in Romania it has been noticed that the zone in which the most important structural damages appear is that of the tronconical roof, where due to the combined action of the hydrostatic pressure and temperature variation, the concrete might be fissurated, leading to a decrease of the tightness and implicitly of the durability. So, we can study only the structural ensemble tronconical roof - cylindrical wall.

If we take into account the physical, geometrical schematism and the links, we have the real structure calculus model. The basic system is obtained by suppressing the continuity links between the structural elements.

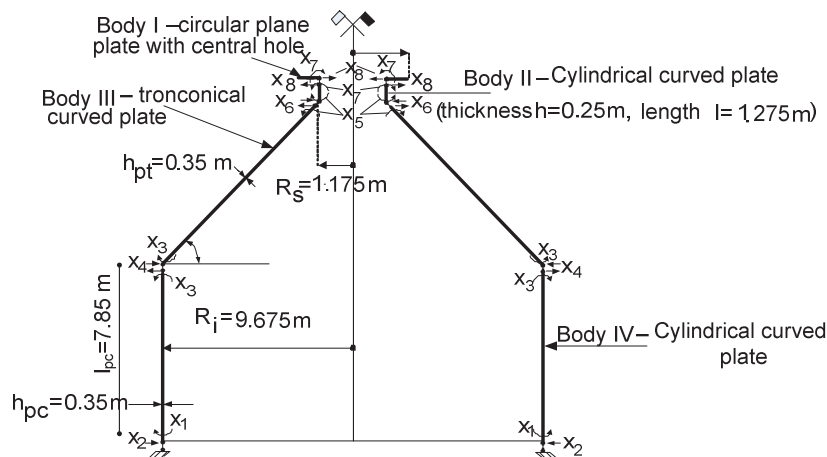


Fig. 3 Basic system of the structural part cylindrical wall - tank roof

2.2. Establishment of the efforts state produced in body 1 (circular plane plate)

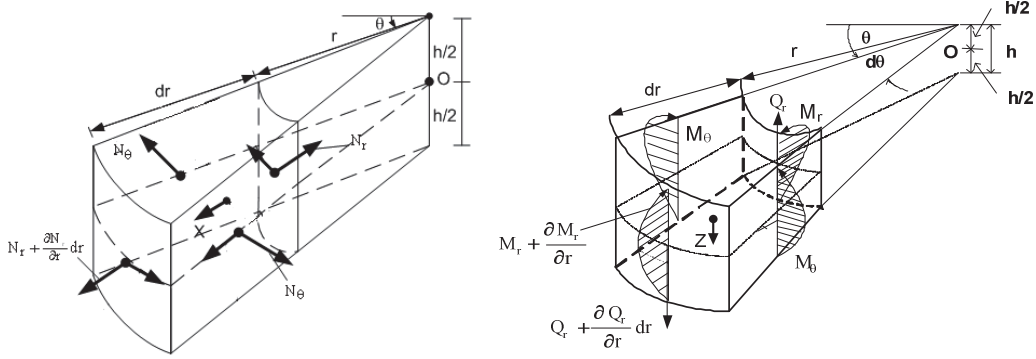


Fig. 4 The sectional positive efforts acting on an infinitesimal plate element

The plate deformations and sectional efforts are calculated with the relations:

$$u(r) = u_p(r) + C_1 \cdot r + C_2 \cdot r^{-1} \quad (1)$$

$$w(\rho) = w_p(\rho) + C_3 + C_4 \rho^2 + C_5 \rho^2 \ln \rho + C_6 \ln \rho \quad (2)$$

$$\chi_r(r) = -\frac{dw(r)}{dr} \quad (3)$$

$$N_r(r) = D \cdot \left[\frac{du(r)}{dr} + \mu \frac{u(r)}{r} - (1 + \mu) \alpha_t T_0(r) \right] \quad (4)$$

$$N_\theta(r) = D \cdot \left[\frac{u(r)}{r} + \mu \frac{du(r)}{dr} - (1 + \mu) \alpha_t T_0(r) \right] \quad (5)$$

$$M_r(r) = -B \left[\frac{d^2 w(r)}{dr^2} + \frac{\mu}{r} \cdot \frac{dw(r)}{dr} + 2(1 + \mu) \cdot \frac{\alpha_t \Delta T_0(r)}{h} \right] \quad (6)$$

$$M_\theta(r) = -B \left[\frac{1}{r} \cdot \frac{dw(r)}{dr} + \mu \cdot \frac{d^2 w(r)}{dr^2} + 2(1 + \mu) \cdot \frac{\alpha_t \Delta T_0(r)}{h} \right] \quad (7)$$

while the $C_1..C_6$ are integration constants and u_p , w_p are the particular solutions of the synthesis differential equations which define the state of efforts and deformations [1],[2].

2.3 Establishment of the efforts state produced in bodies 2 and 4 (cylindrical curved plates)

The synthesis equation which define the state of axial-symmetrical efforts and deformations that appear in the cylindrical curved plate by the simultaneously action of the charges and temperature variations is the following [1],[3]:

$$\frac{d^4 w}{dx^4} + 4k^4 \cdot w = -\frac{Z(x)}{B} + 4k^4 \cdot a \cdot \alpha_t \cdot T_0(x) + 2 \cdot (1+\mu) \cdot \frac{\alpha_t}{h} \cdot \frac{d^2 \Delta T_0(x)}{dx^2} \quad (8)$$

The deformation plate and sectional efforts have the expressions (9),...(14):

$$w(x) = w_p(x) + C_7 \operatorname{ch}(kx) \cos(kx) + C_8 \operatorname{ch}(kx) \sin(kx) + C_9 \operatorname{sh}(kx) \cos(kx) + C_{10} \operatorname{sh}(kx) \sin(kx)$$

$$\chi_x = -\frac{dw(x)}{dx}$$

$$N_x(x) = -\int X(x)dx + C_{11} \quad (11)$$

$$N_\theta(x) = D \left[\frac{w(x)}{a} - (1+\mu) \alpha_t T_0(x) \right] \quad (12)$$

$$M_x(x) = B \left[\frac{\partial^2 w(x)}{\partial x^2} - 2(1+\mu) \frac{\alpha_t}{h} \Delta T_0(x) \right] \quad (13)$$

$$M_\theta(x) = B \left[\mu \frac{\partial^2 w(x)}{\partial x^2} - 2(1+\mu) \frac{\alpha_t}{h} \Delta T_0(x) \right] \quad (14)$$

where $w_p(x)$ is the particular solution of the differential synthesis equation and the $C_7..C_{11}$ are the integration constants.

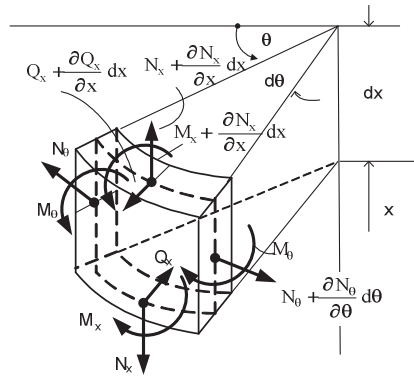


Fig. 5 Sectional positive efforts acting on an infinitesimal element of the cylindrical plate

2.4 Establishment of the state of efforts produced in body 3 (tronconical curved plate)

The synthesis equation which define the axial-symmetrical state of efforts and deformations produced in the tronconical curved plate by the simultaneously action of external loads and temperature variations is:

The behaviour analysis of an anaerobic sludge digester exposed on thermic action

$$L(L(Q_x x) + \frac{E \cdot h \cdot \text{tg}(\alpha)}{B} \cdot Q_x \cdot x = \frac{1}{B} \cdot \left[\frac{dZ(x)}{dx} + \frac{2Z(x)}{x} - \frac{1}{x^3} \left(\int Z(x) + X(x) \text{ctg}(\alpha) \right) x dx - \right. \\ \left. - \frac{\mu X(x) \text{tg}(\alpha)}{x} \right] - E \cdot h \cdot \text{tg}(\alpha) \left[\alpha_t L \left(\frac{dT_0(x)}{dx} \cdot x \right) + 2(1+\mu) \alpha_t \frac{d\Delta T_0(x)}{dx} \cdot x \cdot \text{tg}(\alpha) \right] \quad (15)$$

$$L() = \frac{d^2}{dx^2} () + \frac{d}{dx} () - \frac{1}{x} \cdot (). \quad (16)$$

If we define $\lambda = 4 \sqrt{\frac{12 \cdot (1-\mu^2) \sin^2(\alpha)}{(R_i + R_s) \cdot h^2}}$ the solution of the equation (15) has the form [1],[2]:

$$Q_x(x) = Q_p(x) + C_{12} \text{ch}(\lambda x) \cos(\lambda x) + C_{13} \text{ch}(\lambda x) \sin(\lambda x) + \\ + C_{14} \text{sh}(\lambda x) \cos(\lambda x) + C_{15} \text{sh}(\lambda x) \sin(\lambda x) - 2B(1+\mu) \frac{\alpha_t}{h} \frac{d\Delta T_0(x)}{dx} \quad (17)$$

where the $C_{12}..C_{16}$ the integrations constants. The axial-symmetrical state of efforts produced in the tronconical curved plate by the simultaneously action of charges and temperature variations are calculated with the relations:

$$N_x(x) = Q_x(x) \text{ctg}(\alpha) - \frac{1}{x} \int (X(x) + Z(x) \text{ctg}(\alpha)) x dx + C_{16} \quad (18)$$

$$N_\theta(x) = \frac{R_i + R_s}{2 \sin(\alpha)} \cdot \frac{dQ_x(x)}{dx} - Z(x) x \text{ctg}(\alpha) \quad (19)$$

$$M_x(x) = -B \frac{d\chi_x(x)}{dx} - 2B(1+\mu) \alpha_t \frac{\Delta T_0(x)}{h} \quad (20)$$

$$M_\theta(x) = -\mu B \frac{d\chi_x(x)}{dx} - 2B(1+\mu) \alpha_t \frac{\Delta T_0(x)}{h} \quad (21)$$

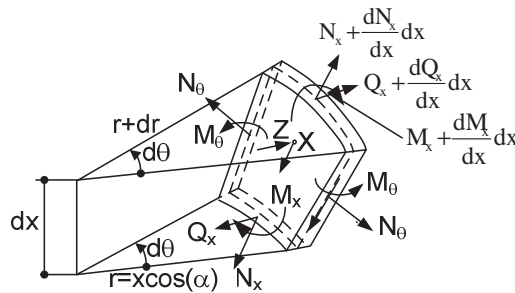


Fig. 6. Sectional positive efforts acting on an infinitesimal element of the tronconical curved plate

Deformation of the plate χ_x and Δ_r may be calculated with the relations:

$$\chi_x(x) = -\frac{\cot(\alpha)}{E \cdot h} \left[(N_\theta - N_x) \cdot (1 + \mu) + x \cdot \left(\frac{dN_\theta}{dx} - \mu \cdot \frac{dN_x}{dx} \right) \right] \quad (22)$$

$$\Delta_r(x) = \frac{x \cdot \cos(\alpha)}{E \cdot h} \cdot (N_\theta - \mu N_x) + x \cdot \cos(\alpha) \cdot \alpha_t \cdot T_0(x) \quad (23)$$

3. Results

In order to determine the efforts state produced by the cumulated action of the charges and of the thermic sollicitation we shall write the compatibility equations system (24) between the real system and the basic system. If we define the matrix $\Delta_i = \Delta_{i,p}$, then the system (24) may be written in a matric form ($i, j = 1..8$):

$$\delta_{ij} x_j + \Delta_i = 0 \quad (24)$$

where Δ_{ij} is the flexibility matrix of the studied structure, and $\Delta_{i,p}$ are the displacements produced by the external loads action on the basal system. The unitary displacements and those produced by the external loads and temperature variations on the basic system are calculated by the relations (1), (2), (3), (11), (12), (21), (22). The state of efforts is obtained by superposing the state of efforts produced by the unknown variables on the basic system and the state of effort produced by the external loads and the temperature variation (fig.7), taking into account the relations (6)-(10),(15)-(19),(22)-(29).

In figure 8 and table 1 we present the state of efforts in the tronconic roof – cylindrical wall part, considering the elastic stiffness hypothesis (hypothesis 1), the hypothesis of the stiffness which is diminuated by 25% compared to the elastic stiffness (hypothesis 2), respectively the hypothesis of the stiffness diminuated by 50% (hypothesis 3), both in case of a noninsulated structure and in case of the thermic insulated structure with a 10 cm mineral cotton layer ($\alpha_i = 500 \text{ W}/(\text{m}^2\text{C})$, $\alpha_e = 24 \text{ W}/(\text{m}^2\text{C})$, $\alpha_b = 1.74 \text{ W}/(\text{m}^2\text{C})$, $\alpha_{iz} = 0.04 \text{ W}/(\text{m}^2\text{C})$, $\alpha_t = 10^{-5} \text{ }^\circ\text{C}^{-1}$).

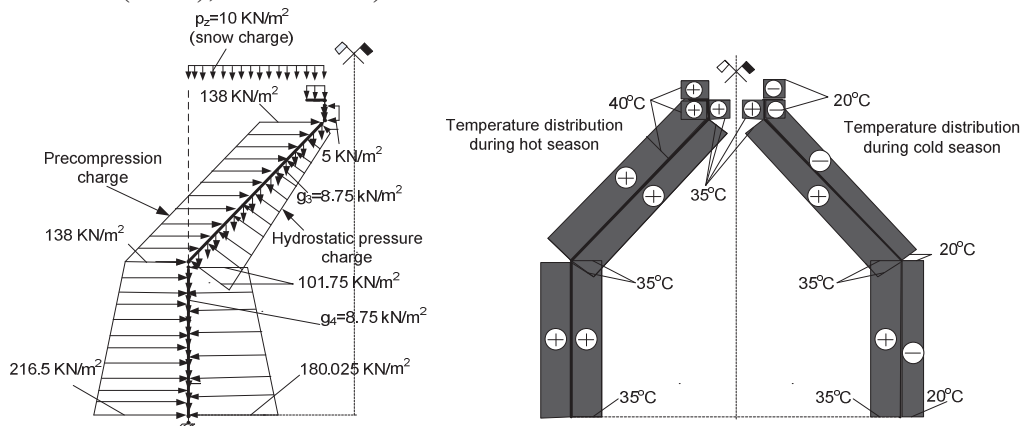


Fig 7 Exterior charges and temperature distribution inside, respectively outside of the tank considered for the studied case

The behaviour analysis of an anaerobic sludge digester exposed on thermic action

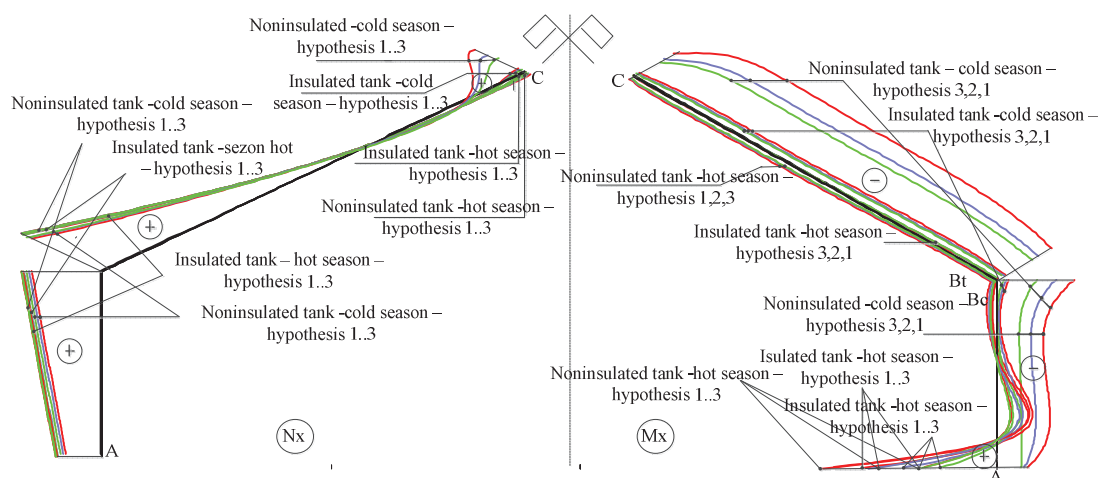


Fig 8 Sectional effort variation N_x (N_r) and M_x in tronconical roof – cylindrical wall structural part

Table 1

Values of efforts in in tronconical roof – cylindrical wall structural part

Structural element	Section	Noninsulated tank - cold season				Isulated tank - cold season			
		Hypothesis 1		Hypothesis 3		Hypothesis 1		Hypothesis 3	
		N_x [KN]	M_x [KNm]	N_x [KN]	M_x [KNm]	N_x [KN]	M_x [KNm]	N_x [KN]	M_x [KNm]
Cylindrical plate	A	69.53	-71.09	80.67	-57.51	88.130	308.34	89.97	132.20
	Bc	138.21	-183.19	149.36	-94.15	156.82	-29.24	158.66	-17.17
Tronconical plate	Bt	195.47	-183.19	211.22	-94.15	221.77	-29.24	224.38	-17.17
	C	138.72	-133.65	38.04	-66.57	17.92	-19.01	7.63	-9.26

Structural element	Section	Noninsulated tank - hot season				Isulated tank - hot season			
		Hypothesis 1		Hypothesis 3		Hypothesis 1		Hypothesis 3	
		N_x [KN]	M_x [KNm]	N_x [KN]	M_x [KNm]	N_x [KN]	M_x [KNm]	N_x [KN]	M_x [KNm]
Cylindrical plate	A	93.28	413.29	92.54	184.68	91.69	381.03	91.75	168.53
	Bc	161.96	13.34	161.23	4.12	160.38	0.24	160.44	-2.43
Tronconical plate	Bt	239.05	13.34	228.01	4.12	236.81	0.24	226.89	-2.43
	C	-15.50	12.7	-9.07	6.6	-4.17	2.95	-3.41	1.72

4. Conclusions

If an analysis in time is done for the cylindrical wall- tronconical roof part, we notice that:

1. In the studied case we obtain in cold season for noninsulated tank in section C, the value of axial force N_x reduced by 72%, respectively in case of a bending moment with 50.2%, in exploitation of the tank. So we can see a variation in time of the state of efforts in the anaerobic sludge digester tank structure, that means a maximum value after the concrete hardening, because in this phase concrete works in its elastic stage, case in which we have maximum values of efforts produced by thermic action.
2. Maximum value of sectional and unitary efforts, while concrete is hardening, leads, when a insufficient reinforcement percentage lacks, to a diminution in time of the stiffness to stretching and bending. So, during exploitation, after a period of time the stiffness value diminishes slowly as soon as fissures appear and this process stabilizes. In the same time, in case of a hydroedilitary construction, to which the fissure opening is limited, there must be imposed percentages of reinforcement corelated to the maximum fissure openings accepted. Thus it appears as necessary the establishment in the future of the bending and stretching stiffness for the plane and curved plates of reinforced fissured concrete, for a better optimization of the resistance structure for hydroedilitary constructions and particularly the anaerobic sludge digesters tanks.
3. In the same time the structure optimization supposes the corelation of the reinforcement percentage to the thickness of the walls and to the degree of thermoinsulation adopted for the walls, so that the energetic efficiency of the anaerobic sludge digester tanks is maximal. For exemplification we present the graphic in figure 9 where it is shown the reinforcement percentage variation on the vertical direction, disposed in the tronconical roof (insulated tank, cold season, hypothesis 3) on the inferior contour, as a function of thermal insulated degree [3], for different reduction values of elastic rigidity.

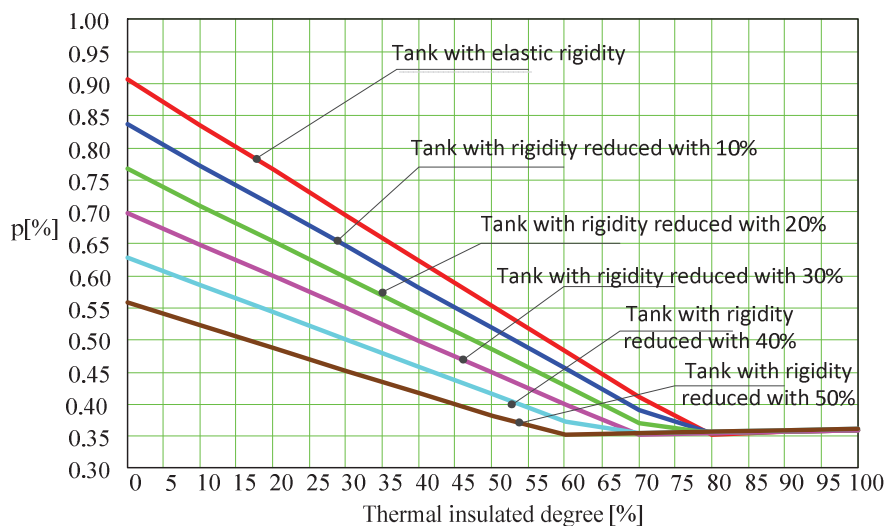


Fig. 9 Variation of the reinforcement percentage p depending upon the value of thermal insulated degree, in case of a tank made of reinforced concrete (C25/30, with reinforcing bars type PC52)

References

- [1] Furiş, D.- „Calculul și concepția structurilor axial-simetrice aplicate în tehnica tratării și epurării apei, luând în considerare rezemarea lor pe mediu elastic”, PhD Thesis, Institutul de Construcții București, 1979.
- [2] Hampe, E. - „Statik rotationssymmetrischer flächentragwerke” Vol 1-4, Veb verlag fur bauwesen, Berlin,1963.
- [3] Sorohan, L. V.- „Studiu privind efectele variațiilor de temperatură asupra construcțiilor utilizate în tratarea apei”, PhD Thesis, Universitatea Tehnică de Construcții București, 2012.

An experimental study on convective drying of quince*

Tzempelikos Dimitrios¹, Bardakas Achilleas², Vouros Alexandros²,
Tsepenekas Dionysios³, Filios Andronikos², Margaris Dionissios¹

¹Laboratory of Fluid Mechanics and Applications, Department of Mechanical Engineering and Aeronautics, University of Patras
GR-26500 Patras, Greece
E-mail: dtzempelikos@meed-aspete.net

²Laboratory of Fluid Mechanics and Turbomachinery, Department of Mechanical Engineering Educators, School of Pedagogical and Technological Education (ASPETE)
GR-14121 Athens, Greece
E-mail: aefilios@meed-aspete.net

³Project Engineer, EKO
GR-15125 Marousi, Greece
E-mail: D.Tsepenekas@eko.gr

Abstract. *A laboratory convective drying unit (LCDU) has been designed, constructed and equipped with an integrated measurement and control instrumentation, in order to evaluate the essential drying characteristics of various horticultural and agricultural products. The current paper presents experimental results from tests with quince slices. Drying kinetics was investigated as a function of drying conditions. Experiments were conducted at air flow temperatures of 40, 50 and 60°C and average velocities of 1, 2 and 3 m/s. Temperature changes of the drying quince samples, the relative humidity and the temperature of the drying air were measured during the drying processes and finally the moisture ratio (MR) was calculated. The experimental MR data were fitted with three mathematical models available in the literature and a good agreement was observed. In the ranges measured, Fick's 2nd law of diffusion was used to fit the experimental data for the determination of the effective moisture diffusivity. The activation energy was determined, assuming an Arrhenius type temperature relationship with moisture diffusivity.*

Keywords: Convective drying, Quince, Experimental, Drying kinetics, Drying rate.

1. Introduction

The drying is used for the preservation and storage of different fruits and vegetables for long periods of time with the removal of moisture content. It is a complex process where a simultaneous heat and mass transfer in transient conditions occurs. Knowing the mechanism of heat and mass transfer of a product, the process drying parameters can be optimized with the ultimate aim of improving the product. The parameters which influence the drying process are the temperature, the velocity and the relative humidity of the drying air. There are many studies in the literature

* Lucrare inclusă în programul conferinței EENVIRO 2013

dealing with the aforementioned parameters and involves a variety of fruits and vegetables. Karathanos et al [1] dealt with drying of some fresh and semi-dried fruits. Margaritis et al [2] studied hot air dehydration of sultana grapes. Kaya et al [3] studied the drying kinetics of quince at low velocities. Babalis et al [4] studied the drying kinetics of figs. Aghbashlo et al [5] modeling potato slices in length continuous band dryer. Velic et al [6] & Zlatanovic et al [7] used a laboratory scale dryer equipment to study the influence of the airflow velocity on kinetics of apple drying. Sacilik et al [8] and Doymaz [9] also studied the drying kinetics of organic apple slices. Drying kinetics of some vegetables like pepper, pumpkin, green pea, carrot, etc. were studied by Krokida et al [10]. The purpose of this study is the experimental investigation of the drying kinetics of quince in accordance with predefined conditions (drying temperature 40, 50 and 60°C and air velocity value of 1, 2 and 3 m/s) that do not exist in the literature and the evaluation of the effective moisture diffusivity as well as the activation energy.

2. Materials and methods

2.1 Materials

Fresh quinces were purchased from a local market in Athens, Greece and used for the drying experiments. The samples were stored in a refrigerator at about 6°C until use. Before drying the quinces were cleaned and sliced manually to a thickness of 10 mm, in order to produce uniform quince pieces. The samples were used to form a thin-layer on a 440 x 400 mm tray with a net weight of 395,5 gr. The initial moisture content (M_0) of quince slices was measured to be around 81,04% in wet basis (w.b.) or 4,27 kg water / kg dry matter in dry basis (d.b.) and was determined by the oven-drying method [11] with repetition in order to assure accurate moisture content average values.

2.2 Experimental apparatus

Fig.1 shows the Laboratory Convective Drying Unit (LCDU) which has been designed and constructed in the Laboratory of Fluid Mechanics and Turbomachinery in ASPETE. The overall dimensions of the facility are 4,7 m (length), 2,5 m (width) and 2,5 m (height). The air ducts are made from steel of 0,8 mm thickness. All the ducts were insulated with 10 mm of Alveolen (Frelen). The square section drying chamber (0,5 m x 0,5 m) is of tower (vertical) type and is equipped with a metal tray which is supported on four, side wall mounted, load cells. A set of four refractory glasses of 10 mm thickness are available to replace the side steel walls when optical clarity and precise visual observations are required. Upstream of the drying chamber, the long rectangular diffuser with a total divergence angle of 6,7°, the tube heat exchanger in which the hot water is provided through a boiler of 58 kW thermal power, the transitional duct with observation window that includes the sprayer for humidifying purposes, the corner duct that incorporates four guide vanes and the flow straighteners section, are located. The flow straighteners consisting of an aluminum

honeycomb are considered necessary aiming for flow uniformity in the drying section. The flow rate is observed and controlled with a custom made and calibrated rake of pitot tubes, namely pitot rake, located at the inlet of the drying chamber.

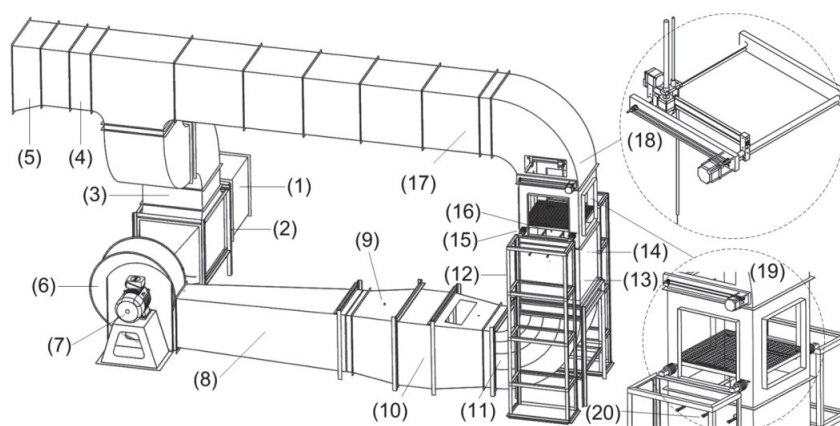


Fig. 1. Schematic diagram of the LCDU: (1) Air inlet, (2) Inlet damper, (3) By pass air damper, (4) Outlet damper, (5) Air outlet, (6) Centrifugal fan, (7) Three-phase electric motor regulated by an AC inverter, (8) Diffuser, (9) Temperature and humidity sensors, (10) Tube heat exchanger, (11) Guide vanes, (12) Metal frame for pressure cells, (13) Flow straighteners, (14) Temperature and humidity sensors, (15) Pressure cells, (16) Metal tray, (17) Temperature and humidity sensors, (18) Computer controlled 3-Axis traverse system, (19) Drying chamber, (20) Pitot rake.

Downstream of the vertical drying chamber, the second corner duct with guide vanes, the elevated horizontal modular constructed duct, the outlet dumper and the exit diffuser, are located. The modular design of the facility allows the easy placement of two or three horizontal drying chambers in tandem arrangement, on the elevated return or exit flow leg. The air flow is established and controlled through a centrifugal fan directly driven by a three phase electric motor of 3 kW with its speed regulated by an AC inverter. Adjusting the air dampers, the laboratory dryer can be used for thermal drying experimental studies in both open circuit and close circuit operations. The mean speed of the air flow at the inlet is the weighted average velocity of the 12 points collected from the pitot rake and the four pressure taps (same level with the contact tip of the pitot tube) in the side wall of the inlet of the drying chamber. Each pitot tube is connected via plastic tubing to a custom made pressure collector system equipped with solenoid valves (Tekmatic 24VDC, 6W) allowing its operation and control via pressure transmitter with the use of a custom application developed in Labview®.

2.3 Instrumentation and measurements

The air and drying product temperatures were measured using calibrated PT100 from UTECO Ltd. with class A tolerance and accuracy $\pm 0,15^{\circ}\text{C}$. A 3-wire transmitter from JUMO Ltd. (type 956533) with accuracy $\pm 0,2^{\circ}\text{C}$ was used for the above PT100's. The relative humidity of the drying air was determined using calibrated humidity transmitters from KIMO Instruments, models TH100 & TH200, with accuracy $\pm 2,95\%$ and $\pm 2,36\%$ respectively. A differential pressure transmitter (Dwyer, model MS-121-LCD) with a calibrated accuracy $\pm 2\%$ of the selected range of 25 Pa was used to measure air drying velocity. The weight was quantified using four load cells

(total nominal load 10 kg) of model F1, class C2, with accuracy $\pm 0,05\%$ and TA4/2 analog transmitter with accuracy $\pm 0,03\%$, from AEP Ltd. All transmitters are connected to a PC with a PCIe-6321 DAQ device (National Instruments®) via NI SCXI-1000 and NI SCXI-1302 modules with accuracy $\pm 0,134\%$ and sampling frequency 3,2 kHz. Custom application in Labview® was used to interface with data acquisition.

2.4 Experimental procedure

The LCDU was started 2h before each experiment in order to achieve the desired steady state conditions. Then the metal tray of the drying chamber was regularly filled with about 700 gr sliced quinces in thin-layer form. Experiments were performed at air drying conditions of 40, 50 and 60 °C with 4, 8 and 12 % relative humidity respectively. The air velocity was adjusted to 1, 2 and 3 m/s in the drying chamber. The volumetric flow rate varied from 900 to 2.700 m³/h, corresponding to a range of Reynolds number varying from $2,64 \times 10^4$ to $8,82 \times 10^4$. Weight, air temperature, probe-surface temperature and relative humidity were automatically monitored and acquisitioned by a PC. Measurements were taken every 10 min. All experiments were twice repeated and the means of measurements were averaged and used to express the data of the moisture content.

2.5 Theoretical considerations

2.5.1 Modeling of drying kinetics

The moisture content of the samples and the dimensionless moisture ratio (MR) during the drying processes were found applying the following equations:

$$M(t) = \frac{w(t) - w_d}{w_d}, \quad MR = \frac{M(t) - M_{eq}}{M_0 - M_{eq}} \quad (1)$$

where $M(t)$ is the moisture content at any moment t (kg water / kg dry matter), $w(t)$ is the dry matter at any moment t (kg) and w_d is the dry matter (kg), M_0 , M_{eq} are initial and equilibrium moisture content (kg water / kg dry matter) respectively. M_{eq} is quite small compared with M_0 and $M(t)$ and in the MR definition may be ignored [12]. The following assumptions were taken into account in order to establish the equations of mass transfer during convective drying: i) The process was isothermal, ii) The main transfer mechanism was diffusion and iii) deformations and shrinkage during drying were negligible [13]. The experimental data were fitted in three, state-of-the art, thin-layer drying models: i) Newton, $MR = \exp(-kt)$ [14], ii) Henderson – Rabis, $MR = \alpha \exp(-kt)$ [15] and iii) Page, $MR = \exp(-kt^n)$ [16], in order to find the best suitable model for describing the drying behavior of a quince slice in LCDU. In the aforementioned models the moisture ratio is a function of the drying time. In order to determine each constant for the tested model, non-linear regression was used. The effectiveness of each model fit was evaluated via statistical criteria such as coefficient of determination (R^2), reduced chi-square (χ^2) and root mean square error (RMSE) between the experimental and the predicted moisture ratio values. The best model describing the thin-layer drying characteristics of quince slices was chosen based on the higher R^2 value and the lower χ^2 and RMSE values.

2.5.2 Effective moisture diffusivity estimations

An analytical solution of Fick's model mass-diffusion equation for drying biological products in a falling-rate period was developed by Crank (1975). For long drying times a limiting of Crank equation is obtained and expressed in a logarithmic form:

$$MR = \frac{8}{\pi^2} \exp\left(-\frac{\pi^2 D_{eff} t}{4L^2}\right), \quad \ln MR = \ln\left(\frac{8}{\pi^2}\right) - \left(\frac{\pi^2 D_{eff} t}{4L^2}\right) \quad (2)$$

where D_{eff} is the effective moisture diffusivity (m^2/s), t is the time (s), L is the half-thickness of samples (m), and n is a positive integer. D_{eff} is determined by the slope of the relationships between the experimental drying data in terms of $\ln MR$ and drying time.

2.5.3 Calculation of the activation energy

The activation energy can be obtained from the Arrhenius correlation, which demonstrates the effective diffusivity reliance on temperature, and taking the natural logarithmic exponential form of Arrhenius, can be expressed as:

$$D_{eff} = D_0 \exp\left(-\frac{E_a}{RT_{abs}}\right), \quad \ln D_{eff} = \ln D_0 - \frac{E_a}{RT_{abs}} \quad (3)$$

where D_0 is the pre-exponential factor of the Arrhenius equation (m^2/s), E_a is the activation energy (kJ/mol), R is the universal gas constant (kJ/mol K), and T_{abs} is the absolute temperature (K). A plot of $\ln D_{eff}$ versus $1/T_{abs}$ from the Eq. (3) gives a straight slope and consequently, the energy activation (E_a).

3. Results and discussion

The drying curves for all drying experiments performed are reported in Fig. 2. In Fig. 2a to 2c the MR was plotted versus the drying time for different values of air drying temperature, while the air velocity value was kept constant. As it can be seen increasing the temperature of the drying air from 40 to 60 °C for all drying velocities, the total drying time decreased about 30%. This effect became less important after approximately 10 – 15 h.

Fig. 2d to 2f show the drying curves for different drying velocities, keeping the drying temperature constant. In these figures the effect of varying the air velocity on the drying rate is shown clearly. The increased air velocity of the air in the drying process results in a reduction of the drying time, a phenomenon that is more pronounced at higher drying temperatures, since heat transfer was increased due to the increasing temperature difference which is the driving cause of the heat transfer. It was observed that after a period of 4 to 5 h, the velocity increase does not affect the drying rate, i.e. the curve for the 3 m/s coincides with the curve of 2 m/s. The reason for this effect can be explained by the flow pattern inside the drying chamber and the dried product that directly affect the heat and mass transfer coefficients.

The statistical results in terms of R^2 , χ^2 and RMSE, as well as drying constants k for Newton, a and k for Henderson – Rabis and k , n for Page models, are shown in Table 1, where V is the air velocity and T is the temperature. The models of Henderson – Rabis and Page (bold numbers in Table 1) obtain an $R^2 > 0,99$ while the small values for the other criteria, show a very good consistence with the experiments.

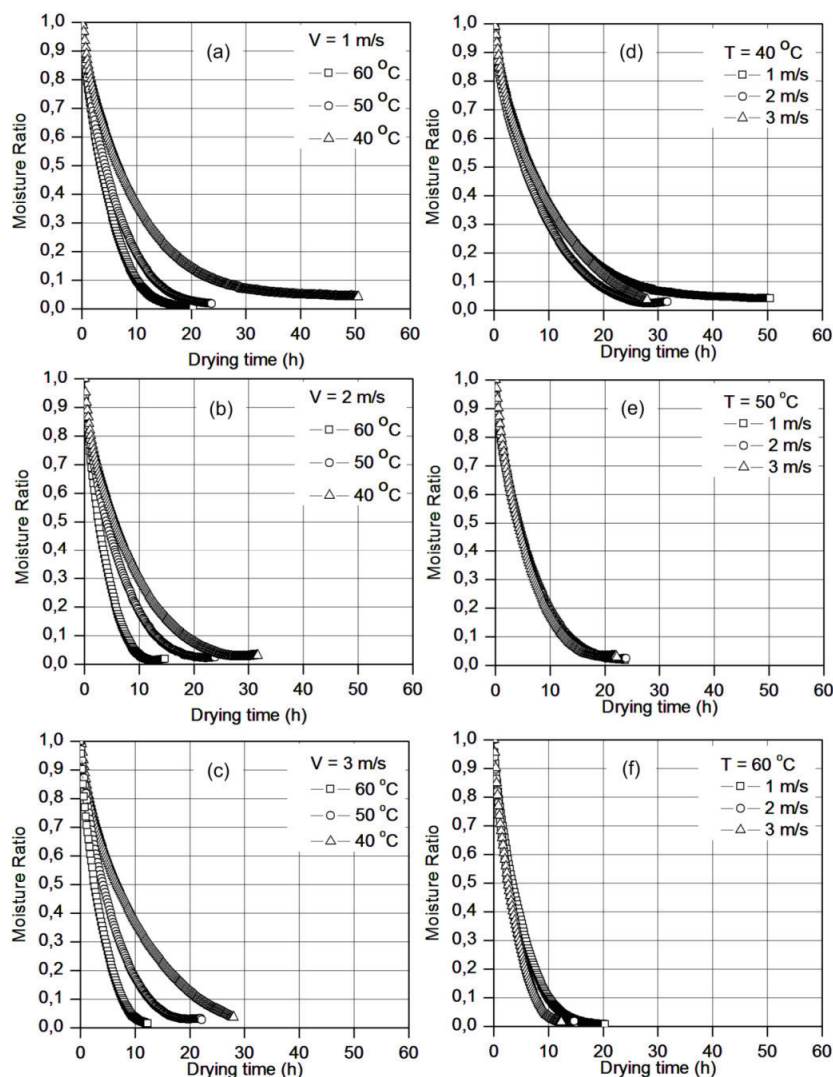


Fig 2. Air temperature (a,b and c) and air velocity (d, e and f) effects on the drying curves.

Table 2 shows the effective moisture diffusivity (D_{eff}) for each test. D_{eff} values varied from $2,67 \times 10^{-10}$ to $8,17 \times 10^{-10}$. These values are in a good agreement with those reported in the literature. As can be seen an increase in either the velocity or temperature increases moisture diffusivity due to the higher mass transfer.

The energy activation (E_a) and the Arrhenius coefficient (D_0) for each value of drying air velocity are presented in Table 3. An increase in air velocity increases both E_a and D_0 . The value of energy activation ranged between 36,996 kJ/mol and 42,593 kJ/mol, similar to those given in the literature for the drying of different foods.

Table 1

Fitting results for different drying conditions

V(m/s)	T (°C)	Model	k	α	n	R ²	$\chi^2 \times 10^{-4}$	RMSE
1	40	Newton	0,0986	0,9386	0,8721	0,9907	4,92	0,0221
		Henderson - Rabis	0,0922			0,9943	3,01	0,0173
		Page	0,1363			0,9972	1,50	0,0122
	50	Newton	0,1676	0,9734	0,9852	0,9974	1,71	0,0130
		Henderson - Rabis	0,1631			0,9981	1,23	0,0110
		Page	0,1727			0,9974	1,68	0,0129
60	Newton	0,2139	1,0094	1,0716	0,9958	2,97	0,0172	
	Henderson - Rabis	0,2158			0,9958	2,96	0,0171	
	Page	0,1882			0,9971	2,04	0,0142	
2	40	Newton	0,1254	0,9448	0,9423	0,9942	3,59	0,0189
		Henderson - Rabis	0,1184			0,9975	1,57	0,0125
		Page	0,1434			0,9955	2,81	0,0167
	50	Newton	0,1736	0,9562	0,9616	0,9955	2,85	0,0168
		Henderson - Rabis	0,1660			0,9975	1,56	0,0124
		Page	0,1874			0,9961	2,49	0,0157
60	Newton	0,2805	1,0112	1,0768	0,9951	3,57	0,0188	
	Henderson - Rabis	0,2835			0,9952	3,53	0,0186	
	Page	0,2497			0,9967	2,40	0,0153	
3	40	Newton	0,1031	0,9628	0,9536	0,9946	3,41	0,0184
		Henderson - Rabis	0,0990			0,9966	2,18	0,0147
		Page	0,1155			0,9956	2,83	0,0167
	50	Newton	0,1745	0,9903	1,0123	0,9979	1,42	0,0119
		Henderson - Rabis	0,1728			0,9980	1,37	0,0116
		Page	0,1703			0,9980	1,40	0,0117
60	Newton	0,2782	1,0024	1,0507	0,9946	3,97	0,0198	
	Henderson - Rabis	0,2789			0,9946	4,03	0,0198	
	Page	0,2578			0,9954	3,45	0,0183	

Table 2

Effective moisture diffusivity coefficient, D_{eff}

Air velocity (m/s)	Temperature (°C)	D _{eff} x 10 ⁻¹⁰ (m ² /s)	R ²
1	40	2,67	0,9993
	50	4,42	0,9989
	60	6,26	0,9933
2	40	3,23	0,9982
	50	4,91	0,9951
	60	7,82	0,9958
3	40	3,06	0,9901
	50	5,36	0,9940
	60	8,17	0,9903

Table 3

Energy of activation E_a and Arrhenius coefficient D₀

Air velocity (m/s)	E _a (kJ/mol)	R ²	D ₀ (m ² /s)
1	36,996	0,9925	4,04E-04
2	38,291	0,9976	7,78E-04
3	42,593	0,9959	3,97E-03

4. Conclusions

The drying kinetics of the quince slices were studied as a function of the drying conditions. Experiments were carried out for three values of the drying air temperature and the averaged velocity. Increasing the temperature or the velocity of the drying air decreases the total drying time. In order to describe the drying behavior of the quince slices, three drying models were fitted to the drying data. The Henderson – Rabis and Page model predicted adequately the moisture ratio, according to the values of R^2 , χ^2 and RMSE. The effective moisture diffusivity was obtained from Fick's 2nd law and observed that increase either velocity or temperature reduces D_{eff} . Finally, the Arrhenius equation was used to describe the energy activation and to increase the drying velocity caused increase E_a .

References

- [1] V.T. Karathanos & V.G. Belessiotis, "Application of a thin-layer equation to drying data of fresh and semi-dried fruits", *Journal of Agricultural Engineering Research*, 74, p.p. 355-361, 1999.
- [2] D.P. Margaris & A. G. Chiaus, "Experimental study of hot air dehydration of sultana grapes", *Journal of Food Engineering*, 79, p.p. 1115-1121, 2007.
- [3] A. Kaya, O. Aydin, C. Demirtas & M. Akgun, "An experimental study on the drying kinetics of quince", *Desalination*, 212, p.p. 328-343, 2007.
- [4] S.J. Babalis & V.G. Belessiotis, "Influence of the drying conditions on the drying constants and moisture diffusivity during the thin-layer drying of figs", *Journal of Food Engineering*, 65, p.p. 449-458, 2004.
- [5] M. Aghbashlo, M.H. Kianmehr & A. Arabhosseini, "Modeling of thin-layer drying of potato slices in length of continuous band dryer", *Energy Conversion and Management*, 50, p.p. 1348-1355, 2009.
- [6] D. Velic, M. Planinic, S. Tomas & M. Bilic, "Influence of airflow velocity on kinetics of convection apple drying", *Journal of Food Engineering*, 64, p.p. 97-102, 2004.
- [7] I. Zlatanovic, M. Komatina & D. Antonijevic, "Low-temperature convective drying of apple cubes", *Applied Thermal Engineering*, 53, p.p. 114-123, 2013.
- [8] K. Sacilik & A.K. Elicin, "The thin layer drying characteristics of organic apple slices", *Journal of Food Engineering*, 73, p.p. 281-289, 2006.
- [9] I. Doymaz, "An Experimental Study on Drying of Green Apples", *Drying Technology*, 27, p.p. 478-485, 2009.
- [10] M.K. Krokida, V.T. Karathanos, Z.B. Maroulis & D. Marinos-Kouris, "Drying Kinetics of some vegetables", *Journal of Food Engineering*, 59, p.p. 391-403, 2003.
- [11] AOAC, "Official Methods of Analysis", 15th Ed., Association of Official Analytical Chemists: Arlington, VA, 1990.
- [12] T. Madhiyanon, A. Phila & S. Soponronnarit, "Models of fluidized bed drying for thin-layer chopped coconut", *Applied Thermal Engineering*, 29, p.p. 2849-2584, 2009.
- [13] R. Lopez, A. de Ita & M. Vaca, "Drying of prickly pear cactus cladodes (*Opuntia ficus indica*) in a forced convection tunnel", *Energy Conversion and Management*, 50, p.p. 2119-2126, 2009.
- [14] C.L. Hii, C.L. Law & M. Cloke, "Modeling using thin layer drying model and product quality of cocoa", *Journal of Food Engineering*, 90, p.p. 191-198, 2009.
- [15] G. Page, "Factor influencing the maximum rates of air drying shelled corn in thin layer", Master Thesis, Purdue University, 1949.
- [16] S. Henderson & S. Rabis, "Grain drying theory: I. Temperature effects on drying coefficient", *Journal of Agricultural Engineering Research*, 6, p.p. 169-174, 1961.